A STUDY ON SEDIMENTATION ISSUE IN MAGNETORHEOLOGICAL FLUIDS

Thesis

Submitted in partial fulfillment of the requirements for the degree of

DOCTOR OF PHILOSOPHY

by

ARUNA M N

(165057 MT16F01)

DEPARTMENT OF METALLURGICAL AND MATERIALS ENGINEERING

NATIONAL INSTITUTE OF TECHNOLOGY KARNATAKA, SURATHKAL, MANGALURU - 575025

JUNE 2021

DECLARATION

I hereby *declare* that the Research Thesis entitled "**A study on sedimentation issue in magnetorheological fluids**", which is being submitted to the National Institute of Technology Karnataka, Surathkal in partial fulfillment of the requirements for the award of the Degree of **Doctor of Philosophy in the Department of Metallurgical and Materials Engineering** is a *bonafide report of the research work carried out by me*. The material contained in this Research Thesis has not been submitted to any University or Institution for the award of any degree.

Place: NITK, Surathkal   Name: **ARUNA M N**

Date: Register Number: **165057 MT16F01**

                                   Department of Metallurgical and Materials Engineering

CERTIFICATE

This is to certify that the Research Thesis entitled "**A study on sedimentation issue in magnetorheological fluids**", submitted by **Mr. ARUNA M N (Register Number: 165057MT16F01)** as the record of the research work carried out by him, is *accepted as the Research Thesis submission* in partial fulfillment of the requirements for the award of the degree of Doctor of Philosophy.

Research Guide

Dr. Mohammad Rizwanur Rahman

Associate Professor

Department of Metallurgical and Materials Engineering

NITK, Surathkal

K. NARAYAN PRABHU

Chairman-DRPC

Date

ACKNOWLEDGEMENTS

I am grateful to NITK for providing an opportunity to carry out my doctoral study in the Department of Metallurgical and Materials Engineering. I thank all faculty members of the Department who taught and helped me.

My sincere thanks to Dr. Pranesh Rao, former Research Scholar, for his help towards Brookfields Viscometer measurements. Special thanks to my friend, Mr. Augustine Samuel Alberts, Research Scholar of the Department for his support in contact angle analyzer study.

I thank our research group members Mr.Arun Kumar D.S, Mrs. Divya Bharathi, Mrs.Pooja M, and Swaroop K.V for their cooperation during the research work.

My heartfelt thanks to my friends Dr.Ramesh S, Dr. Sharath S, Dr.Pradeep V Badiger, Mr.Sandeep,Mr.Manjunath M, Mr.Govind Ekbote, Mr.Jagadeesh C, Mr.Natesh B V, Mr.Sunil Meti, Dr.Anjan B.N, Mr.Basavaraj Padsale, Mr.Sunil B Y for standing by me through my good and bad times. I extend my sincere gratitude to all the research scholars of the department for rendering their support.

I am very much grateful to Mr. Mohan Raj G T of our research group for his skills, criticisms, and suggestions. I am deeply moved by his humbleness, dedication, and helping nature.

I am indebted to my parents Nagaraju M N and Sundramma for having extended their support and faith in me for doing the Ph.D. work. I also would like to thank my brother Mr.Anil M N for the moral support. Without them, surely, this research work

would not have been possible.

I am humbled when I think of extending my thanks to my family members because of whom I exist and because of whom if I am what I am in my life today. To my life coach, my grandfather Late. Narayanagowda and grandmother Late. Puttamma, because I owe it all to him. Lastly, I would like to express my deepest gratitude to my grand parents Late. Sanne gowda (Kaka) and Late.Gowri without whom I would not have pursued higher education

I would like to thank God for giving me the strength, knowledge, ability, and opportunity to undertake this research study and to persevere and complete it satisfactorily.

Abstract

The purpose of this dissertation is to investigate the sedimentation problem in magnetorheological fluids (MRFs). MRFs are the class of smart materials since some of the physical properties can be changed with the application of an external magnetic field. In particular, the shear stress and viscosity characteristics which can modify by varying the intensity of the magnetic field can be varied. The main property of MRFs is the capability of changing their rheological behavior within milliseconds and reversibly with off-state and on-state magnetic field conditions. At present, MRFs are very attractive for a large number of applications such as vibration-dampers, clutches, brakes up to the recent biomedical applications and virtual reality devices. MRFs typically consist of 1-10 μm micron-sized magnetic particles dispersed in a carrier liquid. Sedimentation stability is the main problem that restricts the application of MRFs, and the main factors affecting the stability are high-density magnetic particles, volume fraction, and type of carrier liquids. Therefore, studying the preparation and performance of the MRFs is crucial to use MRFs extensively for various applications. To minimize the settling of magnetic particles used in MRFs various new types of additives, surface modifiers, different carrier fluid with varying viscosity, ferrite particles, and changing the particle volume fraction are used to address the sedimentation issue in the present work. First, the effects of three different clay additives are added in carbonyl iron particles along with poly-alpha-olefin oil for sedimentation effect in MRFs are investigated. Experimental investigations have been carried for sedimentation testing for MRFs which contain with and without additives to know the damping force of fabricated mono-tube magnetorheological (MR) damper. Further, the effect of different surface area fumed silica additive added in silicone oil to minimize the settling of carbonyl iron particles in MRFs. The carrier fluid with varying viscosity plays a major role in the stability of MRFs, so the MRFs were prepared with three different carrier fluids with varying viscosity. The ferrite particles based MRFs are stable against settling than the CIPs based MRFs due to the density of the particles used is very less. The rheological properties of the MRFs,

including field-dependent yield-stress, were measured at off-state and magnetic fields applied using a parallel plate design magnetorheometer. Hence, in this present work minimize the sedimentation of the particles in MRFs with slight variation in the rheology properties have been formulated in lab-scale at cost-effective than the commercial available MRFs.

Table of Contents

CHAPTER 3

CHAPTER 4

CHAPTER 5

RHEOLOGICAL, SEDIMENTATION, DAMPING FORCE CHARACTERISTICS OF CIPs BASED MRF WITH/WITHOUT ADDITIVES…………………………………….93

CHAPTER 6

INFLUENCE OF DIFFERENT FUMED SILICA BASED MRF FOR SEDIMENTATION EFFECTS…………………………………………………………..107

CHAPTER-1

INTRODUCTION

This chapter presents an overview of magnetorheological fluids (MRFs), including their description, properties, applications, and working modes.

1.1 Background of MRFs

J. Rabinow of the US National Bureau of Standards patented the use of MRFs in 1948's (Rabinow 2013).MRFs are smart materials that can be controlled by an applied magnetic field. MRFs consist of typically micron-sized (i.e.1-10μm) magnetic particles that are uniformly distributed in the carrier fluid, which can be mineral oil, synthetic oil, water, silicone oil, and hydrocarbon oil (Carlson 2005).
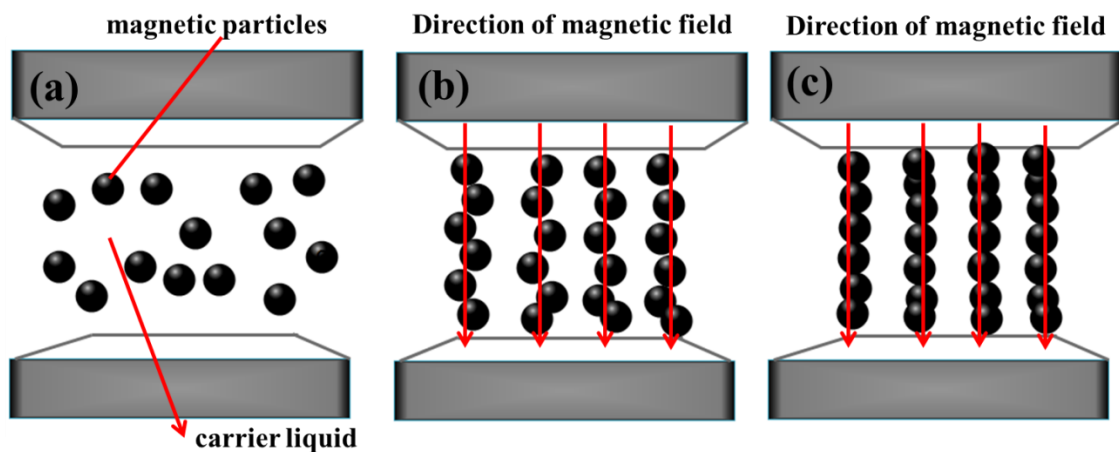
Fig.1.1 Schematic representation of MRF (a) off-state (b) on-state (c) columnar-like structure in the direction of applied magnetic field

As shown in Fig.1.1(a)-(c), an external magnetic field modifies the macroscopic appearance of MRFs by allowing them to transition from a viscous free-flow liquid in the absence of a magnetic field to a quasi-solid state in the presence of a magnetic field. In other words, polarization between two induced dipoles causes suspended particles in MR fluids to form a chain-like microstructure that corresponds to the direction of the applied magnetic field (Jolly et al. 1999). The magnetic chain arrangement alters the rheological properties of the suspension. Meanwhile, the

rheological properties of MR fluids change dramatically, with the shear viscosity of MRFs suddenly increasing and yield stress required to start the flow of MR fluids. However, at a magnetic field of 150–250 kA/m, MR fluids can only exhibit yield stress of 50–100 kPa. When MR fluids are exposed to a magnetic field, the particles acquire a dipole moment that is associated with the flux lines of the field (Ashour et al. 1996). As this phenomenon is studied on a microscale, it can be demonstrated that it contributes to the formation of linear chains of particles, resulting in a solid-like MR aggregate on a macro-scale. MRFs gain strength from the formation of chain structures. From an application standpoint, the field-dependent yield stress, viscosity, and sedimentation stability of the MRFs under gravity are critical parameters.

1.2 Electro rheological fluids (ERFs)

In recent years, because of their ability to adjust their flow resistance when subjected to magnetic or electric fields, MRFs and electro-rheological (ERFs) fluids have sparked a lot of research interest. ERFs are composed of electrically polarizable particles suspended in an insulating medium.
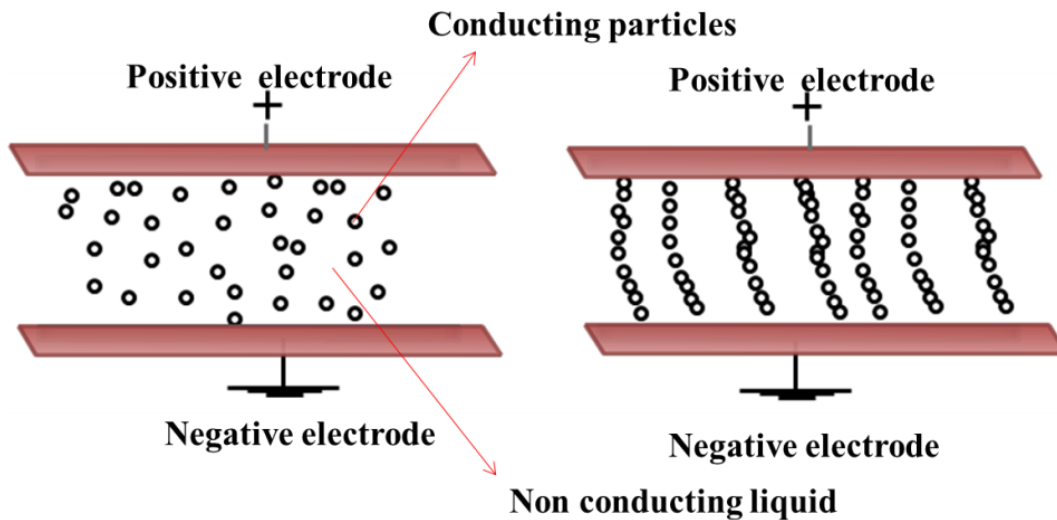
Fig.1.2 Electrorheological fluids (a) absence (b) presence of an electric field

If the ER fluid is free of the electrical field, the particles are evenly distributed in the fluid and flow as a Newtonian fluid, as shown in Fig. 1.2(a). When exposed to a high-intensity electrical field of up to 5 kV/mm, however, the particles form a chain-like structure parallel to the electrical field's direction, as shown in Fig.1.2.(b). As a

consequence, the flow resistance or apparent viscosity gets regulated by the electrical field strength. The original properties of the ER fluids could be recovered after the electrical field is removed. Due to their high dielectric constants, ferroelectric particles such as $BaTiO_3$ and $SrTiO_3$ are also commonly used in ERFs. The electro-rheological (ERFs) effect is influenced by the electrostatic field, while the magnetic field influences the MRFs effect (Stanway et al. 1996). The MRF products have yield stress that is 20-50 times higher than the comparable ERF products. All of these advantages of MRF technology have given rise to a very high level of interest in the launch of MRF-based products over the last few years. Table 1.1 offers a summary of the ERFs and MRF's main features.

Table 1.1 Major characteristics of MRF and ERF (Chaudhuri et al. 2005)

Property	Features of MRF	Features of ERF
Maximum yield stress	50–100 [kPa]	2–5 kPa
Reaction time	Few milliseconds	Few milliseconds
Power supply	2–25 [V], 1–2 [A]	2–5 kV @ 1–10 mA
Working temperature	−40 to 150 [°C]	25 °C up to +125 °C
Operational field	250 kA/m	4 kV/mm
Energy density	0.1 J/cm^3	0.001 J/cm^3
Stability	Good for most impurities	Poor for most impurities

1.3 Ferrofluids and MRFs

 A ferrofluid is a liquid that contains a stable colloidal suspension of ferromagnetic or ferri-magnetic particles. Ferrofluids were discovered in the 1960s at a research center run by the United States' National Aeronautics and Space Administration (NASA).
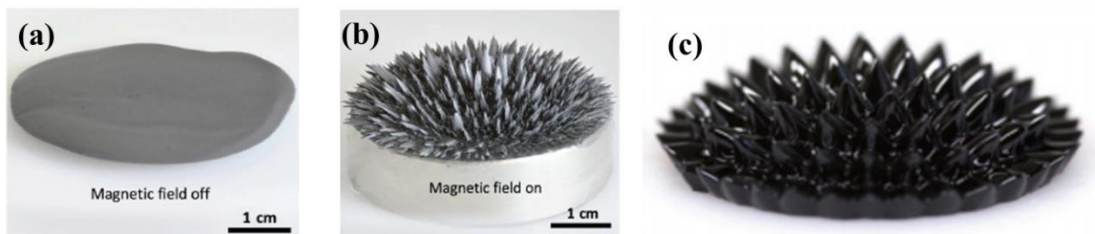
Fig.1.3 (a) MRFs with magnetic field of (b) with the magnetic field on (Jackson et al. 2018) (c) Ferrofluids (Branch and Knudsen 2018)

In MR fluids, the iron particles are in the range of 1-10 μm, while in ferrofluids, the iron oxide particles are about 10 nm. As a result, the magnetic moment of micron particles in MRFs is field-induced, and their Brownian motion is negligible, whereas magnetic nanoparticles in ferrofluids have a permanent dipole moment and undergo extreme thermal motion. MRF changes state from liquid to semi-solid when a magnetic field is triggered, while ferrofluid remains liquid even in a strong magnetic field, as shown in Fig.1.2.When making a ferrofluid, it is important to keep the particles from clumping together and settling. As a result, the size of the magnetic particles must be below a critical limit, allowing Brownian motion to counteract gravitational agglomeration and sedimentation (Vékás 2008). The interaction of the magnetic dipole and the Van der Waals forces facilitate particle agglomeration. Ferrites, such as Fe_3O_4, Fe_2O_3, and $CoFe_2O_4$, are widely used particles that are prepared using various techniques (Holm and Weis 2005). Since the particles in ferrofluids are smaller, they remain in constant Brownian motion, preventing gravitational settling. Only MR fluid expresses yield stress under an external field due to this difference, which defines the effect of Brownian motion within the fluid. Table 1.2 shows the comparison of smart fluid materials.

Table 1.2 Comparisons of Smart Fluids

Particulars	Ferrofluid	MR fluid
Particles	Magnetite, Iron, ferrites, etc.	Carbonyl iron, powder, cobalt, nickel, etc
Particle Size	2-10nm	1-10μm
Carrier Liquid	Oil-based, water-based, etc	Oils, Polar Liquid, water
Density (g/cc)	1-2	3-4
Operating Temperature	-40 to 150°C	-40 to 150°C
Required Field	Magnetic Field	Magnetic Field

1.4 Rheology background to the MRF

In its simplest form, rheology is the study of the flow and deformation of matter. To design magnetorheological devices and predict how they operate, it would be important to find a clear relationship between shear stress and shear rate in the MRFs.
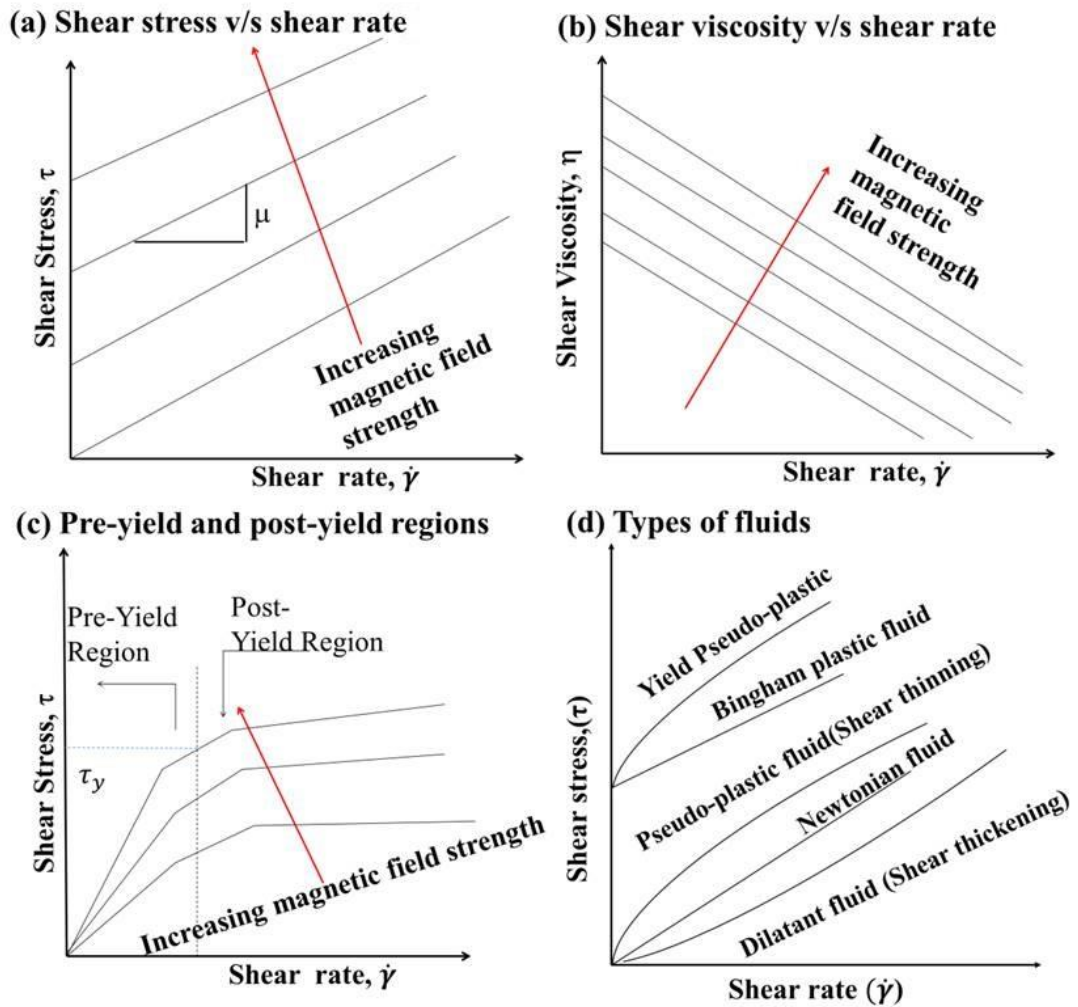
Fig.1.4 Under various magnetic field strengths of MRFs (a) shear stress (b) shear viscosity of (c) pre and post-yield regions and (d) types of fluids

There are two ways to express viscosity-dynamic and kinematic viscosity.

Dynamic viscosity is defined by equation

$$\eta = \frac{\tau}{\dot{\gamma}}, \tag{1.1}$$

where τ =Shear stress (N/mm^2), $\dot{\gamma}$=shear rate (1/s), $\eta (Pa.s)$.

Kinematic viscosity is defined by

$$\vartheta = \frac{\eta}{\rho},$$

(1.2)

where, $\rho =$ density $\left(\frac{Kg}{m3}\right)$, $\vartheta =$ Kinematic viscosity $\left(\frac{m2}{s}\right)$, 10^4 stokes, 10^6 cSt. Fig. 1.4(a), shows that shear stress which increases with an increase in the external magnetic field strength. The MR fluid can be called a Newtonian fluid in the absence of a magnetic field, with a linear relationship between stress and strain rate (Eshaghi et al. 2015). Figure 1.4(b) shows that as the shear rate increases, the viscosity decreases, indicating that MR fluids shear thin. The chain structures formed by the magnetic particles within the MRF under the applied magnetic field are continuously broken under shear deformation (Ju et al. 2013). As the magnetic field strength increases, the magnetic interaction force between the particles increases, resulting in increased shear viscosity. The shear stress-shear rate properties of the MR fluid can be investigated in two regions referred to as pre-yield and post-yield regions, as shown in Fig.1.4(c). To model the entire pre-yield and post-yield behaviour of the MR fluids, two simple viscoelastic models, Bingham-plastic and Herschel-Bulkley, are commonly used: Two parameters, including shear viscosity and shear stress, are used in these models to describe the behaviour of MRFs. The Bingham plastic model is used when shear stress is proportional to shear rate in the post-yield regime (Çeşmeci and Engin 2010). As a result, the behaviour of MR fluid is frequently represented as Bingham plastic with variable yield stress. An equation represents the Bingham plastic model (Chaudhuri et al. 2006).

$$\begin{cases} \tau = \tau_y(H) + sgn\left(\frac{du}{dr}\right) + \mu\frac{du}{dr} & |\tau| \geq |\tau_y|, \\ \qquad \frac{du}{dr} = 0 & |\tau| \ll |\tau_y|, \end{cases}$$

(1.3)

where τ represents the shear stress, τ_y represents dynamic yield stress, H is the applied magnetic field intensity, du/dr is the shear-strain rate, and μ is the plastic viscosity of the MRFs.

The fluid behaviour under field is nonlinear and different in the pre-yield and post-yield regimes with pseudo plastic properties shear stress is typically described by the

Herschel–Bulkley equation. As depicted in Fig.1.4(d), the above relation describes the Newtonian fluid when $\tau_y = 0$ and $n = 1$ and when the dynamic viscosity of the fluid is constant.The Herschel–Bulkley model reduces to the Bingham plastic model for $n = 1$. The equation demonstrates shear thinning and shear thickening fluids for $n < 1$ and $n > 1$ respectively(Wang and Gordaninejad 1999).

$$\begin{cases} \tau = \tau_y + k \left|\frac{\partial u}{\partial z}\right|^n & |\tau| \geq \tau_y, \\ \frac{\partial u}{\partial z} = 0 & |\tau| \ll \tau_y, \end{cases} \tag{1.4}$$

where τ, τ_y, k, and u denote shear stress, yield stress, plastic viscosity, and velocity of the fluid, while the exponent n is a flow behaviour index.

Casson developed the most widely used empirical model for describing time-independent viscosity. The Casson fluid model represents the fluid's continuous shear thinning behaviour, with viscosity decreasing from infinite at zero shear rate to zero at infinite shear rate. Based on the equation relationship between shear stress (τ) and shear rate ($\dot{\gamma}$) becomes (Sidpara et al. 2009a).

$$\sqrt{\tau} = \sqrt{\tau_y} + \sqrt{\eta\dot{\gamma}}, \tag{1.5}$$

where η is a shear viscosity of suspension at an infinite shear rate, τ is the shear stress, τ_y is the dynamic yield stress, and shear rate is ($\dot{\gamma}$)

1.3 Critical factors of MRFs

Several key issues must be addressed to successfully apply MR fluids in various applications. The major challenges of MRF are depicted in Figure 1.5. One of the most significant challenges in the application of MRFs is that their magnetic particles tend to settle due to the density difference between the dispersed phase (ρ=7.9 g/mL) and the carrier fluid medium (ρ=0.95g/mL), making them difficult to re-disperse in the suspension. Sedimentation can be especially problematic when MRF-based devices are used infrequently. Understanding the sedimentation process is required for MRF application success. As a result, the sedimentation stability of the MRF used in the specific device may become a greater concern in the current work.

When MRFs are subjected to a large number of loading cycles, they exhibit an increase in OFF state viscosity at high stress and high shear rate over time, causing

the fluid to thicken. A good magnetorheological fluid should be able to withstand the in-use thickening that occurs during use (IUT) (Carlson 2003).
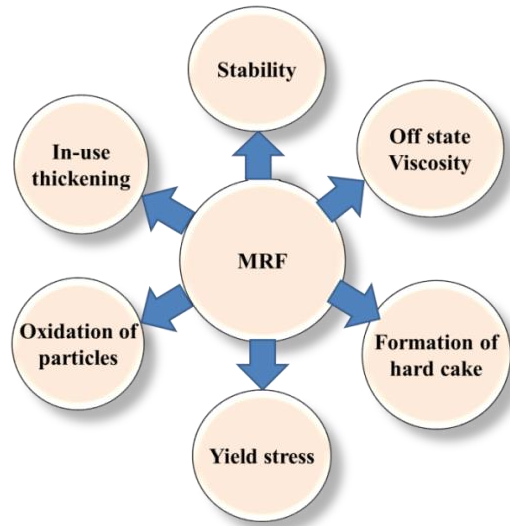
Fig.1.5 Challenges of MRF (Kumar et al. 2019)

The commercial MR fluid manufacturing process differs significantly from laboratory MR fluid mixing. Due to the sophisticated manufacturing process, the price of commercially available MRF is expensive from Lord. Corporation (MRF-132DG $ 816.00 per 1 Litre). Many more applications would become commercially viable very quickly if the material cost of MRFs could be reduced.

Particle oxidation is a chemical reaction that takes place in the presence of air and moisture. This causes rusting of iron particles used in magnetorheological fluids, which can have serious consequences for magnetorheological fluid results such as yield strength and response time.

Han et al., (2015) studied the effects of using corroded iron particles to synthesize magnetorheological fluids, and their output in MR devices was investigated. Shear stress values were found to be very low, and response time was found to be very fast. Another significant challenge of MRFs is their low off-state viscosity in the absence of a magnetic field, which is a critical requirement for MRF device applications. Despite these obstacles, MR technology is increasingly used.

1.5 Magnetic properties of materials

Magnetization (M) is the total magnetic moment of dipoles per unit volume. The magnetization unit is $A.m^2$ per m^3.
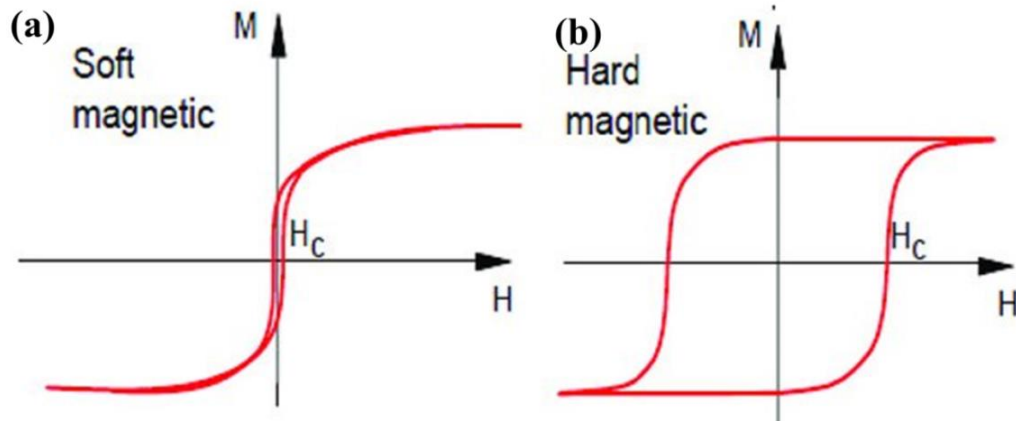
Fig.1.6 Hysteresis curve of soft/hard magnetic materials (Branch and Knudsen 2018)

Magnetic induction, also known as magnetic flux density B, is the flux per unit area expressed in Wb/m^2 or Tesla units (T). The equation (1.6) gives the induction in free space.

$$B = \mu_o H, \tag{1.6}$$

Where, μ_0 is the permeability of free space ($4\pi \times 10^{-7}$ H/m). If space is filled with any magnetic substance in which the induced magnetization is $\mu_0 M$. The MR effect on MR fluid quantitatively depends on dispersed magnetic particle size, subject to the scale of micro and nano as well particle's detail magnetization given in equation (1.7)

$$B = \mu_o(H + M) \tag{1.7}$$

Susceptibility is defined as given by the Eq.(1.8)

$$\chi = \frac{M}{H}. \tag{1.8}$$

The M-H hysteresis curves for ferromagnetic soft and hard magnetic materials are shown in figure 1.6. When the applied magnetic field is zero, remanence is a measure of the remaining magnetization. Coercivity, on the other hand, is a measure of the reverse magnetic field required to drive the magnetization to zero after it has been saturated. Figures 1.6(a) and (b) show the difference in hysteresis loops between soft

and hard magnetic materials in terms of remanence region. Soft and hard magnetic materials, the most important criterion for differentiating between soft and hard magnetic materials, as well as the energy product $B_r H_C$, required to demagnetize the magnetic material, is coercivity, which is defined as the material's resistance to magnetization reversal. Magnetically soft materials have coercivity values less than 50 Oe, while magnetically hard materials have values greater than 100 Oe.

1.8 MRF applications

Potential applications of MRFs are in devices that involve rapid, continuous, and reversible changes in rheological characteristics. Based on MRF characteristics, many devices have been developed. According to their survey, the promising features of MRF technology, such as rapid response, the simple interface between electrical power input and mechanical power output, and even precise controllability, make them the next technology choice for many applications

1.8.1 MR damper working principal

Recently, some small MRF dampers have been developed, RD-1097-01X damper, which is the smallest commercial damper and still has a force of 100N. Figure 1.7 depicts the structure of a traditional MRF damper. Changes in the applied excitation current affect the strength of the magnetic flux density of the electromagnets, which in turn affects the rheological properties of the MR fluid (Wang and Meng 2001). Low off-state viscosity is an important property in these devices. As a result, by modulating the electrical current to the damper, the resistance of the damper can be continuously changed in real-time. The passive dampers are tuned to a specific performance condition and achieve high force only when the stroke velocity is high. In the case of MR suspensions, maximum force can be achieved instantly because they can be continuously adjusted to support various operating conditions. When no force is applied, the gas chamber in the mono-tube damper provides a spring effect to the force generated by the damper and keeps the damper in extended length (Yao et al. 2002). Changes in the applied excitation current affect the strength of the magnetic flux density of the electromagnets, which in turn affects the rheological properties of

10

the MR fluid. The force-displacement and force-velocity curves in Fig. 1.7(b) and (c) show the damping behaviour of the mini-damper, which are nonlinear hysteretic characteristics.
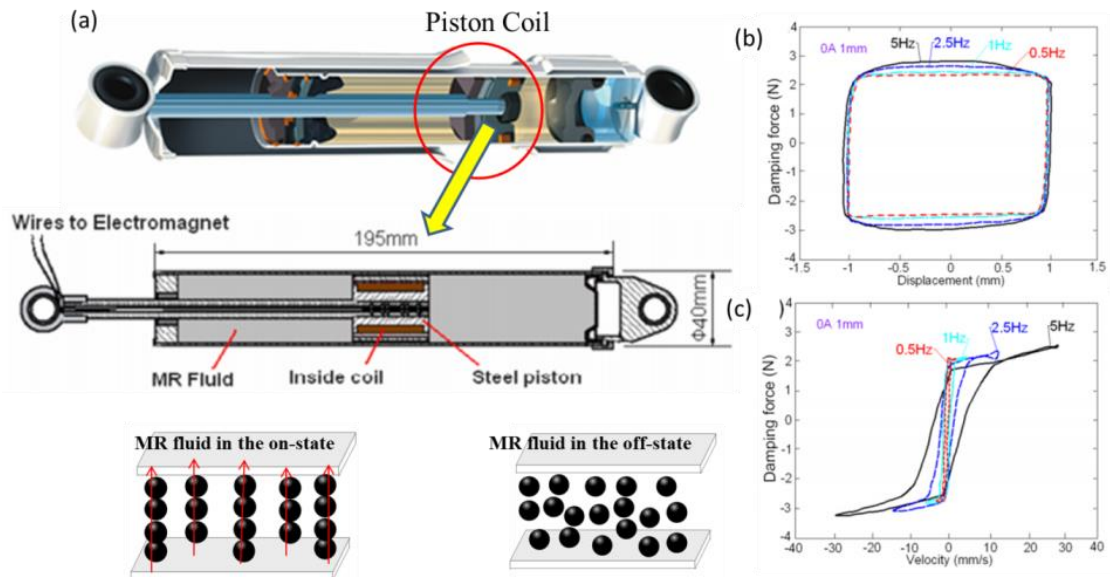
Fig.1.7 (a) MRF damper (b) damping force v/s displacement (c) damping force v/s velocity for different frequencies (Huang et al. 2017)

1.8.2 MR fluid in automobiles, civil structures, and prosthesis applications

The construction of smart and controllable MR linear dampers is one of the most intriguing engineering applications of MR fluid. The main advantage of an MR-based damper is its controllability, which can be adjusted to provide the desired level of damping by simply changing the supply current. An electromagnet is used to create a magnetic field. As shown in Fig.1.8, MR dampers are widely used in vehicle suspension systems to improve ride comfort and stability. By varying the viscosity of the MR Fluid, a controlled set of algorithms improves the shock-absorbing capacity of suspension (Yao et al. 2002). As shown in Fig. 1.8, the results show a significant reduction in vibrations of the bridge structure. The MR Dampers can be used as seismic dampers, operating at the building's resonance frequency and absorbing shock waves and oscillations that can cause harm within the structure. They are also used to avoid the seismic activity depicted in Fig. 1.8(c). As a result, the dampers can make

any building earthquake-proof. The MR Dampers can be used in the prosthetic knee to provide quick shock absorption and give the user the sensation of walking on natural feet (Dyke et al. 1998).
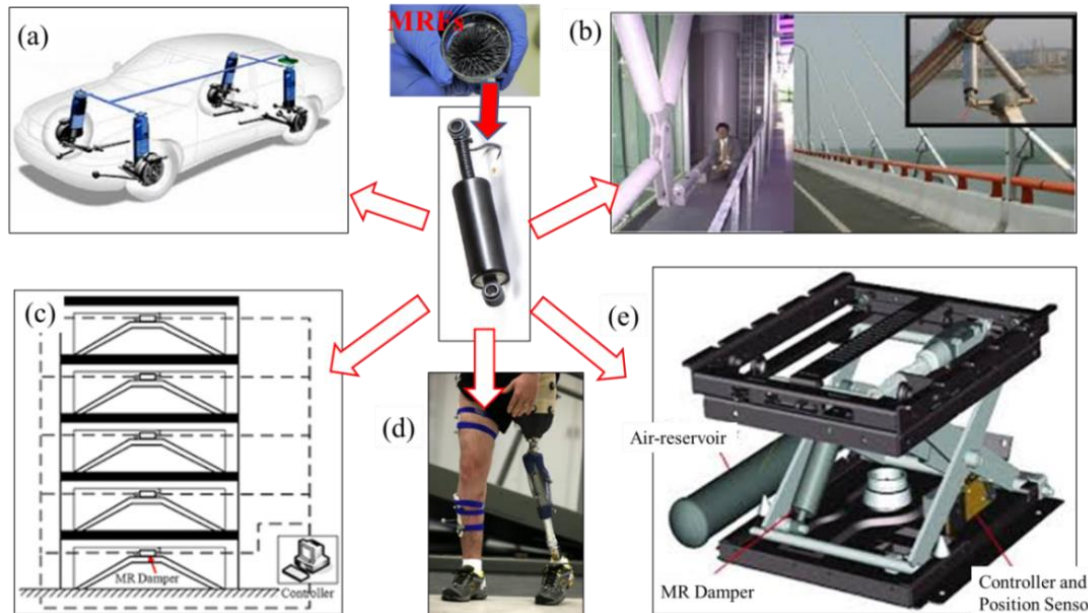
Fig.1.8 MR damper applications in (a) vehicle suspensions (b) cable-stayed Bridges (c) civil buildings (d) human prosthetic leg (e) lord's seat suspension system

Figure 1.8(d) depicts a prosthetic leg with an MRF damper that reduces the shock delivered by the patient's leg during jumping. As a result, the patient's mobility and agility will improve. A small magneto rheological fluid damper is used in such systems to control the motion of an artificial limb in real-time based on inputs from a group of sensors (Gao et al. 2017). This is accomplished by employing a small MR fluid damper to absorb the shocks caused by the motion of a prosthetic knee, as shown in Fig.1.8(d) Ride quality in heavy-duty dump truck or tractor is not only a comfort issue but also a health and safety issue for the operator. Fig.1.8(e) shows the seat suspension system consists of an MR damper that can control vibration.

1.8.3 MRFs in haptic, polishing, and automobile applications
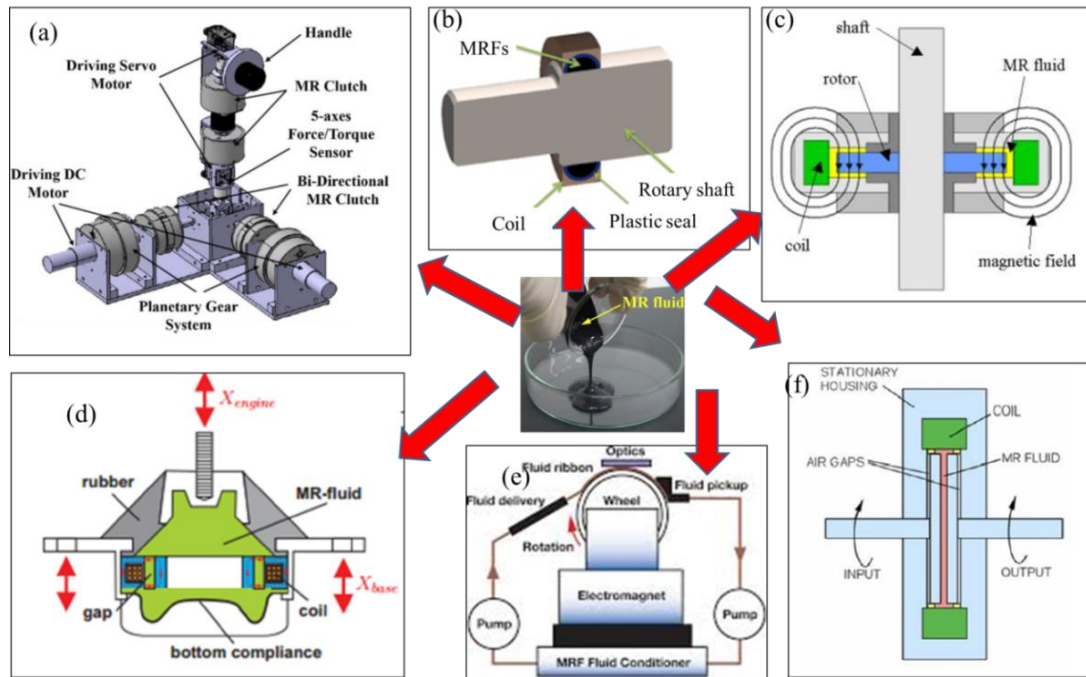
Fig.1.9 Schematic of (a) haptic devices (b) MR fluid seal (c) MR brake (d) MR engine mount (e) MR polishing devices (f) MRF clutch

The schematic diagram of the system's haptic devices is shown in Fig. 1.9 for the study of the coupling of the human sense of touch and a computer-generated environment. Haptics is a tactile feedback technology that simulates the user's sense of touch by using forces, vibrations, or motions. To generate a sufficient sense of touch to human skin, haptic devices should have high performance in their output characteristics, such as low friction in off-state, the constant force with constant input, and quick response with dynamic input. The MR seal was formed by controlling the viscosity of the MR fluid confined by a magnetic field in the working gaps between mating parts with the same structure as the Ferro-fluid seal, as shown in Fig. 1.9(b). The seal's characteristics are as follows: simplicity in structure, provision of high sealing, lack of wear of mating parts, and ease of maintenance (Kordonski and Gorodkin 1996). Recently, MR brakes have been investigated as an alternative to conventional hydraulic brakes for road vehicle applications. The torque transmissibility of an MR brake is heavily influenced by MR fluid properties such as

dynamic yield stress and viscosity (Kumbhar et al. 2015). Magneto-rheological (MR) mount for a cabin of heavy equipment vehicles were designed for improving vibration isolation in both low and high-frequency domains (Zhang et al. 2011). The mounts shown in Fig. 1.9(d) operate similarly to a hydraulic mount except that while the fluid moves between the mount chambers, its viscosity can be changed by applying a magnetic/electric field across the passages connecting the chambers (Hong and Choi 2005). Magnetorheological (MR) polishing achieves precise control of polishing forces by utilizing the rheological properties of an MR polishing fluid in the presence of a magnetic field. An MR polishing fluid is transformed into a stiffened fluid ribbon that serves as the polishing tool during the MR polishing process. MR effect polishing, also known as magnetorheological finishing, is a new magnetic-assisted hydrodynamic polishing method shown in Fig.1.9(e). This polishing is commonly used on optical glasses, ceramics, plastics, and some nonmagnetic materials (Singh et al. 2015). As shown in Fig. 1.9(f), an MR clutch consists of a driving shaft, a driven shaft, two parallel transmission disks, namely a driving disk, a driven disk, a coil, and MR fluid filled in the working gap between the two disks (Shafer and Kermani 2011).

1.9 Magnetic flux density (B) versus H curve relationships
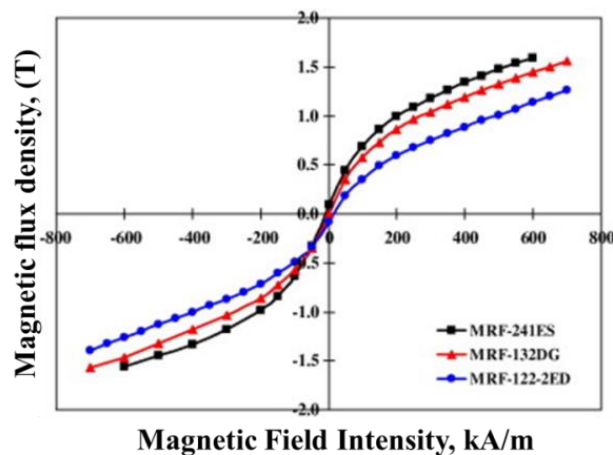
Fig.1.10 Typical magnetic properties of tested MRFs (Purandare et al. 2019)

The static magnetic properties of MRFs, which can be characterized by B-H and M-H hysteresis, are important in the design of any MRF-based device. The magnetic flux

density (B) is proportional to the applied field (F). As a result, the B-H curve for an MRFs suspension is depicted in Fig. 1.10. A vibrating sample magnetometer (VSM) can measure hysteresis loops in a maximum field of 1.25 T, while a Quantum Design MPMS-2 magnetic-property measurement system equipped with a superconducting magnet can measure them in a maximum field of 5 T.Fig.1.10 depicts the magnetic flux density versus magnetic field intensity of commercially available tested MR fluids. Up to 200 kA/m of applied field intensity, MRFs have approximately linear magnetic properties. The magnetic flux density of MRF-241ES is higher than that of the other MR fluids. The magnetic properties of MRFs differ significantly because MRF-241ES (3.80–3.92 g/cm^3) has a higher particle density than MRF-132DG (2.98–3.18 g/cm^3) and MRF-122-2ED (2.32–2.44 g/cm3) (Mazlan et al. 2009).

1.10 Shear yield stress and magnetic field strength relation
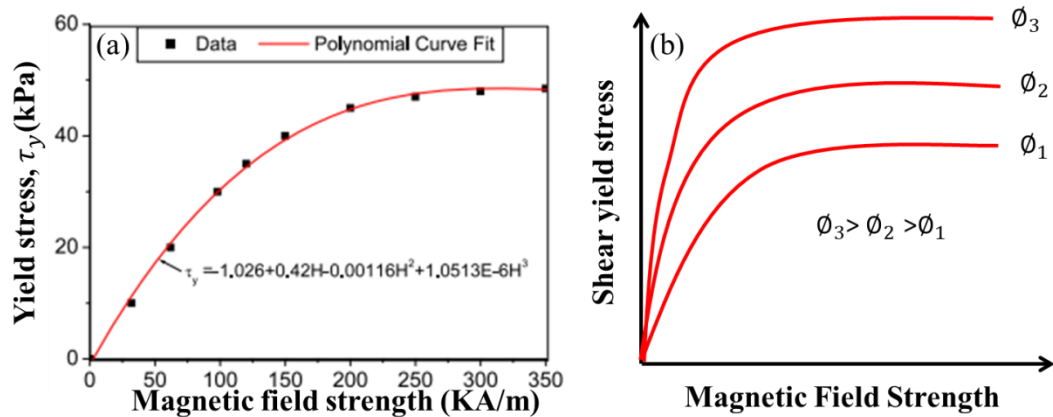
Fig.1.11 (a) Yield stress v/s magnetic field strength (b) shear yield stress v/s magnetic field strength at different volume fractions

The shear stress yield, which is the maximum stress that the fluid can withstand before beginning to flow, is the most important parameter for MR fluids. Taking into account how MRFs change their properties as the magnetic field strength changes, a constitutive model for shear yield stress was developed, consisting of expressions that relate to the volume fraction, magnetic field strength, and particle materials. The saturation shear yield stress occurs when the shear yield stress of a magnetic field becomes constant due to particle alignment. As per Ginder et al., (1996) microscopic

model is given in equation (1.9), for yield stress calculations concerned with the details of forces between interacting particles.

$$\tau_y = C.271700.\emptyset^{C_3} \tanh (C_4 \times 10^{-6}H) \tag{1.9}$$

While (Weiss et al. 1994) macroscopic model, suggests a linear dependency on solid loading and a sub quadratic field dependency, shown in equation (1.10) for the yield stress calculation

$$\tau_{y_s} = C_5.\varphi.\mu_0 H^{C_6}M_s^{1-C_6} , \tag{1.10}$$

where M_s is the saturation magnetization for the MR fluid, and φ represents iron volume fraction. In MR fluid design, this value is fundamental since it is directly related to the maximum power that can be dissipated by an MR instrument. One potential way to increase the yield stress of MR fluids is to choose a material with a greater magnetic saturation (Jolly et al. 1996)

The induced yield stress of the MRFs as a function of the applied magnetic field intensity is shown in Fig. 1.11(a). (Nguyen et al. 2014b) et al given the least square curve fitting method, the yield stress of the MR fluid was approximately expressed by

$$\tau_y = C_O + C_1H + C_2H^2 + C_3H^3 \tag{1.11}$$

In equation (1.11), the unit of the yield stress (τ_y) is kPa, while that of the magnetic field intensity (H) is kA m^{-1}. The coefficients C_0, C_1, C_2, and C_3 are respectively identified as 0.3, 0.42, −0.001 16, and 1.0513×10^{-6}.

(Si et al. 2008) described the model to calculate yield stress in terms of magnetic field intensity, particle size, and iron particle volume fraction. The model is illustrated in Fig. 1.12, where h denotes the gap between the two plates, τ_0 is the shear yield stress per unit area, and F_a is the external force applied to the upper plate in the lateral direction. The bottom plate is held stationary.The applied magnetic field in an upward direction. The analysis showed that the yield stress of MR fluid under that

$$\tau_o = F_a sin\theta_\alpha \tag{1.12}$$

where θ_α is the angle between the centerline of the chain and these conditions can be given as

16
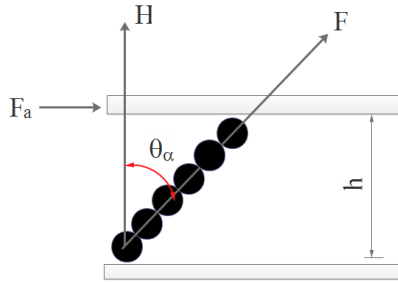
Fig 1.12 Shear yield stress

$$\tau_0(H) = \sum_{n=1}^{K_P} \frac{\mu_O}{12n^2} \frac{r\emptyset_v(\mu_{mr}-1)^2 H^2}{(2r+\delta_p)} \sin\theta_a \cos\theta_a . \qquad (1.13)$$

Where μ_{mr}—relative permeability of the MR fluid, $\mu_{mr} = 1 + \kappa v$, K_v— susceptibility, K_P—average number of particles in each chain, and kp = A_{fh}/V_sN_s, A_f—flat plate area, V_s—average volume of solid particles, N_s-number of chains in a unit area.

1.11 MRF common operational modes

There are three modes of MRF operation depending on the fluid flow and rheological stress. MR devices can also be used in a combination of these modes. In many applications, the three most common modes of operation for MR fluids are flow mode, shear mode, and squeeze flow mode.
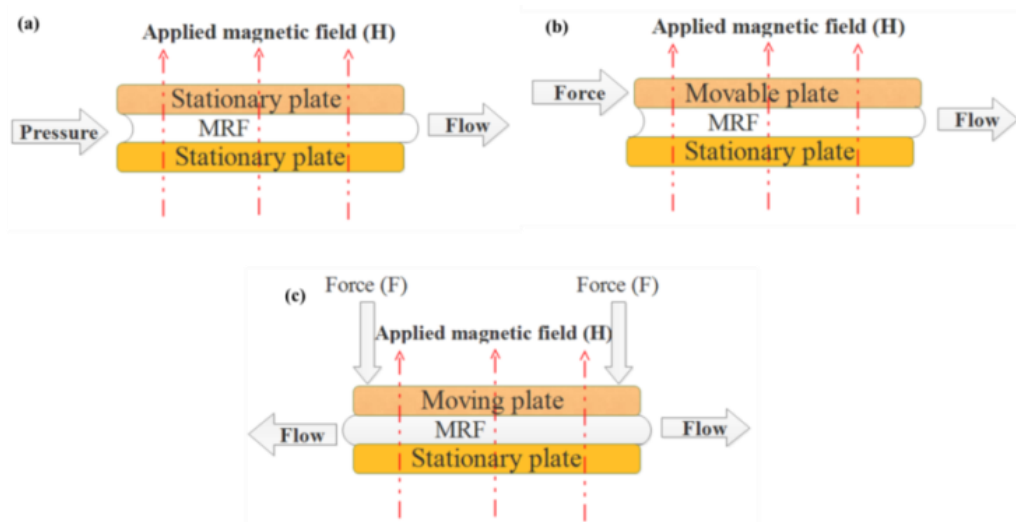
Fig.1.13 The concept of basic operational modes of MR fluids (a) flow mode, (b) shear mode, and (c) squeeze mode.

17

The first mode is flow or valve mode, in which the fluid is passed between two stationary elements, with the magnetic flux flowing perpendicular to the flow of the fluid from one element to the other, as shown in Fig. 1.13. (a).The valve mode as an operational mode is used in dampers or shock absorbers. The pressure drop created in this mode e.g. in a damper is the sum of the viscous (pure rheological) component (ΔP_r) and the magnetic field dependent (magneto-rheological) component (ΔP_{mr}). The value of this pressure drop is defined using the following approximation equation (1.14) (SUNG et al. 2005).

$$\Delta P = \Delta P_r + \Delta P_{mr} = \frac{12\eta QL}{g^3 w} + \frac{f\tau_{mr}L}{g}. \tag{1.14}$$

In this equation, (Pa s) represents dynamic viscosity, Q (m³/s) is the flow rate, and L, w, g (m) represents the flow channel's geometric length, width, and gap size. Direct shear mode is shown in Fig. 1.13 (b). The two magnetic poles move relative to each other in this mode, and the MR fluid is sheared between them. A layer of MR fluid is squeezed between the two magnetic poles in squeeze-film mode. When two magnetic pole plates move relative to each other, the magneto-rheological fluid between them is sheared. The magneto-rheological (MR) fluid is sandwiched between two moving paramagnetic surfaces. The MR fluid is in a shear mode in this case. One of the drawbacks of an MR fluid in shear mode is that it has weak interactions between magnetic particles when their chains are strained by an external force. In the shear mode, the connection total force can be divided into a viscous (pure rheological) component F_r and a magnetic field dependent (magneto-rheological) component F_{mr}. Equation 1.15 is used to calculate the total shear force (Boelter and Janocha 1997). Figure 1.13 depicts the direct shear mode, which is used in brakes and clutches (b).

$$F = F_r + F_{mr} = \frac{\eta SA}{g} + \tau A \tag{1.15}$$

In equation (1.15), η (Pa s) represents the dynamic viscosity, S (m/s) represents the relative speed, A = the working interface area, and g = gap size of the flow channel (in meter). In the magnetic field dependent component F_{mr} (N/mm²) is the yield stress developed in response to the applied magnetic field.

When MR fluid is subjected to an external magnetic field between two parallel surfaces, it enters squeeze mode. One surface is fixed, while the other can only move in the direction of the magnetic field (Sapiński and Gołdasz 2015). As a result, this mode is typically used for low-motion, high-force applications. There are two types of squeeze modes: compression and tension. In the squeeze mode, the total amount of force is estimated by

$$F_s = \frac{\pi r^4}{4} \left(\frac{6\mu\dot{h}}{h^3} + \frac{3\rho\ddot{h}}{5h} - \frac{15\rho\dot{h}^2}{14h^2} \right) \qquad (1.16)$$

where and $r, \mu\ \dot{h}, \rho\ \ddot{h}, h$ are the plate radius, the distance between the two parallel plates, the viscosity of the MRF, the gap acceleration, the gap speed, and the density of the MRF, respectively.

1.12 Outline of the thesis

The thesis has been presented in 9 chapters:

Chapter 1 outlines the introduction to MRFs, properties of MRFs critical factors of MRFs, MRFs operational modes and applications of MRF.

Chapter 2 describes the detailed review of the published literature relevant to the present study. The literature review presented mainly includes earlier research work carried out on the development of MR fluids stabilization methods such as surface modification, additives added, Nano-particles, high-density carrier fluid, and different types of magnetic particles are discussed. The research gap, motivation, and objectives of the present research work are discussed.

Chapter 3 describes materials used for synthesizing MRFs, fabrication of mono-tube MR damper, and proper dispersion mechanism of additive are discussed. In addition to that, various characterization techniques such as analysis of morphology, saturation properties, sedimentation, surface tension, chemical compositions, and rheological characteristics are discussed.

Chapter 4 In this chapter, the effects of additives on the synthesis of carbonyl iron suspension on the rheological and sedimentation characteristics of magnetorheological (MR) fluids are discussed.

Chapter 5 In this chapter, the preparation of MRFs, morphology, damping force properties using an MR damper, sedimentation quality characteristics, magnetization saturation studies, and rheological property characteristics are all discussed.

Chapter 6 outlines the various fumed silica as a thixotropic additive on carbonyl magnetorheological fluids for sedimentation effects rheological properties characteristics are discussed in

Chapter 7 explains the sedimentation and rheological properties using various carrier fluids are outlined.

Chapter 8 describes the effect of varying percentages of Mn-Zn ferrites particles based on MRF were discussed.

Chapter 9 presents the conclusions reached based on the findings of this research project, as well as prospects.

CHAPTER-2

LITERATURE REVIEW

This chapter presents a detailed literature review of published research articles related to MRFs. This chapter provides a review of the literature on MRF preparation, MRF constituents, sedimentation techniques, and MRF rheological properties. As a result, understanding the properties of MRFs is critical for applying them to real-world applications of MRFs devices such as MR prosthetic knees and MR dampers.

2.1 Constituents of MRFs

An MRF typically consists of three main constituents: base fluid, magnetizable particles, and a stabilizer to reduce magnetic particle settling. The base fluid functions as a carrier medium for magnetic particles. Petroleum-based oils, mineral oils, rubber, polyester, polyether, water, and synthetic hydrocarbon oils are commonly used as base oils in the preparation of MRFs (Ashtiani et al. 2015). This is a medium in which magnetic particles are dispersed to prepare the MRFs. Figure 2.1 shows the flow chart of MRF constituents.
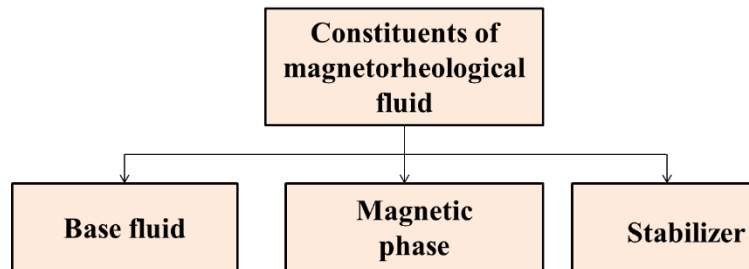
Fig.2.1 Constituents of MRF fluid

2.1.1 Liquid phase

The base fluid, which can be either polar or non-polar, is usually chosen for its rheological properties and temperature stability. Other factors to considered while choosing a base fluid include magnetic particle compatibility, chemical stability, surface tension, and so on. Another important feature of the carrier fluid in MRFs is its low vapor pressure, because it is not necessarily vaporized and can thus be used at

a wide range of temperatures. The carrier liquid's viscosity should be appropriate, which means that when the magnetic field is zero, it should have less viscosity, and provides better MRF characteristics. The sedimentation increases as the viscosity decreases. The fact that the MR fluid has a low cooling point and a high-temperature point confirm that it has a high working temperature with different operating ranges. A low viscosity carrier fluid should be used in MRFs. It should also include other critical characteristics for operating temperatures and particle redistribution (Charles 2002). One of the most important characteristics of the continuous process of MRFs is viscosity.

2.1.2 Dispersed phase

Many metals, alloys, and ferrite-based magnetic particles can be used as magnetic phases in the fabrication of MRFs. Because of their high magnetic permeability and saturation magnetization, ferromagnetic binary alloys appear to be another option for MR fluids. Among magnetic alloys, FeCo, FeNi, and Nico are the most commonly tested in both bulk and nano forms. Some of the most commonly used magnetic particles are ferrite-particles, iron-cobalt alloy, and carbonyl iron.As previously stated, the magnetic particle which is most commonly used in MRF preparation is a high purity iron powder known as carbonyl iron particles (ρ=7.91 g/cm^3), which was chosen for its high saturation magnetization of 2.1 Tesla and availability of various particle sizes (average particle size: 1-10 μm). Carbonyl iron particles (CIPs) are free-flowing powders which are manufactured in large quantities by BASF through the thermal decomposition of liquid Fe(CO)$_5$. The reagent is produced as uniform spherical particles suitable for direct use as a result of this process.

$$\text{Fe}(\text{Co}_5) \rightarrow Fe(s) + 5Co \uparrow (g) \qquad (2.1)$$
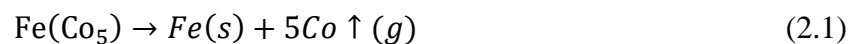
2.1.3   Stabilizers

To prevent magnetic particle sedimentation in MR fluids, various methods, such as polymer coating on magnetic particles to reduce the mismatch dispersed phase and continuous phase are used. The use of additives such as thixotropic agents, surfactants, or fillers that can intercept magnetic particle physical contact is another technique identified by the researchers. Section 2.2 discusses the detailed study of sedimentation methods.

2.1.4 General preparation of MRFs

MRFs are made up of two components: solid phase and liquid phase. The solid phase is added to the liquid phase and thoroughly mixed for a set amount of time. The resulting mixture is then left undisturbed to observe the magnetic particle settling characteristics. The preparation method and materials used in MRFs are shown in Table 2.1. MR fluids containing magnetic particles must, in general, have a high saturation magnetization and a low coercivity/remnant magnetization, as well as be resistant to settling, irreversible flocculation, and chemical degradation/oxidation.

Table 2.1 Preparation method of MRFs

Magnetic/dispersed phase	Method of preparation	Stabilizers used	Ref
Carbonyl iron/ lubricant oil	Mechanical Stirring	CI nanoparticle	(Kim et al. 2012a)
Carbonyl iron particles/ silicon oil	Mechanical Stirring at 1000 rpm	cellulose nanoparticles	(Rabbani et al. 2019)
$Fe_{78}Si_9B_{13}$ particles/ silicon oil	Mechanical stirring and supersonic dispersion for 1.5 h	Na	(Yu et al. 2016)
Iron powder/Silicone oil	Mechanical stirrer at 400 rpm in room temperature	Grease	(Premalatha et al. 2012)

2.2 Sedimentation in MRFs

Sedimentation caused by density differences between magnetic particles and carrier fluids is a major challenge in MRFs. The MRF experiences phase separation due to the large gravity difference between dispersed phase density (7.5 g/cm3) and carrier fluid density (1 g/cm3). The effect of sedimentation on MRF is shown in Fig 2.2 (a): on the left, a homogeneous MRF before sedimentation; on the right, the fluid after

sedimentation with an obvious sedimentation layer at room temperature. Fig 2.2(b) shows the position changes of the boundary between a clear and turbid portion of carrier oil (Bell et al. 2008)..
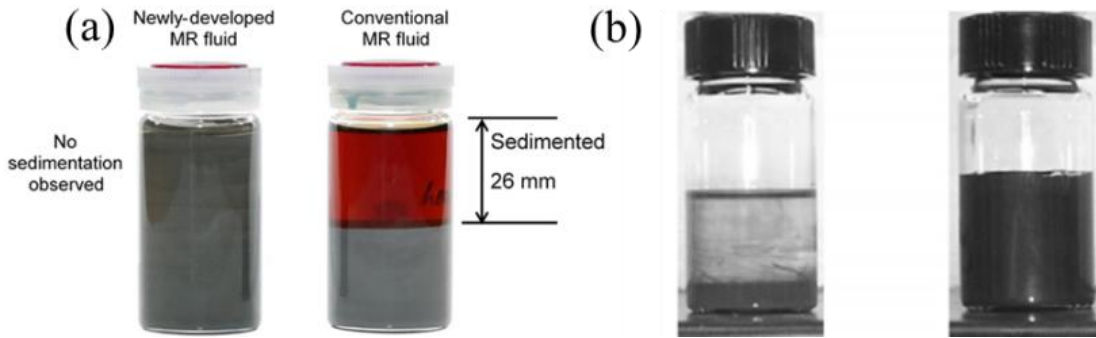
Fig.2.2(a)The conventional MRF (New Energy and Industrial Technology Development Organization) (b) Iron particles dispersed in silicone oil along with micro wires

Sedimentation rate is calculated using the general equation given (2.2)

$$\text{Sedimentation rate (\%)} = \frac{b}{a+b} \times 100 \qquad (2.2)$$

Where: a - the length of the clear fluid, b - the length of the turbid fluid.

The general sedimentation stokes law predicts that a decrease in particle-fluid density mismatch reduces particle sedimentation velocity. The general sedimentation law is described by the equation (Wang et al. 2017a)

$$V(\phi, d) = \frac{|\rho_p - \rho_c| \times g \times d^2}{18 \times v \times \rho_c} \frac{[1-\emptyset]}{\left[1 + \frac{4.6\emptyset}{(1-\emptyset)^3}\right]}. \qquad (2.3)$$

Where V represents the particle migration velocity (m s^{-1}), ρ_p is the particle density (kg m^{-3}), ρ_c indicates the continuous phase density (kg m^{-3}), v designates the kinematic viscosity of continuous phase, g is gravitational acceleration (9.81 m/s^2), d represents for the particle diameter, and ϕ represents the volume fraction.
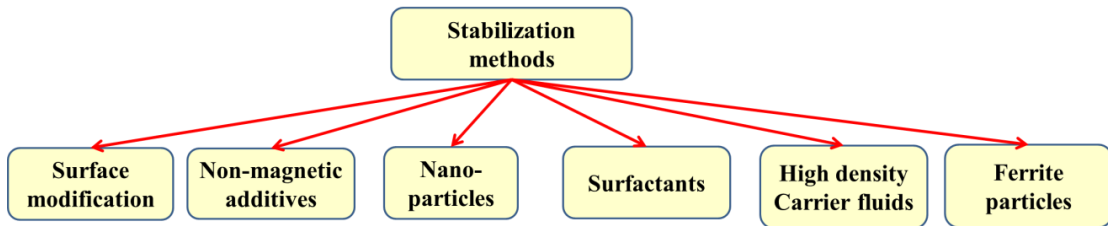
Fig.2.3 Method to address sedimentation problem in MRF

Various methods used to address the stabilization are shown in Fig.2.3. Researchers have identified six major methods for reducing sedimentation they are: surface modification of magnetic particles, Non-magnetic additives, nano-particles, Surfactants, and high-density carrier fluids.

2.2.1 Non–magnetic additives

Many techniques have been developed to mitigate the sedimentation issue of MRFs, with the use of additives being one of the simplest. The effects of additives on the stability of MRFs will be discussed in detail in this section.
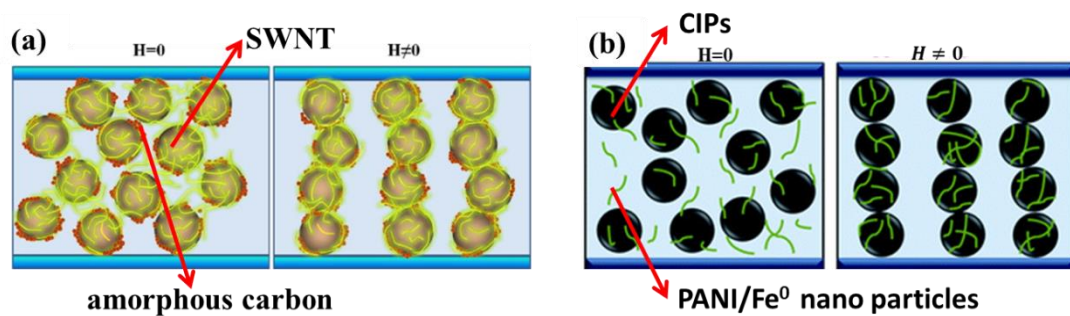
Fig.2.4 (a) Supposed morphology of SWCNT additives added MRFs (Fang et al. 2009). (b) PANI/Fe^0 additive CIPs based MRF with and without magnetic field (Piao et al. 2015).

Red dots and yellow lines in Fig. 2.4(a) represent amorphous carbon and SWNT, respectively. When the magnetic field is absent, nano-scaled amorphous carbon and SWNT dispersed in CIPs suspension are randomly adhered to the surface of CI particles, preventing CIPs from coming into direct contact. When an external shear field is applied, these additives-wrapped CIPs may exhibit flocculation due to SWNT entanglement among adjacent CIPs (Fang et al. 2009).

25
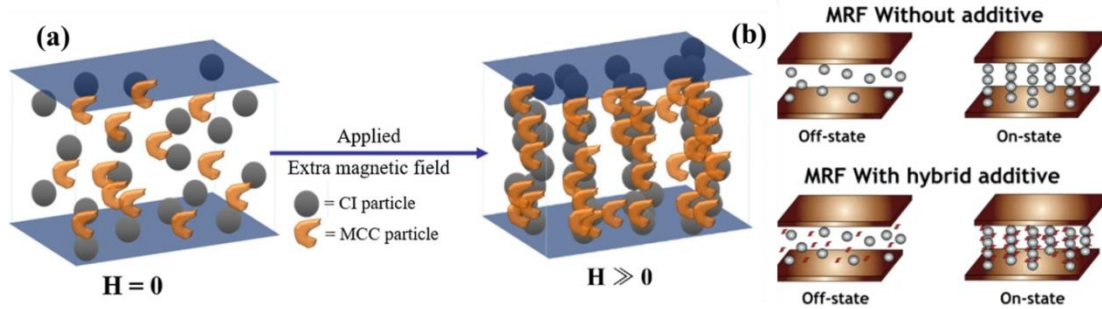
Fig.2.5 (a) Microcrystalline cellulose added CIPs MRFs (Bae et al. 2017) (b) magnetic hybrid additives added MRF with and without magnetic field (Manzoor et al. 2018)

Many different additives have been used to stabilize or improve the performance of MRFs to date, but their efficiency ranking is still lacking. To create effective MRFs, it is necessary to investigate the overall effects of the additives on their complex behavior. The most important criterion for additive selection is compatibility with the carrier matrix, which must be determined even before determining the amount of additive to be used in specific MR fluids.

Among these additives, sub-micron-sized particles have attracted the interest of researchers because they can significantly reduce particle sedimentation by occupying the interspaces of magnetic particles, as shown in Fig. 2.5.(a). In the absence of a magnetic field, however, microcrystalline cellulose can prevent direct contact between the CIPs. (Bae et al. 2017). Fig.2.5(b) shows the MRF without and with hybrid additives such as molybdenum disulfide (MoS_2), graphene-oxide, Fe-rGO-MoS_2, and non-magnetic rGO-MoS_2 that play a significant role in improving yield and sedimentation by application of magnetic field (Manzoor et al.2018).

Lim et al. (2004) discussed the CIPs based MRFs with the addition of fumed silica to enhance the re-dispersibility of MR fluid. The fumed silica fills the interspace between the particles which might help in the formation of chain-like structure and found that adding a specific amount of fumed silica to the MRFs was considerably successful in preventing sedimentation of CIPs shown in Fig. 2.6(i) and 2.6(iii). The shear stress and shear viscosity higher values with magnetic field as shown in Fig. 2.6(ii)
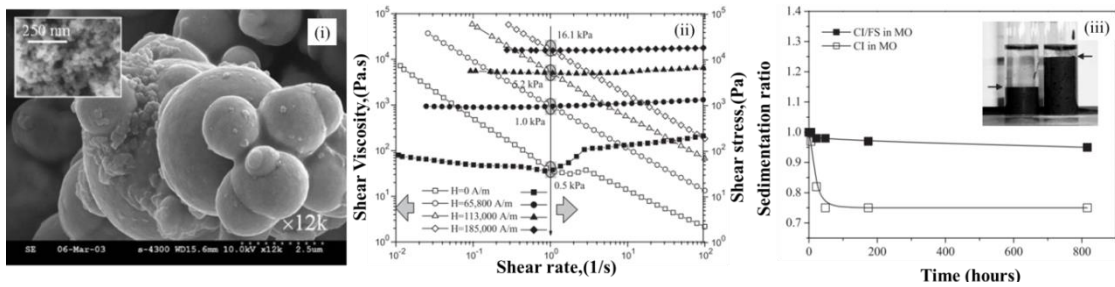
Fig.2.6 (i) SEM image of CI and fumed silica (FS) mixture (ii) shear viscosity and shear stress as a function of shear rate (iii) changes of sedimentation ratio with time

Chae et al. (2015) discussed the sepiolite, a fibrous clay mineral (0.1wt.%) that was added to a mineral oil along with carbonyl iron (CI) (70 wt. %.) and particle-based MRFs was prepared. When the external magnetic field was present, both MRFs (with and without clay MRF) exhibited a Bingham behaviour with non-vanishing yield stress under the magnetic field. The dispersion stability of CI/sepiolite suspensions was better than that of pure CI MRFs.
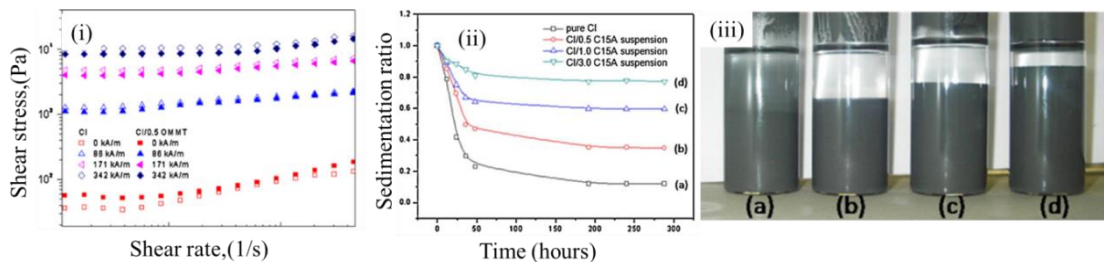
Fig.2.7 (i) shear stress versus shear rate (ii) sedimentation ratio versus Time (iii) Images of sedimentation after settling of particles.

In a successful research, Hong et al. (2013) prepared the 70wt.% concentration of CIPs, with 1.0 wt. % and without halloysite additive added in MRFs. On the other hand, these additive particles prevented the hard caking of magnetic particles in the MRFs suspension. The dispersion stability of CI/halloysite was superior to that of pure CI MRFs. The flow curves measured from a rotational rheometer revealed non-Newtonian Bingham fluid behaviour under an applied magnetic field.

In another study, Hato et al. (2011) studied the effect of adding submicron organoclays to an MRF based on CIPs and noticed that the addition of up to 1 wt.% organoclays improved redistribution and stability of the suspension. Fig.2.7(i) shows the shear stress at different applied magnetic field strength, and the pure CIPs based

MRFs shows larger shear stress than the additive added MRF. As can be seen from Fig.2.7(ii) the sedimentation rate showed a considerable reduction with the addition of different weight percentages of organo-clay additives.

In a similar research, Lim et al., (2005), employed sub-micron sized organoclays to stabilize an MRF containing carbonyl iron particles. It was observed that the addition of organoclay without much change in the MR effect improved the stability of the MRFs. A descending trend for yield stress was reported at first which was later changed to an ascending trend by increasing the magnetic field.

The yield stress as a function of magnetic field strength for two different regions of low and high field can be obtained by using the universal yield stress equation (Morillas and de Vicente 2019). A general universal relationship dependence on $\hat{\tau}$ and H_0 was introduced in the previous study as given below (Kim et al. 2012b)

$$\hat{\tau}(H_0) = \alpha {H_O}^2 \left(\frac{tan\sqrt{H_0/H_C}}{\sqrt{H_0/H_C}} \right) \tag{2.4}$$

$$\hat{\tau}(H_0) = \alpha {H_O}^{\frac{3}{2}} {H_c}^{\frac{1}{2}} \, tanh \left(\sqrt{\frac{H_O}{H_C}} \right). \tag{2.5}$$

Where α is associated with the susceptibility of the fluid regarding the volume fraction of magnetic particles. In this case, the critical magnetic field strength is located between two regimes as given by the following equation

$$\tau_Y = \alpha {H_0}^2 \quad H_O << H_C \tag{2.6}$$

$$\tau_Y = \alpha \sqrt{H_C {H_O}^{3/2}} \, , \text{ for } H_O >> H_C \tag{2.7}$$

$\tau_{Y,}$ possesses two limiting behaviours around a critical magnetic field strength H_C concerning H_0, Eqn. (2.6) indicates that τ_Y is proportional to ${H_0}^2$ at low magnetic field strength and Eqn (2.7) indicates that τ_Y is proportional to ${H_O}^{3/2}$ when the H_0 exceeds H_C at high magnetic field strength.

Bae et al. (2017) demonstrated about the microcrystalline cellulose (MCC) particles, fabricated from rice husk, which were introduced as an additive to CI-based MRFs.

The rheological properties of MR fluids with and without MCC additive were compared under an external magnetic field using a rotational rheometer. Although the MR property of CI/MCC-based MR fluid decreased slightly due to the addition of MCC, while a reduction in sedimentation rate was observed.

Cvek et al., (2018) studied the addition of carbon allotropes (fullerene powder, carbon nanotubes, graphene nano platelets) to the carbonyl iron-based MRF (60% weight fraction CIP) to examine their effects on stability. The results showed that carbon nanotubes had the highest stabilization effect. The measured sedimentation ratio was about 20% after 100 h.

Manzoor et al. (2018) discussed the hybrid rGO-MoS_2 additives for high-performance MRFs.Two different kinds of hybrid additives; non-magnetic rGO-MoS_2 and magnetic Fe-rGO-MoS_2, were synthesized by using a hydrothermal method. The rGO-MoS_2 added suspensions remained stable for the first 90 min whereas the CIP MRFs settled down quickly (65%) in the first 10 minutes. There was an increase in the shear stress and yield stress after the addition of additives.

Wu et al. (2006) used guar-gum to generate cell-type structures in silicone oil. Upon the application of a magnetic field, the iron microparticles line up along the field lines and the cells underwent distortion. The optimum amount of guar gum was 3wt. % of the amount of the iron powders, which led to an MR fluid with yield stress (i.e.52.5 kPa at 0.4 T) and zero-field viscosity (i.e.0.70 Pa.s) at a shear rate of 100 s^{-1} and the MRFs showed only 2–3% sedimentation after 3 months period.

Chae et al. (2015) used attapulgite (ATP) fibrous nano clay mineral adopted as an additive in soft magnetic carbonyl iron (CI)-based MRFs. Two different types of MRFs prepared with same particle concentration of CI at 70 wt. % with one having the 0.1 wt. % of ATP additive. Fig.2.8 (a) and (b) show the shear stress of the CIPs based MRFs showing higher shear stress and shear viscosity values than the ATP mixtures-based MRFs and behave like non-Newtanion type. The sedimentation test showed that the addition of ATP additive improved the sedimentation time of CIPs in carrier fluid as shown in Fig.2.8(c).
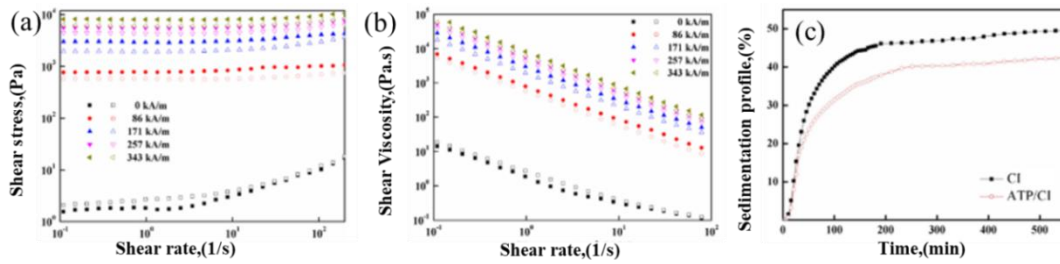
Fig.2.8 (a) shear stress (b) shear viscosity v/s shear rate (c) sedimentation profile for CIPs and ATP additive MRFs

Piao et al. (2015) proposed a Fe^0 nanoparticle-supported polyaniline (PANI/ Fe^0) composite nano-fibers additive for CIPs/mineral oil based MRFs and dispersed in mineral oil. The results showed that the sedimentation rate reduced while the MR properties were enhanced with the addition of additives. Fig.2.9 shows the shear stress, shear viscosity, and sedimentation profile curves. They observed that the addition of Fe^0- PANI nano-clay additives without much change in the MR effect improved the stability of the MRFs.
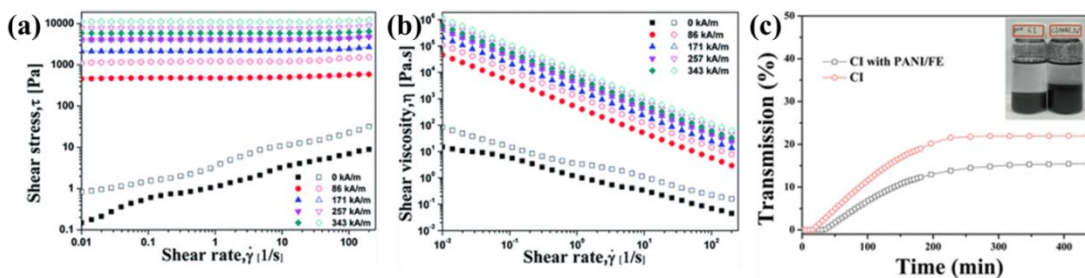
Fig 2.9 (a) shear stress (b) shear viscosity versus shear rate (c) Sedimentation profile PANI/ Fe^0 based MRFs

The incorporation of additives into MRFs is a well-known method of improving MRF performance and stability. This method is simple effective, and it does not require any special or toxic chemicals, which appears to be beneficial from an environmental standpoint. Because of their large surface areas and nano-scaled dimensions, they have triggered a lot of interest in nanotechnology. Table 2.2 provides a list of the additives and their intended use.

Table 2.2 Summary of various additives in MRFs

Sl no	Carrier fluid	Particle type (size μm)	Type and % of additive	Sedimentation time and sedimentation ratio.	Rheological studies details			
					Shear stress (Pa)	Shear viscosity (Pa.s)	Magnetic field strength kA/m	Reference
1	Mineral oil	CIPs 4.65μm (70 wt.%)	Attapulgite 0.1 wt.%	0 to 500 minutes CIPs based MRF- 50%, CIPs/ATP mixture MRF- 40 %	10^0-10^4	10^1-10^5	0-343	(Piao et al. 2015)
2	silicone oil	CIPs 4.25 μm, (70 wt.%)	Halloysite 1.0 wt.%	0 to 6 hours CIPs based MRF- 80%, CIPs/Halloysite MRF- 61 %	10^1-10^4	10^2-10^5	0-342	Liu et al. 2013
4	Mineral oil	CIPs 7 μm (70 wt.%)	Sepiolite 0. 1 wt%	0 to 300 minutes CIPs based MRF- 70%, CIPs/Halloysite MRF- 68 %	10^{-1}-10^4	10^1-10^6	0-343	(Plachý et al. 2019)
7	Mineral oil	CIPs 4.5–5.2 μm (80wt.%)	Fumed silica 3wt%	0 to 800 hours CIPs based MRFs-75% CIPs/Fumed silica MRFs-99%	10^1-10^4	10^2-10^5	0-185	(Lim et al. 2004)
8	Mineral oil	CIPs 4.5–5.2 μm (70 wt%)	Microcrystalline cellulose (0.1 wt%)	0 to 400 minutes CIPs based MRFs-80% CIPs/MC mixtures-78%	10^0-10^4	10^1-10^5	0-343	(Choi et al. 2017)
9	lubricant oil	CIPs 4.25 μm (25 wt.%)	Organoclay (0.5-3.0 wt.%)	0 to 300 hours CIPs based MRFs-20% CIPs/ 3wt%. Organoclay-90%	10^2-10^4	10^2-10^4	0-343	(Hato et al. 2011)

2.2.2 Surface modification of magnetic particles

While CIPs have been widely used as MRFs, researchers have concentrated on the problems of dispersed magnetic particles for industrial applications with improved dispersion stability and re-dispersibility. It has been observed that, in comparison to the ease of use of solid additives, the surface modification of particles is the most commonly used method used to reduce sedimentation. One of the criteria that will improve the sedimentation stability of MRFs is particle density, which can be reduced by coating with polymers. Therefore, several techniques for improving MRFs sedimentation properties were applied such as Pickering emulsion polymerization (Kim et al. 2013), surface-initiated atom transfer radical polymerization, (Cvek et al. 2015) and in situ dispersion polymerization (Fang et al. 2010), and solvent casting methods (Fang et al. 2012). The polymer encapsulation method of the magnetic particles has been regarded as one of the popular techniques, because it can reduce the particle density and improve the chemical resistance of magnetic particles.
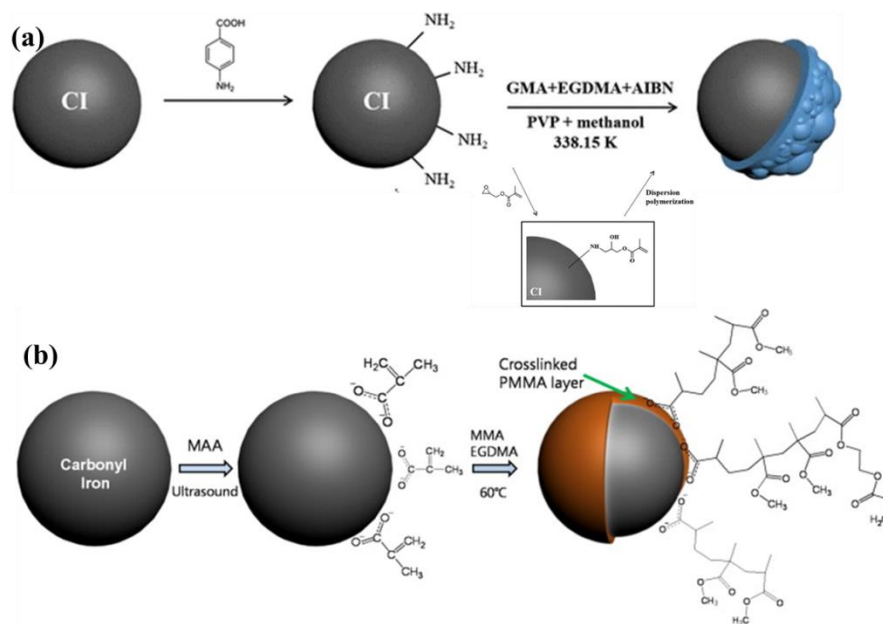
Fig.2.10 Synthesis mechanism of (a) PGMA-coated CI particle (Ahn et al. 2015) (b) encapsulation process of CI/ PMMA particles (Park et al.2009).

Fig.2.10(a) shows a schematic of the synthesis of the CI/PGMA particles using a dispersion polymerization method. Ethylene glycol dimethacrylate (EGDMA) was a introduced as a grafting agent which improved the affinity of PGMA to the surface of the CI particles (Ahn et al. 2015) Fig.2.10(b) shows the magnetic hybrid composite microsphere that was synthesized via a dispersion polymerization in the presence of CI, in which the PMMA was cross-linked

using ethylene glycol dimethacrylate during polymerization for enhancement in both chemical resistance and surface hardness (Park et al. 2009).
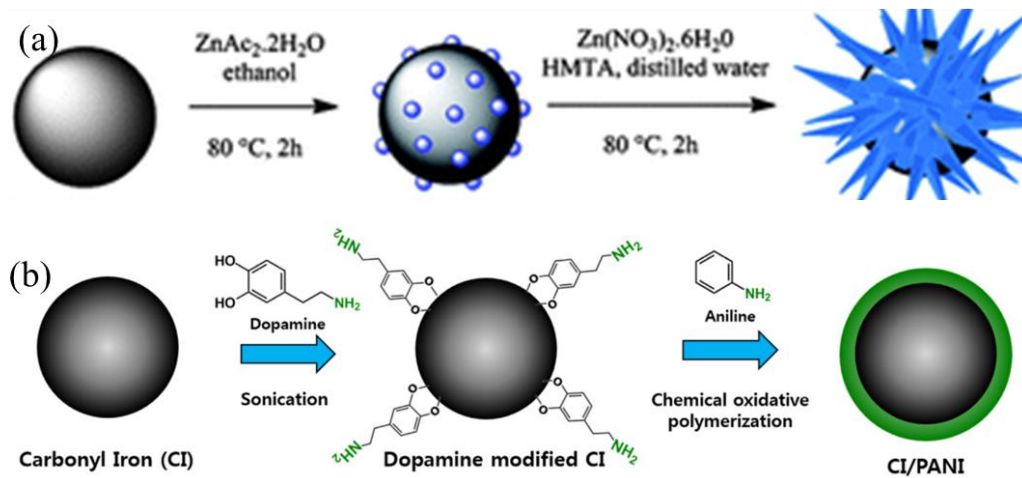
Fig.2.11 Synthesis mechanism of (a) CI/ZnO particles (Machovsky et al., 2014) (b) CI/PANI particles (Kim et al. 2008)

Fig.2.11 (a) shows the synthesis of seeding of CI particles with ZnO nanocrystal and used as a dispersed phase for MRFs preparation. Fig.2.11(b) presents the synthesis done via a chemical grafting method using dopamine hydrochloride as the grafting agent.The CI particles were initially modified using dopamine as a chemical grafting agent to strengthen the affinity between PANI and the CI particles.

Nguyen et al. (2014a) synthesised chemically stable core-shell structured silica coated on carbonyl iron (CI) microspheres and applied the MRFs for a specially designed small-sized MR brake. The results showed that except for the settling time, the response times were faster than those of the pristine CI-based MR fluid.

Cvek et al. (2015) prepared two different MR suspensions (20 vol.%) based on both the pure CI and CI/PGMA particles dispersion in silicone oil. Moreover, the density of the PGMA-coated particles was reduced to 6.96 g/cm^3, which is about 10 wt.% decrease, compared to 7.68 g/cm^3 of pure CIPs. As a result decrease in the sedimentation rate was observed. Fig.2.12(a) shows the shear stress increased with the increasing applied magnetic field strength. At each magnetic field strength, the shear stress exhibited a wide plateau range for all shear rates. Fig.2.12(b) shows the lower magnetic moment (Pure CIPs: 175 emu/g; CI/PGMA: 85 emu/g), due to the non-magnetic coating by cross-linked PGMA. Fig.2.12(c)

shows that the sedimentation rate of CI/PGMA was observed to be slower than that of the pure CI particles after 100 min.
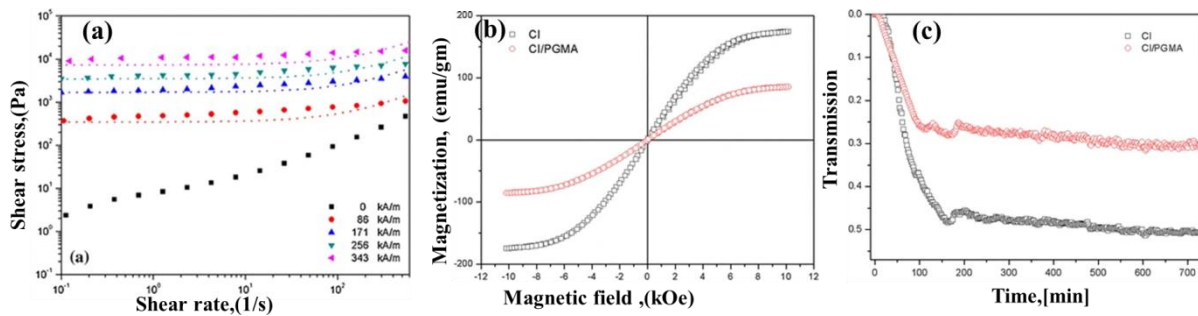
Fig.2.12 Shear stress (b) magnetization curves (c) sedimentation curve of CIPs/PGMA MRFs

Fang et al. (2007) added single-walled carbon nanotube (SWNT) to a suspension of carbonyl iron CIPs particles in lubricant oil. It was shown that adding SWNT could improve both MRF stability and the MR effect. This behaviour was attributed to more robust chain-like structure of the SWNT-containing MRF in the presence of a magnetic field. Fig.2.13(a) shows that shear stress increases with an increase in the magnetic field strength. Fig.2.13(b) shows the magnetization of C-MWNT MRFs is slightly reduced. Fig.2.13(c) shows the stability of C-MWNT MRFs of about 10% for 20 Hours.
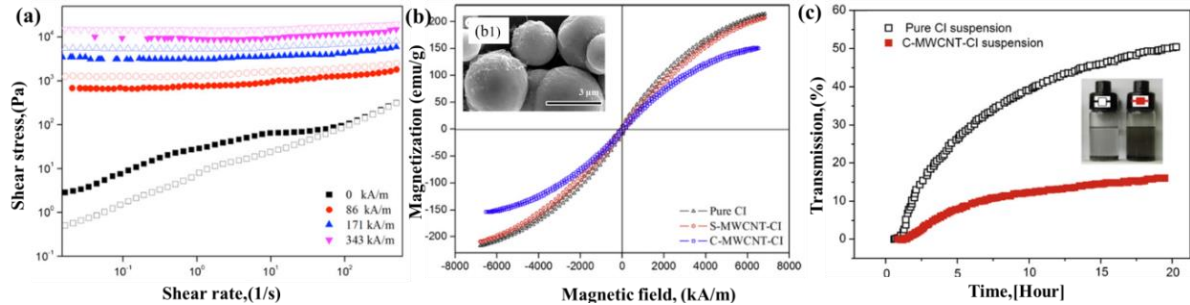
Fig.2.13 Shear stress v/s shear rate (b) hysteresis curve (c) sedimentation curve of CIPs/MWCNT based MRFs

Moon et al. (2016) discussed the polyaniline-coated magnetic carbonyl iron using the dispersion polymerization method. The coated particles and pure CIPs were dispersed in silicone oil with a sample concentration of 20 vol.%. The rheological properties showed that the non-Newtonian fluid and sedimentation rate was considerably improved for the coated MRFs.

Quan et al.,(2013) prepared the two kinds of MRFs based on pure CI and PS-coated CI particles. Each of the two systems was dispersed in the silicone oil with the same particle volume fraction of 20 v/v%. Fig.2.14 (b) shows the saturation magnetization of CI and PS-

coated to be 250 and 240 emu/g, respectively. A slight decrease of magnetic property for the coated particles was observed. Fig.2.14 (a) shows the shear stress versus shear rate, without the magnetic fields and the two suspensions show typical Newtonian behaviours. When the external magnetic field was present, the two systems exhibited Bingham fluid behaviour. Fig 2.14(c) indicates that the PS-coated CI was more stable than the CI suspension.
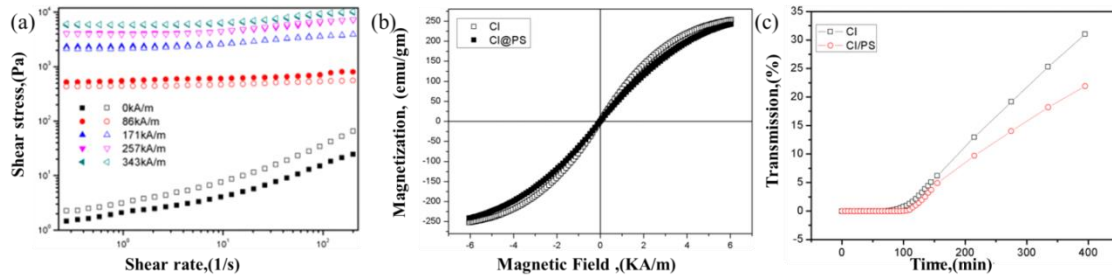
Fig.2.14 Shear stress versus shear rate (b) magnetization versus applied magnetic field (c) sedimentation curve (Quan et al.2013) of PS and CI/PS MRFs

Mrlík et al., (2013) prepared the CIPs coated with a low-density substance, cholesteryl chloroformate dispersed in silicone oil for improving the sedimentation and thermal oxidation stability of MRFs. The CI-cholesteryl particles showed slightly lower magnetization saturation in comparison with the bare ones due to a compact layer of cholesteryl groups on the surface shown in Fig.2.15b. The sedimentation ratio after 30 h was about 0.55 for modified CI particles with a compact layer of cholesteryl groups. As is apparent from Fig. 2.15, both suspensions exhibited Newtonian behavior in absence of magnetic field was applied. A list of the polymer coating material used are shown in Table 2.3
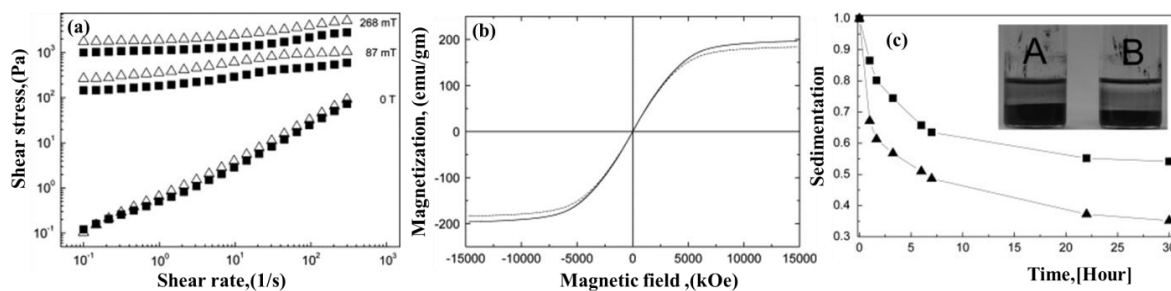
Fig.2.15 (a) Shear stress versus shear rate (b) magnetization versus magnetic field (c) sedimentation (Mrlík et al., 2013)

Table 2.3 Summary of coatings added into the MRFs

Sl no	Carrier fluid	Particle size (μm) and volume fraction	Type of coating used	Sedimentation time and ratio.	Rheological studies details			
					Shear stress (Pa)	Shear viscosity (Pa.s)	Magnetic field strength	References
1	Silicone oil	CIPs 4.25μm 35 vol%.	MWCNT	0 to 20 hours CIPs based MRF- 50% C-MWCNT CIPs MRF-10%	10^0-10^4	Na	0-343 kA/m	(Fang et al. 2012)
3	Silicone oil	CIPs (ES grade) 40 wt.%	cholesteryl chloroformate	0 to 30 hours Bare CIPs MRF-35% CIPs- cholesteryl chloroformate MRF-60%	10^{-1}-10^3	Na	0 to 268 mT	(Mrlik et al. 2014)
5	Silicone oil	CIPs	poly(butyl acrylate)(PBA) shell	0 to 60 Hours Bare CIPs MRF-80% CI-PBA MRF-10%	10^0-10^4	10^0-10^4	0-287mT	(Mrlik et al.2016)
6	Silicone oil	CIPs 3.5 μm 80 wt.%	Polyaniline (PANI)	0 to 200 Hours Bare CIPs MRFs-50% CIPs/PANI MRFs-95%	10^2-10^4	10^1-10^4	0-0.3 T	(Moon et al. 2016)
7	Silicone oil	CIPs	Poly(glycidyl methacrylate) (PGMA)	0 to 700 minute Pure CIPs MRFs-50% CI/PGMA MRFs-25%	10^{-1}-10^3	10^1-10^5	0-343 kA/m	(Kim et al. 2014
9	Silicone oil	CIPs 40 wt% .	urchin-like ZnO	0 to 30 hrs Bare CIPs-30% ZnO/CI urchin-like MRFs-55%	10^{-1}-10^3	Na	0-272mT	(Machovsky et al. 2014)

2.2.3 Nanoparticles magnetic additives into the MRF systems

Nonmagnetic materials, on the other hand, improve the sedimentation problem while decreasing the MR effect. As a result, the use of a magnetic nanoparticle additive system is regarded as an effective method of improving both dispersion stability and MR behaviour (Jang et al. 2015). The presence of micro-sized magnetic particles is responsible for the strong MR response under an external magnetic field. Fig.2.16(a) shows the absence of an external magnetic field, the addition of magnetic nano-particles will improve the kinetic stability of the system. Fig.2.16 (b) represents the schematic mechanism of the movement of carbonyl iron and magnetic additives in lubricant oil. The CI and magnetic nanoparticles are oriented in the magnetic field direction forming a chain structure under an applied magnetic field. This combination forms more regular chains of particles in the magnetic suspension fluid and increases the yield stress and sedimentation rate considerably.
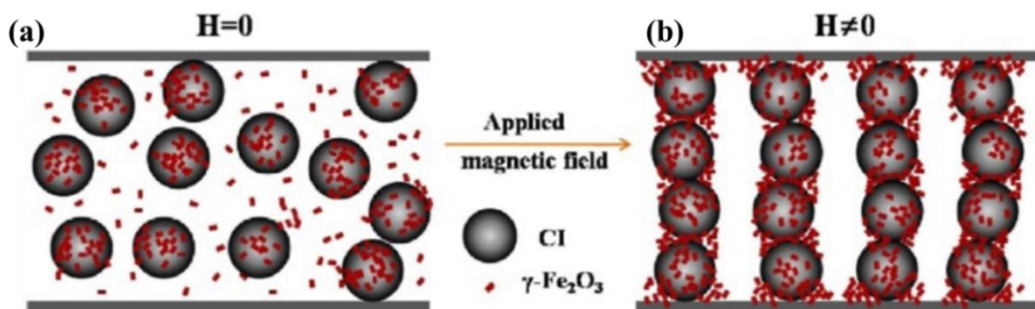
Fig.2.16 MR effect (a) absences of magnetic field (b) presence of magnetic field (Kim et al. 2016)

Jang et al. (2015) discussed experimental suspensions of pristine CI (70 wt.%) and MR fluids with different concentrations of the CI/γ-Fe$_2$O$_3$ mixture (0.5, 1, 1.5, and 2 wt.%) were added in silicone oil. The sedimentation rate decrease due to the gap-filling of γ-Fe$_2$O$_3$ between the micron C particles. All fluids show Bingham fluid behaviour under an applied external magnetic field, demonstrating that the MR performance is strongly influenced by the additives.

Kim et al. (2017) introduced the hard magnetic chromium dioxide nanoparticles with a rod-like shape which as an additive to a carbonyl iron (CI)-based (MR) fluid. Compared to the CI-based MRFs without chromium dioxide nanoparticles, the MR fluid with the chromium dioxide additive exhibited remarkably higher yield stress, shear stress behaviour with increasing

magnetic field strength, enhancing its MR performance and dispersion stability as shown in Fig.2.17(a),(b) and (c)
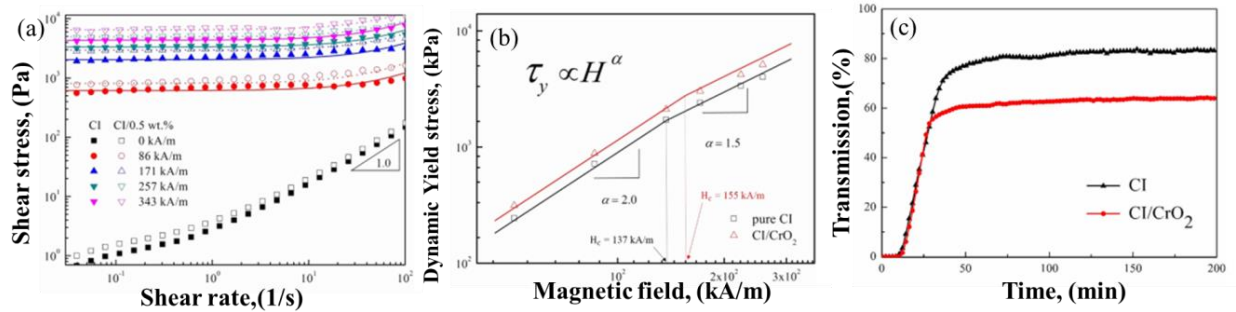
Fig.2.17 (a) Shear stress versus shear rate (b) dynamic yield stress versus magnetic field(c) sedimentation curve of CI/Cro$_2$ based MRFs

Han and Choi (2018) compared the MR performance of ferrites, non-stoichiometric zinc-doped spinel ferrite (Zn$_{0.417}$Fe$_{2.583}$O$_4$) nanoparticles with a high saturation magnetization value and a truncated octahedron like shape were synthesized using a simple thermal decomposition process with benefits of mono-disperse and high crystallinity. Fig.2.18(a) shows the flow curves of shear stress increase with magnetic field strength and exhibit a non-Newtonian behaviour in the presence of a magnetic field. Fig.2.18(b) shows that the M$_s$ values for CI, Zn$_x$Fe$_{3-x}$O$_4$, and the CI/Zn$_x$Fe$_{3-x}$O$_4$ mixture are 184.6, 105.8, and 197.3 A·m^2/kg at 770 kA/m, respectively. The addition of 0.5 wt.% Zn-doped ferrite (Zn$_x$Fe$_{3-x}$O$_4$) to the MR fluid enhanced not only the MR performance but also sedimentation stability, as confirmed by Turbiscan shown in Fig.2.18(c).
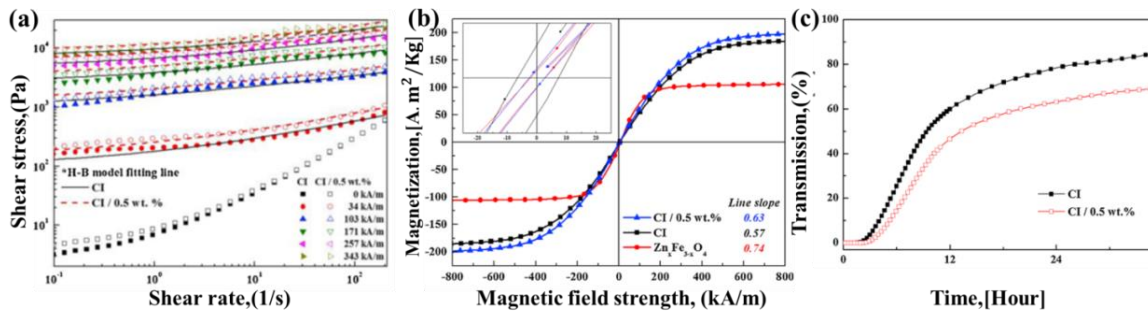
Fig 2.18 (a) Shear stress versus shear rate (b) magnetization curve (c) sedimentation curve of CI/Zn$_x$Fe$_{3-x}$O$_4$ based MRFs

Hajalilou et al. (2016) synthesized the Ni-Zn ferrite nanoparticles that via a thermo-mechanical alloying route and used it as additive for micron-sized CI-based MRFs. This study indicated that Ni-Zn ferrite nanoparticles fill the micron-sized CI particles cavities and are orientated in the direction of the applied field and consequently make a strengthened structure with improved properties.

Liu et al. (2015) studied the sedimentation stability of CIPs based MRF with strontium hexaferrite ($SrFe_{12}O_{19}$) nanoparticles as additive. The results indicated that the stability of MRFs improved remarkably by adding $SrFe_{12}O_{19}$ nanoparticles and the sedimentation ratio was only 88 % in 20 days when the content of the nanoparticles added 10 wt.%. Also, the rheological properties of MRF could be predicted well using the improved H–B model.

Dong et al. (2018) discussed about the CI MR fluid which was prepared by dispersing 50 wt.% of CI particles in silicone oil, and the $CI/CoFe_2O_4$ MR fluid was prepared by adding 0.1 wt.% of $CoFe_2O_4$ nanoparticles to the CI MR fluid. Fig. 2.19(a) shows the $CI/CoFe_2O_4$ MR fluid showed a higher shear stress value than the CI MR fluid at each magnetic field strength, indicating that the $CoFe_2O_4$ additive played an active role in the MR response. Fig.2.19(b)shows the magnetization as a function of magnetic field strength, demonstrating a saturation magnetization (Ms) of about 200 emu/g, 175 emu/g, and 74.4 emu/g for $CI/CoFe_2O_4$ mixture, pure CI, and $CoFe_2O_4$ particles, respectively Furthermore, $CI/CoFe_2O_4$ mixture MRFs results showed that the sedimentation ratio after 1400 min had improved by about 78%. The summary of various types of Nano-particles additive added MRF are discussed in Table 2.4
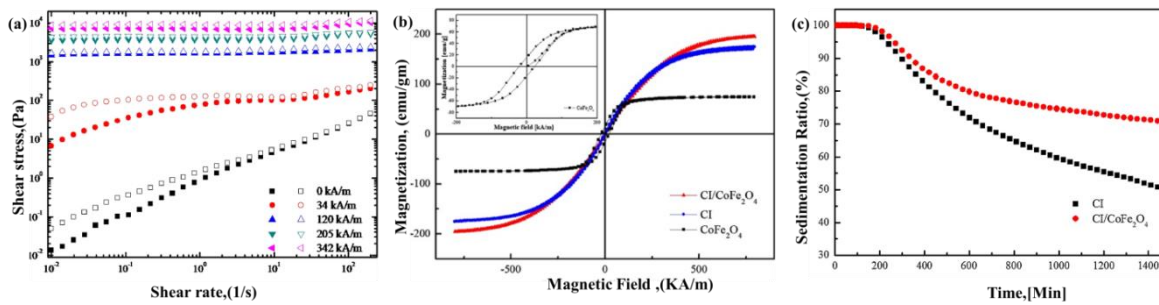
Fig.2.19(a)Shear stress flow curve (b) hysteresis loop (c)sedimentation curve of $CI/CoFe_2O_4$ MRF

Table 2.4 Summary of nanoparticles additives added into the MRFs systems

Sl no	Carrier fluid	Particle type (size μm)	Type and % of additive	Sedimentation/Transmission Time and ratio.	Rheological studies details			Reference
					Shear stress (Pa)	Shear viscosity (Pa.s)	Magnetic field strength	
1	silicone oil	CIPs 4 μm (50 wt.%)	$CoFe_2O_4$ 0.1 wt.%	0 to 1400 minutes CIPs based MRF- 82%, CIPs/ $CoFe_2O_4$ MRF- 50 %	10^{-2}-10^4	10^0-10^5	0-342 kA/m	(Dong, Piao et al. 2018)
2	Silicone oil	CIPs 4 μm (50 wt. %)	CrO_2 (0.5 wt. %)	0 to 200 minutes CIPs based MRF- 80%, CIPs/ $CoFe_2O_4$ MRF- 60 %	10^0-10^4	10^1-10^5	0-342 kA/m	(Hajalilou et al. 2018)
3	Silicone oil	CIPs 4-μm 30 wt%	$Ni_{0.5}Zn_{0.5}Fe_2O_4$ + Fe_3O_4 1 wt%	0 to 600 minutes CIPs based MRF- 40%, CIPs +$Ni_{0.5}Zn_{0.5}Fe_2O_4$ + Fe_3O_4=70%	10^{-1}-10^7	10^{-1}-10^8	0 to 558.18kA/m	(Park et al. 2001)
4	Silicone oil	CIPs 7 μm (70 wt%)	γ-Fe_2O_3 particles (0.5, 1, 1.5, and 2 wt%)	0 to 400 minutes CIPs based MRFs-80% CIPs+ γ-Fe_2O_3 2wt%.-70%	10^1-10^4	10^0-10^5	0-343 kA/m	(Mazlan et al. 2016)
5	Poly-alpha-olefin (PAO) oil	CIPs (63.5vol.%)	$ZnFe_2O_4$ nanoparticles 1 vol.%	0 to 7500 Minutes Pure CIPs MRF- 40% CIPs/ $ZnFe_2O_4$ MRF-70%	10^1-10^3	10^1-10^4	0 to 500 mT	(Hajalilou et al.,2018)
6	Silicone oil	CI Particles (2-4 μm) (50 wt%)	$Zn_xFe_{3-x}O_4$ (0.5 wt%)	0 to 24 Hours CIPs MRF-80% CI/ $Zn_xFe_{3-x}O_4$ MRF-60%	10^1-10^4	10^1-10^5	0 to 343 kA/m	(Han et al. 2016)

2.2.4 Ferrite based MRFs

Conventionally, a high yield strength value can be expected from the MRFs containing metallic magnetic (Fe, Co, Ni or their alloys) particles having high saturation magnetization (Anupama et al. 2018). However, MRFs containing these metallic particles suffer from poor dispersion stability and extreme difficulty of re-dispersibility. The merit of ferrite particles used in preparing MRFs is that the ferrite particles settle down slower than the CIPs due to their much lower density (4–5 g/cm^3) and sufficient magnetic behaviour in MRFs (Nugroho et al. 2020).

Guangshuo Wang et al., (2017) discussed two different MR fluids prepared by dispersing the CI particles and the CaFe$_2$O$_4$ nanocrystals clusters in silicone oil. The particle weight fraction of each MR fluid was 25%. As shown in Fig. 2.20(a), without an external magnetic field, the MR fluid exhibits typical Newtonian behaviour. The lower shear stress for CaFe$_2$O$_4$ nanocrystal is due to the low saturation magnetization (65.7 emu/g) as shown in Fig. 2.20(b). Fig 2.20(c) shows the sedimentation ratio of CaFe$_2$O$_4$-based MR fluid to be about 78% in 15 days, suggesting that the dispersion stability of CaFe$_2$O$_4$-based MR fluid was superior to that of CI-based suspension (63%).
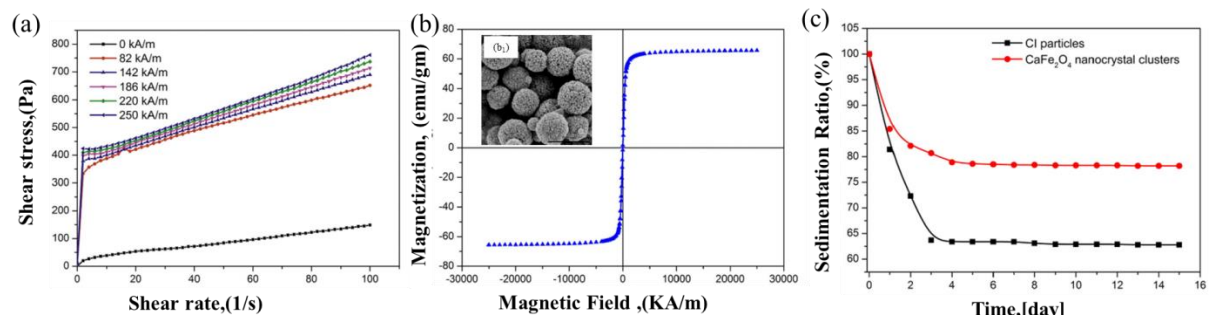
Fig.2.20 (a) Shear stress versus shear rate (b) magnetization versus magnetic field applied and (c) sedimentation curve for CaFe$_2$O$_4$ nanocrystal MRFs (Guangshuo Wang et al., 2017)

Wang et al. (2016) synthesised the magnesium ferrite (MgFe$_2$O$_4$) nanocrystal clusters using an ascorbic acid assistant solvothermal method and used for the preparation of MRFs. The MgFe$_2$O$_4$ nanocrystal clusters-based MRFs demonstrated enhanced sedimentation stability compared to the CIPs based MRFs. The values of dynamic yield stress increase with the magnetic field strength and form a robust columnar-like structure between the particles.

Anupama et al. (2019) discussed about the soft-magnetic Mn$_{0.7}$Zn$_{0.3}$Fe$_2$O$_4$ powder particles containing 40 wt. % of these particles which were prepared using thin silicone oil as a carrier

medium. The result shows that an increase in the yield stress increases with an increase in the magnetic field strength (τ_y=0.5 kPa at B = 1.2 T) . Also, the thermal, oxidative, and chemical stability of these ferrite particles are advantageous for their application in corrosive and high-temperature environments.

Wang et al. (2016) investigated the porous $MnFe_2O_4$ nano-flakes which were synthesized by a facile one-step solvothermal method, and the obtained products were employed as new magnetic. Fig.2.21(a) shows that the shear stress increases with an increase in magnetic field strength. Fig.2.21(b) shows the value of saturation magnetization (M_s) for the $MnFe_2O_4$ nanoflakes which is about 58.8 Am^2 /kg, which is sufficient for generating sufficient yield stress. Fig.2.21(c) shows that the $MnFe_2O_4$ based MRFs demonstrated enhanced sedimentation stability in 15 days.
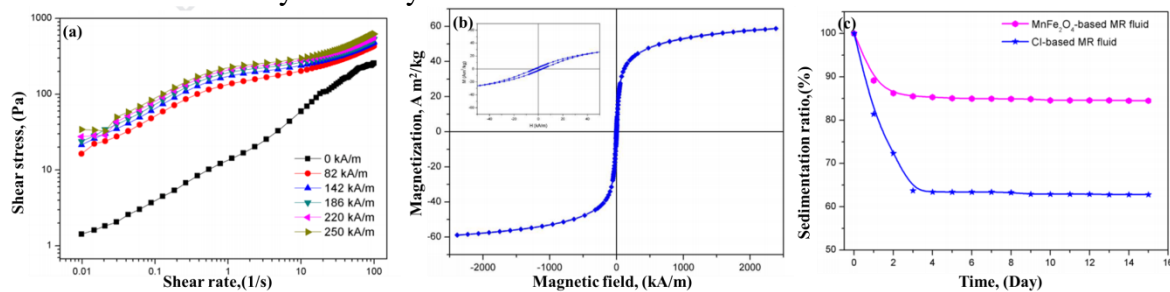
Fig.2.21 (a) Shear stress flow curve different magnetic field strengths (b) Hysteresis curve (c) sedimentation curve of CI/$MnFe_2O_4$ based MRFs

Anupama et al., (2018) showed about the magnetically soft nickel-zinc ferrite ($Ni_{0.5}Zn_{0.5}Fe_2O_4$) powder with high saturation magnetization synthesized by solution combustion route using metal nitrates as precursors and glycine as fuel. The particles were found to have irregular morphology. Three different concentrations of MRFs were prepared by dispersing 10, 20, and 40 wt. % of these particles in thin silicone oil. The behaviour of the MRFs were studied under steady shear conditions at different applied magnetic field strengths (B). The list of additives used in the ferrite particles is shown in Table.2.5.

Table 2.5 Summary of ferrite particles used in preparing MRFs

Sl no	Carrier fluid	Particle type (size μm)	Sedimentation/Transmission time and ratio.	Rheological studies details			
				Shear stress (Pa)	Shear viscosity (Pa.s)	Magnetic field strength	Model used
1	Silicone oil	$MnFe_2O_4$/GO	0 to 15 days CIPs based MRFs- 62% $MnFe_2O_4$/GO based MRF- 85%	0-6000	Na	0 to 250 kA/m	(Zeng et al.2020)
7	silicone oil.	Li–Zn ferrite ($Li_{0.4}Zn_{0.2}Fe_{2.4}O_4$)	Na	10^{-1} to 10^3	10^{-1} to 10^5	0 to1.2T	(Anupama et al. 2018)
4	Silicone oil	calcium ferrite ($CaFe_2O_4$) nanocrystal clusters	0 to 14 days CIPs MRF-60% $CaFe_2O_4$ MRF-80%	0 to 700 Pa	0 to 200 Pa.s	0 to 250 kA/m	(Wang et al. 2017)
5	silicone oil	$Mn_{0.7}Zn_{0.3}Fe_2O_4$	Na	10^{-1} to 10^3	10^{-1} to 10^5	0 to 1200 mT	(Anupama et al. 2019)
2	Silicon oil	$MgFe_2O_4$	0 to 14 days CIPs based MRFs-65% $MgFe_2O_4$ MRFs-83%	0 to 500 Pa	0 to 180 Pa	0 to 250 kA/m	(Ma et al. 2017)
3	Silicone oil	$MnFe_2O_4$ 30 wt%.	0 to 15 days CI particles MRFs-62% $MnFe_2O_4$ MRFs-85%	1 to 1000 Pa	Na	0 to 250 kA/m	(Baek et al. 2021)

2.2.5 Different types of surfactants in MRF systems

Surfactants can be used to avoid particle aggregation by enhancing steric repulsion among the particles. Surfactants reduce the interfacial tension at the iron/oil surface and increase wettability. Surfactants can improve the polarity of the carbonyl iron surface and make it more compatible with the carrier fluid. The surface coating of carbonyl iron with surfactants is therefore one of the common ways to strengthen the stability of sedimentation. Many researchers have used a variety of solutions to solve this problem.

Yang et al. (2016) discussed the role of oleic acid, dimer acid hydrophobic, hydrophilic interactions and the effect of surfactants on MRFs. MRFs were prepared with 20 vol.% modified carbonyl iron using high-speed mechanical ball milling followed by sonication. The off-state viscosity of MRFs showed non-Newtonian behaviour due to high-volume fraction and remnant magnetization of CIPs. The CI/dimer acid-based MRFs showed enhanced settling ratio than the bare CIPs MRFs in a long sedimentation time (i.e. 0.71% for 30 days) duration.

Fei et al. (2015) prepared solid loading of 70 wt. % of CIPs in MRFs by using the two typical surfactants including polyethylene glycol and oleic acid which has Hydrophilic-Lipophilic Balance (HLB) parameters. The sedimentation stability (8.8%) of lipophilic surfactants were superior to the hydrophilic surfactants (12.15%) added MRFs. The shear stress values showed was values of 40.78 kPa and 39.97 kPa, (HLB) respectively for a magnetic field of 0.6 Tesla

Du et al. (2010) studied the effect of four surfactants such as oleic acid; sodium dodecyl benzene sulfonate, OP4 emulsifier, and Tween 80. The high-performance MRFs were prepared by CIPs particles dispersed in silicone oil along with different concentrations of surfactants compounding. The result showed that the oleic acid and SDBS compounding treated MRF possesses higher sedimentation stability (17% up to 14 days) and smaller zero-field viscosity (0.464Pa.s).

Lijesh et al. (2016) prepared nine MRFs samples using three types of surfactants (oleic acid, citric acid, and tetramethylammonium hydroxide) and three different carrier fluids (water, silicone oil, and DTE light mineral oil) along with CIPs. Minimum shear stress and highest settling values were obtained for DTE oil with a surfactant of 10% weight of CIPs. Also, the dispersibility of the MRFs was enhanced by adding the surfactants.

Yang et al. (2017) prepared the MRF which contained carbonyl iron particles mixed in mineral oil with 12-hydroxy stearic acid (12-HSA) surfactant. It was interesting to note they that the addition of 12-HSA caused high shear stress with non-Newtonian behaviour and also increased with increasing concentration of 12-HSA. The concentration of 2g/HSA MRF formed a longer gel network formation where longer, provides strong flocculation in the suspension and improved stability.

Ashtiani et al. (2015) studied the stable MRFs with promising MR effect. Four hydrophobic acids such as (Lauric acid, Myristic acid, Palmitic acid, and Stearic acid) with the same functional group but different numbers of carbon atoms were added to the suspension of 62 wt.% CI particles and silicone oil. The surfactant added MRFs yield stress and stability increased up to 22 times (at H = 362 kA/m) and 7 times, respectively, in comparison to the surfactant-free MRF it observed that 3 wt.% of stearic acid improved stability and MR effect. Another study was conducted by the same research group (Rabbani et al., 2015) on the effect of adding two hydrophobic (stearic and palmitic) acids on the stability and MR effect of a suspension of 60 wt. % CIPs in silicone oil was studied. The results showed that adding 3 wt. % of stearic acid to the MR fluid resulted in relatively low off-state viscosity, high yield stress, and 92% stability enhancement of the suspension even over a period of one month.

Cheng et al., (2021) discussed about oleic acid, isopropyl tri(dioctylpyrophosphate) titanate and sodium stearate which were used as compound surfactants to modify carbonyl iron powder. MRF consisted of 25 vol.% of CIP particles and 75 vol.% of mineral oil mixed at 2300 RPM for 2 h. Fig.2.22(a).(b).(c) shows the MRFs sample shear stress values of about 20 kPa and sedimentation stability was considerably reduced. The modified surfactant compounding CIPs show lower saturation magnetization values compared to pure CIPs. Table 2.6 shows the summary of various surfactants used in MR suspensions.
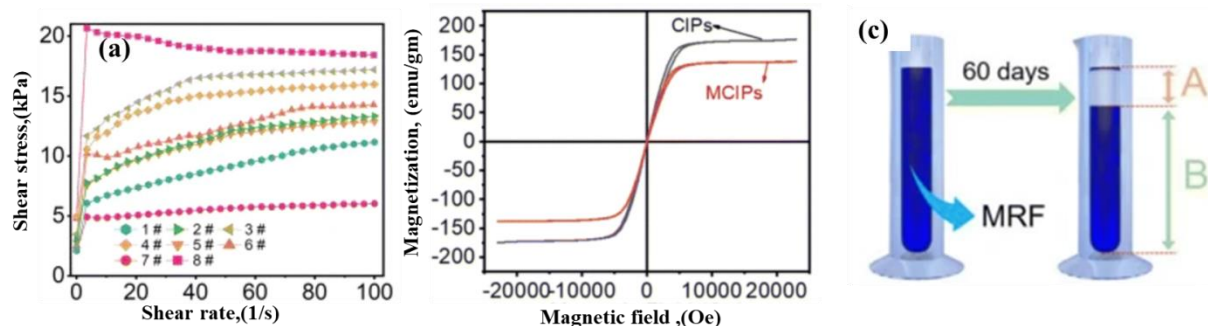
Fig.2.22 Shear stress curves (b) Hysteresis curve (c) sedimentation of CIPs and MCIPs MRFs

Table 2.6 Summary of various surfactants are added into the MR suspension

Sl no	Carrier Fluid	Particle type (size μm)	Type and % of surfactants	Sedimentation/Transmission time and ratio.	Rheological studies details			Reference
					Shear stress (Pa)	Shear viscosity (Pa.s)	Magnetic field strength	
1	silicone oil	CIPs 5.35 μm	Dimer acid Oleic acid	Na	0 to 80 Kpa	1 to 1000 Pa	0.2 to 1 Tesla	(Yang et al. 2016)
2	Mineral oil	CIPs 4–5μm	12-hydroxy stearic acid	0 to 600 min A_n/A_0 0 gm/l- 0.3% 1gm/l- 1.5% 2 gm/l-1%	10^0-10^4	10^1-10^5	0.03 T to 0.71 T	(Yang et al. 2017)
4	Silicone oil	Carbonyl iron particles	Stearic acid	0 to 1000 hours CIPs based MRF-60% CIPs/stearic acid MRF-20%	0 to 14000 Pa 0 to 25000 Pa	0 to 8000 Pa.s 0 to 20000 Pa.s	0 to 1.5 kA/m	(Rabbani, et al. 2015)
5	Mineral oil	CIPs	oleic acid/ sodium stearate	0 to 60 days	0 to 20 kPa	0 to 750Pa.s	0 to 391 kA/m	(Cheng et al. 2021)
6	silicone oil.	CIPs	OA and anhydrous alcohol	0 to 150 hours self-made-55% commercial MRF-58%	Na	Na	Na	(Zhang, et al. 2020)

2.2.6 Different types of bi-dispersed magnetic particles with irregular shapes

The shape and size of the magnetic particles have a significant impact on the stability of MRFs. Because of the larger surface area and higher frictional force induced between the particles, sedimentation was lower in the case of plate-like particles. Nonetheless, smaller Nano-sized magnetic particles, which are easier to disperse, have low magnetic saturation and yield stress of about 5 kPa. Bidisperse MRFs are produced by partially replacing micrometer-scale Fe particles with nanometer-scale Fe particles.

Wereley et al. (2006) discussed the bi-dispersed MRFs containing Fe particles at micron and Nanometer-scale with a solid loading of 60 wt.%. An important finding was that addition of nanoparticles reduced the sedimentation rate. The Bingham fluid model was fitted to observe the dynamic yield stress value of 10.25 kPa for the micron level-based MRF, while the bi-dispersed Fe particles-based MRFs caused an increase in the yield stress to 12 kPa.

Jiang et al. (2011) prepared the dimorphic MRFs with 60 wt.% CIPs by adding different weight ratios of wire-like nanostructures. The dynamic yield stress values varied between the 5 to 25 kPa with the magnetic flux density varied between the 0 to 0.5 Tesla. The shear stress and the dynamic yield stress markedly increased with the increase in magnetic field strength. Fig.2.22(a),(b), and (c) shows the typical magnetization, yield stress, and sedimentation values.
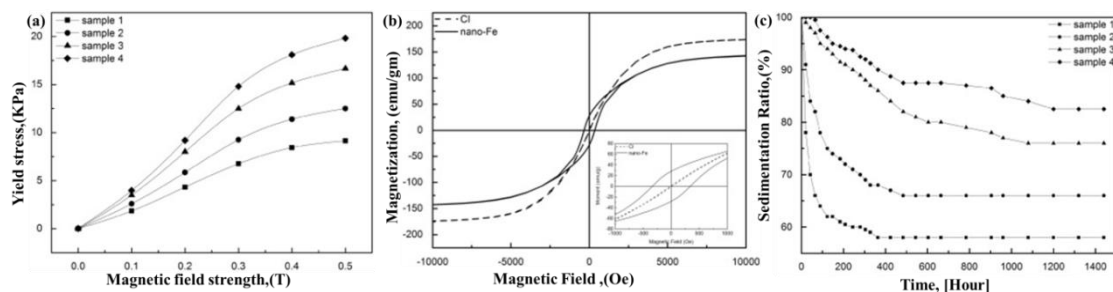
Fig.2.22 (a) Yield stress (b) magnetization curve (c) Sedimentation of CIPs dimorphic MRFs

Shah et al. (2014) focused on the preparation of bi-dispersed MRFs using the plate-like small particles (2 µm) and large iron particles (19 µm), and tested in damper against sedimentation for 48 Hours. The yield stress reached 32 kPa, when the magnetic field applied of was about 255kA/m. The fabricated damper showed a damping force of 5 to 30 N without changing any transient behaviour and dynamic motion after left for 2 days in the MR damper.

Lee et al. (2019) discussed the two types of MRFs prepared by dispersing each of the different shaped CIPs at 50 wt.% in silicone oil. However, rheological properties of shear stress, shear viscosity, and storage modulus of the (CI-F) MRF surpassed those of the (CI-S) under applied magnetic field. The CI-F MRF also demonstrated superior sedimentation stability compared with the CI-S. The saturation magnetization of the flake-shaped (CI-F) obtained to be slightly lower than that of spherical-shaped (CI-S) as shown in Fig.2.23(b). This was due to the large surface area, suggesting that the anisotropy of CIPs plays an important role in their MR performance.
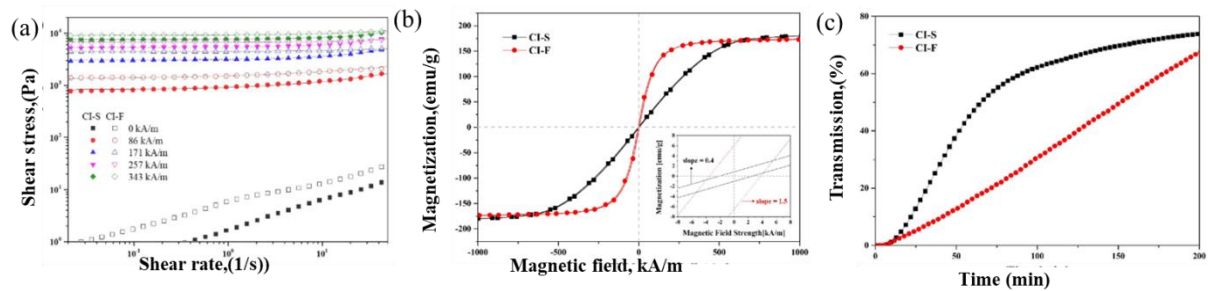
Fig.2.23 (a) Flow curves shear stress curves (b) Hysteresis curve (c) sedimentation of plate and sphere particles based MRFs

Ngatu et al. (2008) discussed about the partial substitution of the micron-sized iron particles with rod-shaped nanowires which constitutes a dimorphic MR fluid. A variety of conventional and dimorphic MR fluid samples were considered for this study with iron loading ranging from 50 to 80 wt.%. These substitutions significantly reduced the rate of particle settling, enabling the MR fluid to maintain a uniform dispersion without marked sedimentation for an extended period.

Xia et al. (2017) synthesized the novel nickel nanowires (NiNWs) and nickel nanospheres (NiNSs) were used as MRFs material. The effect of these two types of MRFs was compared. Moreover, MRF containing NiNWs possessed shear stress 15 times as strong as the one with the same volume of NiNSs, even though the saturation magnetization of NiNWs was smaller than NiNSs. Furthermore, MRF with a higher fraction of NiNWs had a more stable suspension, and NiNWs dispersed much better than NiNSs with the same volume fraction. Table 2.7 shows the list of magnetic particles with irregular shapes of MRFs

Table 2.7 Summary of types of magnetic particles with irregular shapes in the MR suspensions

Sl No	Title of paper/fluid properties/Ref	Yield stress (kPa) magnetic field strength kA/m	Sedimentation/ (%)	Solid fraction/magnetic particle type	Carrier fluid	Types of stabilizers
2	The influence of particle size on the rheological properties of plate-like iron particle based MRF (Shah and Choi 2015)	36.16 kPa (200 kA/m)	0.8 %/day	16 vol.% Plate like iron particles	Heavy paraffin oil	Bi disperse particles large size 19 μm and small size (2 μm)
3	Iron nanoparticles-based MR fluids: A balance between MR effect and sedimentation stability (Zhu et al. 2019)	0 to 4 kPa 0 to 234 mT	0.6% for 8 days	40 vol.% of Iron nano particles	silicone oil	Na
4	Preparation of spherical and cubic $Fe_{55}Co_{45}$ microstructures for studying the role of particle morphology in MR suspensions(Arief and Mukhopadhyay 2014)	0 to 1.2 Tesla	0.65% for 36 hours	$Fe_{55}Co_{45}$ particles 8 vol.% MR fluids	silicone oil	Na-citrate Na-acetate/PEG
5	Hierarchically Structured Fe_3O_4 Nanoparticles for High-Performance MRFs with Long-Term Stability (Choi et al. 2020)	10^0 to 10^4 0 to 343 kA/m	40% for 1 Week	10 vol. %	silicone oil	Na
7	Properties of cobalt nanofiber-based magnetorheological fluids (Dong et al. 2015)	0 to 40 kPa 0 to 250 kA/m	0 to 15 days	Co nano-fibers based 12 vol.%	Silicon oil	Na

2.2.7 High-density carrier fluid in MRFs.

The function of MRF carrier fluid is to provide an environment where magnetic particles are uniformly dispersed. Low viscosity and excellent physico-chemical stability in absence of magnetic fields are required for carrier fluid selection. Viscosity is one of the most important characteristics of the continuous phase in MRFs. For the highest MRF effect, the viscosity of the fluid should be small and almost independent of temperature. The carrier liquid is the major constituent approximately 50-80 percent by volume used in MR fluids. But the increasing zero-field viscosity would result in increase in on-off response time, as a result the application field would be restricted. Ionic is also an interesting carrier fluid because, unlike conventional ones, the properties of ionic liquids can be tuned by varying the composition of their ion Gómez-Ramírez et al. (2012). Furthermore, ILs are considered to be very stable and environmentally friendly compounds owing to their negligible vapor pressure, negligible flammability, and liquid state in a broad temperature range.

Recently, it was demonstrated that the use of magnetite ferrofluid as carrier media is an effective way of reducing the sedimentation of micron-sized particles of an MRF. In a successful research, (Patel 2011) studied the mechanism of chain formation in nano fluid-based MRFs. To obtain the stable ferrofluid magnetite particles coated with oleic acid and dispersed in kerosene. Fig.2.22(a) shows the mechanism of chain formation in the conventional MRFs and bi-dispersed, nano-particles which filled the microcavities between the large particles. Their findings showed that the ferrofluid-based MRFs to be more stable than the conventional MRFs.

Marinicə et al. (2016) used the carbonyl iron powder, with saturation magnetization of (M_s=210A.m^2/kg) in a highly concentrated transformer oil-based ferrofluid with magnetite volume fraction (ϕ_{FeO}=20%), and saturation magnetization of the MRF of M_s=74 kA/m). A collection of 12 composite magnetic fluids with Fe particle volume fractions differing in a large interval was prepared. There were no more additives used. The magnetization of Composite Magnetic Fluids (CMFs) by saturation varies linearly with the total magnetic particle material. An optimum volume fraction of Fe

particles (ϕ_{Fe}=20%) based MRFs, has a maximum magneto-viscous effect. This was justified by the substantial increase in the effective viscosity of high-volume Fe particle samples in the absence of an external magnetic field.

In another research, (Chand et al. 2014) investigated the varying concentrations of magnetic particles mixed in Ferro-fluid. They observed that the nanoparticles provide better stability, increased viscosity, and provides a strong chain-like structure with the presence of a magnetic field, fill the micro-cavities between the particles shown in Fig.2.24(c) and 2.24(d).
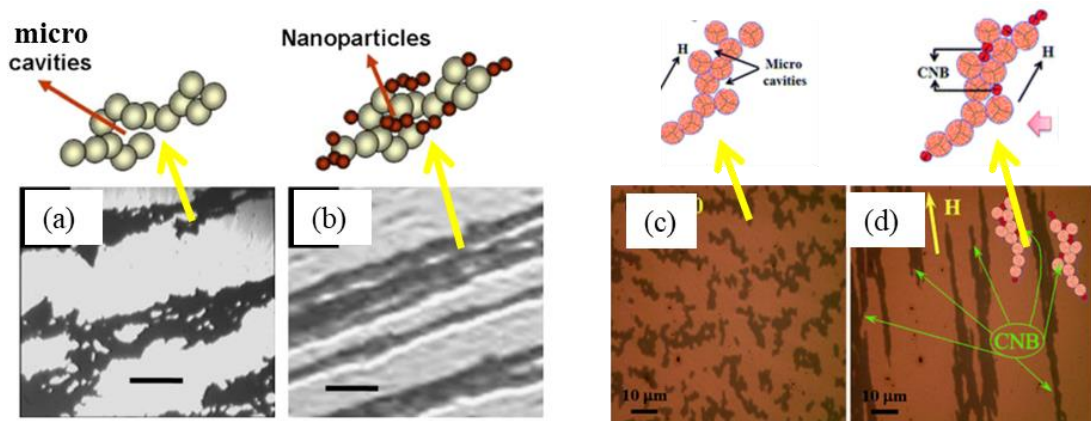
Fig.2.24 (a)Mechanism of chain formation in MRF (b) bi-dispersed MRFs with Nano-particles (c) without magnetic field (d) formation of columnar like structure and colloidal Nano-bridge (CNBs) in presence of magnetic field

Park et al. (2001) showed that sedimentation rate of MRFs considerably reduced by adding the hydrophilic CIPs in water-in-oil emulsion along with Tween 80 surfactants. The volume ratio of water in the continuous phase was ϕ (0.1–0.3) and surfactant contents were 3 wt.% of the oil phase. The values of yield stress which depend on the particle volume ratio of the particles showed that the linear relation with the magnetic field varied between 0.08 to 0.3 T.

Shetty and Prasad (2011) showed MRFs with a non-edible vegetable honge oil as a carrier liquid. Three samples of such MR fluid containing different percentages by volume of CIPs as suspensions were prepared for comparing their rheological properties. It was observed that one of the samples containing 40 per cent by volume

as suspensions exhibited a maximum viscosity of 334 Pa-s and yield stress of 13.23 kPa at a magnetic field of 0.3816T.

Zhang et al. (2018) discussed the polytetrafluoroethylene (PTFE) micro powders dispersed into silicone oil to viscosity changeable PTFE-oil organogell along with 10 vol.% of CIPs to fabricate MRFs. Fig.2.25 (a) and (b) show that the shear stress and shear viscosity increased with of PTFE organogell constant and obtained by the H-B model fit. Specifically, the PTFE powder provided internal thixotropic microstructures formation and possessed an excellent sedimentation stability of the MRFs as shown in Fig.2.25(c)
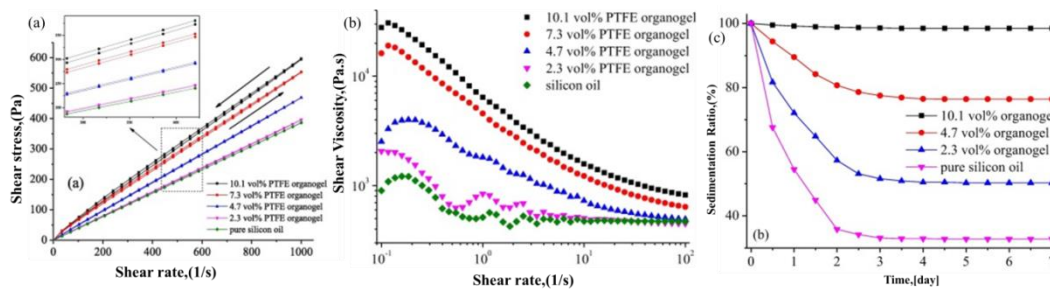
Fig.2.25 (a) Shear stress curves (b) shear viscosity as a function of shear rate (c) sedimentation profile as a function of time of PTFE/CIPs based MRF

In this regard, Guerrero-Sanchez et al. (2007) prepared eight different Ionic liquids with magnetite nano and microparticles as a magnetic phase. The sedimentation rate depended upon the kind of Ionic liquid used and the composition of magnetic particles. Furthermore, the rheological properties showed a quasi reversible modification and long-chain structure of magnetic particles in the Ionic liquid-based MRFs.

Xu et al. (2013) presented that MR gels as one of the categories of magnetic smart materials, whose mechanical properties change significantly in the presence of a magnetic field. In their paper, considering the significant effect of PU matrix content on the rheological response of MR materials, PU-based MR soluble gel (MRSG) with the carbonyl iron powder (CIP) weight fraction of 40%, 60%, and 80% were developed.

Table 2.8 Summary of various carrier fluids in the MR suspensions

Sl no	Carrier Fluid/Ref	Particle type (size μm)	Type and % of additive	Sedimentation/ Transmission Time and ratio.	Rheological studies details			
					Shear stress (Pa)	Shear viscosity (Pa.s)	Magnetic field strength kA/m	Model used
1	PTFE-silicone oil organo-gel (Yan et al. 2018)	CIPs	PTFE micro-powders	0 to 7 days Silicone oil based MRF-40% 10.1 Vol.% Organogell MRF-99%	0 to 600 Pa	10^{-1}-10^5	0 to 120	H-B model
2	water (Ghatee et al. 2020)	CIPs d_{50}=5 μm	Cetyltrimethyl ammonium bromide (CTAB)	0 to 50 Hours CR1-16% CR2-8%	10^{-2} to 10^{-4}	10^2 to 10^8	0 to 76	B-P Model
3	Poly(ethylene oxide) (PEO) solution (Cruze et al.2021)	Carbonyl iron particles	PEO powders	0 to 28 hours PEO MRF-27%	10^1 to 10^3	10^{-1}-10^5	0 to 342 kA/m	Na
4	water-in-oil emulsion (Park et al. 2001)	CIPs	Span 80	0 to 140 hours 97-%	10^1 to 10^4	Na	0 to 300 mT	Bingham fluid model

2.3 Techniques to analyze and evaluate sedimentation profiles

To measure the sedimentation or settling rate of MR fluid, the particle concentration must be measured at different time intervals. In MRFs, the main reason of sedimentation is due to the density difference between the magnetic particle (about $7.91g/cm^3$) and carrier fluid (about $1g/cm^3$). Such sedimentation deteriorates the designed performance of MRF-based systems such as MR dampers that operated for longer period. Therefore, the characterization of the sedimentation behaviour of MRFs is an essential factor in the design process of MRF-based systems. Table 2.9 list the techniques used to analyze the sedimentation study of MR fluids.

Table 2.9: Methods applied used for sedimentation study in MR fluids

Sl. No	Method of Sedimentation/ Reference	Remarks
1	Visual observation (Jun et al. 2005)	Visual inspection consists of a comparison of the heights (H_d) of the phase dispersed and the phase fixed at different time intervals to give an idea sedimentation ratio
2	Turbiscan instrument (Fang et al. 2011)	This system emits pulsed near-infrared light to the sample and then detects the beams from the other side. By comparing the obtained lights with the transmitted beam, the sensor ensures a distribution of the sample density.
3	Thermal conductivity monitoring (Cheng et al. 2016)	Thermal conductivity testing is a technique that can provide a test that does not cause magnetic fields in the MRF column and can provide data on the concentration of the particles
4	Nephelometer (Lambrou et al. 2010)	Nephelometer is a device that measures scattered light passing through a sample fluid, provides better sensitivity to measure the concentration of particles.
5	Inductance based	In this procedure a change in inductance of the

	monitoring system (Chambers and Wereley 2017)	circuit occurred due to sedimentation of magnetic particles. The relationship between LC circuit and magnetic permeability μ_r of the sample provided the volume fraction ϕ, and the change in volume fraction with time gave the sedimentation rate.

2.4 Magnetorheological testing

The most popular geometry used for magnetorheological of MRF testing is a parallel plate measuring system with varying magnetic field strength. The schematic diagram of the rheometer is shown in Fig.2.26 (a). A standard gap of 1mm is used to separate the parallel disks. The magnetic circuit is designed so that the magnetic flux lines are normal to the parallel disks. The MR cell is capable of continuously varying the magnetic field applied to the MR fluid sample. The MR cell also included a water-based heating/cooling system to maintain a temperature of 25°C. The top disk rotates while the bottom disk remains stationary. After placing the sample between the plates, the magnetic circuit is closed. As the upper plate rotates, a sensor measures the torque and calculates the corresponding force exerted on the moving plate. The shear stress at a designated point on the plate is then evaluated. A shaft encoder measures the angular rate and the corresponding shear rate. Both on-state and off-state behaviour were measured, for shear-rates ranging from 10^{-1} s^{-1} to 10^3 s^{-1} for the on-state characteristics, and shear-rates ranging from $10^{-3}s^{-1}$ to 200 s^1 for the off-state characteristics. Fig. 2.26(b) shows the MR Rheometer for placing the MRF sample between the plates with temperature-controlled yoke, hall sensor and coils for generating the magnetic field. Field-responsive fluids were distinguished by the steady-shear and linear viscoelastic properties that can be calculated using rheological instruments. The two most widely used configurations are shown in the figure, in which small volumes of fluid sample are tested between two coaxial circular parallel plates or between a small angle cone and plate, under shear, oscillatory flows(Guo et al. 2018b).

In this case as shown in Fig.2.26(c)and (d) of cone and plate type, measuresonly with the dispersion of particles in the liquid less than the 10μm. Parallel plate useful for measuring dispersion containing coarse particle paste, printing inks, gel-like materials, and polymer solution. The rheometry measuring systems consist of cone and plate type, parallel plate, and concentric cylinders for measuring the absolute values of samples. The concentric cylinder is shown in Fig.2.26(e) type for measuring the low viscosity liquids and solvent-borne coatings. Radius R, cone angle α, truncation); plate-plate (with radius R, the distance between plates H); and concentric cylinders (with bob radius R_i and cup radius R_e and internal angle α at the tip of the bob) are shown in the figure below.
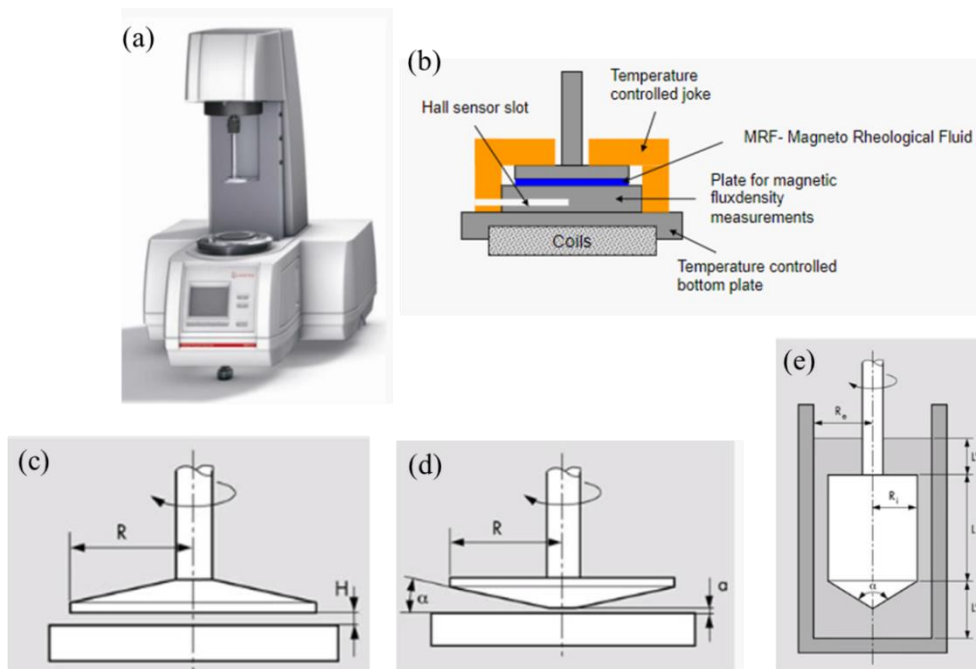
Fig.2.26 MCR 301 Rheometer (b) Schematic representation of magnetorheometer working (c)Parallel plate (d) cone and plate type arrangements (e) concentric type geometry (Permission taken from Anton Paar)

2.5 RESEARCH GAP

Several approaches have been explored to solve the sedimentation problem and search for a better magnetic material, which can suit a particular application. The

sedimentation stability methods such as non-magnetic additive, different carrier fluid, and ferrite particles are the most suited techniques to achieve the desired properties for a particular application of MRFs without compromising the properties such as low off-state viscosity, MR effect, and sedimentation rate.

2.6 MOTIVATION

Though enormous research works have been reported in the field of MRFs, the following studies are worth investigating to improve the performance of MRFs.

> There are significant works available based on the experimental characterization of MR damper against sedimentation days. But a limited work has been done in the settling of MR fluids in an MR damper. Better sedimentation MR fluid constituent plays a crucial role in enhancing the performance of MR damper; hence there is still scope for considerable work to be carried out in this area.

> The magnetic particles which are having lower density can have better sedimentation. The particular composition of low density particles based MRFs is to characterize in terms of sedimentation and rheological properties, which allows the MR damper weight to be minimum. It can be used for small damping force applications

> The cost of the commercials available for MRF in the market is very high. To synthesis, cost-effective MRFs in lab-scale is a major concern for use of MRFs to a larger extent in various applications.

> The spherical carbonyl iron particles CIPs have been widely used in magnetic particle, while the sedimentation methods such as non-magnetic additives, different types of carrier fluids, ferrite magnetic particles, and surface modifier using thixotropic additive are most appropriate methods to improve the settling of particles

2.7 OBJECTIVES OF PROPOSED WORK

➢ To study the effect of additives on the synthesis of carbonyl iron suspension on rheological and sedimentation properties of magnetorheological (MR) fluid.

➢ Study the different fumed silica as a thixotropic additive on carbonyl particles magnetorheological fluids for Sedimentation Effects

➢ Investigation of sedimentation, rheological, and damping force characteristics of carbonyl iron magnetorheological fluid with/without additives

➢ Investigating sedimentation and rheological properties of magnetorheological fluids using various carrier fluids

➢ An experimental investigation of manganese-zinc ferrite particle-based magnetorheological fluids under three different volume fraction was made.

2.8 SCOPE OF THE RESEARCH WORK

Owing to the numerous benefits of MRFs, then scope of applications is expanding. MRFs are increasingly being used in an array of applications such as robotics, aerospace, military, electrical, construction, automotive and biomedical field.

CHAPTER-3

MATERIALS AND METHODOLOGY

The present chapter focuses on materials used for the preparation of MR fluids. In the first approach, the effect of three clay additives is used to synthesis MRFs and to study rheological properties. In the second approach, the effect of with and without clay additives was tested in MR damper against sedimentation days. In the third approach, the effect of thixotropic fumed silica additive on MRF properties was studied. In the fourth approach, the different types of with varying viscosities of MRFs were prepared. In the last approach, the low-density Mn-Zn ferrite particles were used as magnetic phase with surfactants to increase the sedimentation time. Further discussions were made regarding the experimental techniques that were used to characterize particle morphology, crystal structures, and magnetic properties using scanning electron microscopy (SEM), energy-dispersive X-ray (EDX), X-ray diffraction (XRD), and vibrating sample magnetometry (VSM). Rheological properties of prepared MRFs under different magnetic field strengths were evaluated using commercial Anton Paar Physica MCR series Rheometer with MR attachment cell (MRD- 180®).

3.1 Materials

3.1.1Flow chart and preparation technique of clay additives in CIPs MRF

Fig.3.1 shows the flow chart for preparing MRFs samples. Initially, 1 wt.% molyvan 855 was used as a friction reducer agent (R.T.vanderbiltcompany) which contains molybdenum.To this material poly-alpha-olefin (PAO) oil was purchased from KK India Pvt. Ltd., which has a kinematic viscosity of 16.7 cSt at 40°C and used as the liquid carrier medium using a mechanical stirrer for certain time intervals. Three different clay additives were added into the suspensions containing 1wt.% of claytone APA, garamite-1958 (BYK additive Pvt. Ltd.), and baragell 10 purchased from (Elementis specialties Pvt. Ltd). For the synthesis of MRFs samples, carbonyl iron particles (CIPs) of CM grade (BASF, Germany, avg. d_{50} diameter 6.5-9 μm, density

7.86 kg/m^3) were mixed using a mechanical stirrer. Table 3.1 shows the properties of CIPs used in the preparation of MRFs. To prepare the MRFs, 81wt% each of CIPs and 1 wt.% each of additives were separately dispersed in PAO oil. The compositions were well mixed using a mechanical stirrer for certain intervals of time to obtain the homogeneous dispersion.

```
┌─────────────────────────────┐   ┌─────────────────────────────┐
│        Base oil             │   │   Friction reducer agent    │
│ (poly-alpha-olefin oil)     │   │      (molyvan 855)          │
│   viscosity: 16.7 cSt       │   │                             │
└─────────────────────────────┘   └─────────────────────────────┘
              │                                   │
              └──────────┐            ┌───────────┘
                   ┌──────────────────────────┐
                   │  Stirred with low shearing│
                   │  using mechanical Stirrer at│
                   │        350 rpm            │
                   └──────────────────────────┘
                                │
┌──────────────────────┐   ┌──────────────────────────┐   ┌──────────────────────┐
│   Clay additives     │   │ Stirred with high shearing│   │  Carbonyl iron powder│
│ Claytone APA, Baragell 10│ │ using mechanical Stirrer at│ │  6.5-9 microns scale │
│  and Garamite 1958   │   │        1200 rpm           │   │   ρ=7.91 kg/m³       │
└──────────────────────┘   └──────────────────────────┘   └──────────────────────┘
                                │
                       ┌──────────────────┐
                       │ MRFp-1, 2 ,3 and │
                       │        4         │
                       │     samples      │
                       └──────────────────┘
```
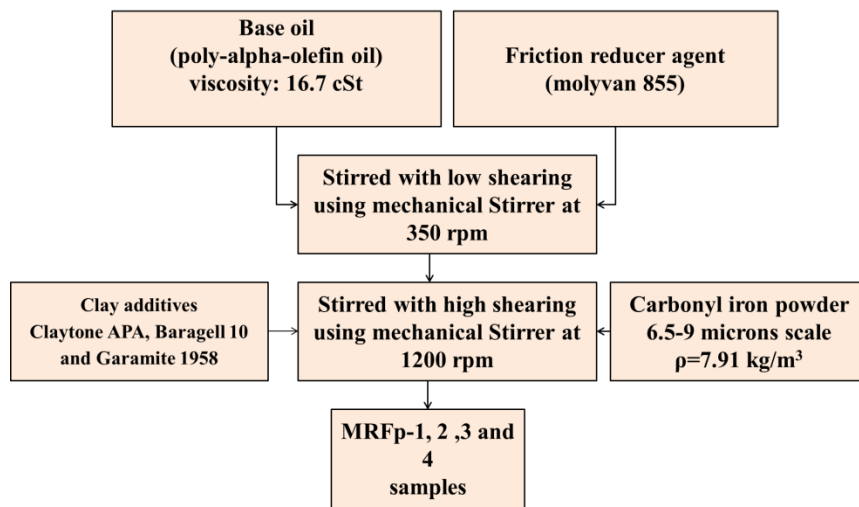
Fig.3.1 Flow chart of three different additives based MRFs

The schematic representation of the synthesis of MR fluids is shown in Figure 3.2. The PAO oil-based MRF samples are coded as MRFp-1, MRFp-2, MRFp-3, and MRFp-4, respectively. Table 3. 1: Formulation of MRFs.
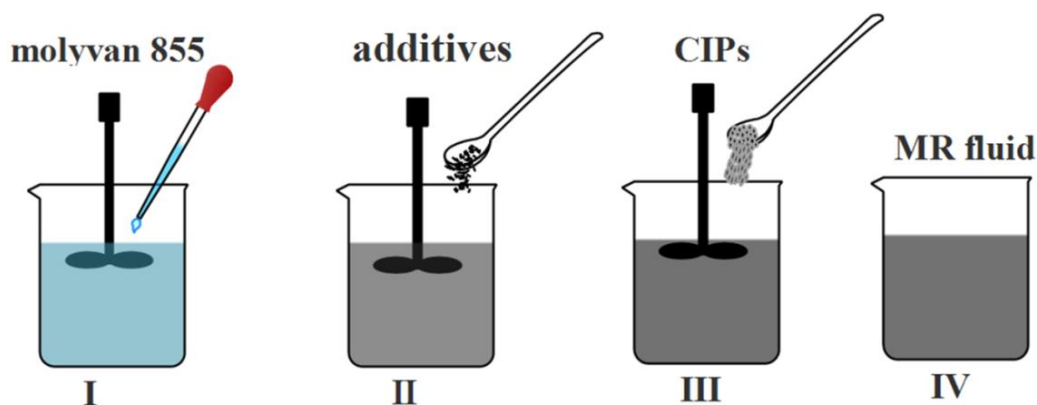
Fig.3.2 Schematic representation of the preparation of MR fluids

Table 3.1 Compositions used in the preparation of MR fluids.

Sample	Magnetic phase wt. (%)	Carrier fluid wt. (%)	Clay additives wt. (%)	Friction reducer agent wt. (%)
MRFp-1	Carbonyl particles (81)	PAO oil (19)	NA	NA
MRFp-2	Carbonyl particles (81)	PAO oil (17)	Claytone APA (1)	Molyvan 855 (1)
MRFp-3	Carbonyl particles (81)	PAO oil (17)	Baragell 10 (1)	Molyvan 855(1)
MRFp-4	Carbonyl particles (81)	PAO oil (17)	Garamite 1958 (1)	Molyvan 855(1)

3.2 Preparation of Carbonyl MRF With/Without friction reducer additives

3.2.1 MRFs materials used
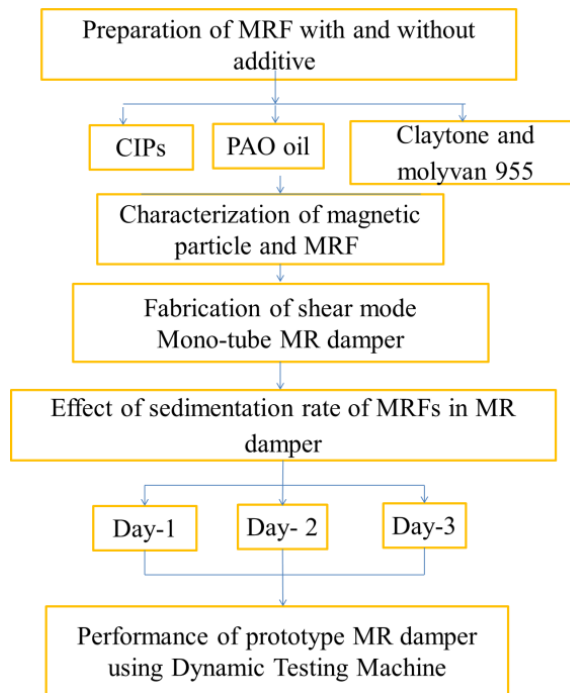
Fig. 3.3 Flow chart of Testing of MRFs

Fig.3.3 shows the flow chart for preparation of MRF and damper fabrication to test at different sedimentation time. These MRF sample constituents were completely homogenized by stirring at 1000 rpm for 4 hours The MRF rheological and damping force properties were evaluted using rheometer and dynamic testing machine respectively. The effect of sedimentation rate in MR damper without disturbance kept for three days was determined to evaluate the damping force characteristics.

For preparing the MRFs, 70 wt.% CIPs composition was added to both the samples. Moreover, 1 wt.% claytone APA was used as an additive to improve the sedimentation in the MRFs, with 1 wt.% molyvan 855 friction reducer agent. Carbonyl iron particles (CIPs) with d_{50} avg. particle size ranging from 6-7 µm (CS-grade) used as soft magnetic (99.5% Fe) dispersed phase particle were purchased from BASF Corp. Poly-alpha-olefin (PAO) oil with a kinematic viscosity of ($\nu=17.2$ mm^2/s) at 40°C with a specific gravity (S.G=0.818) was used as the carrier medium for the MRFs. Table 3.2 shows the composition and samples of pure CIPs and CIPs/claytone APA MRFs.

Table 3.2 Composition and Constituents used in MRFs

Sample Code	CIPs	PAO oil	claytone APA	molyvan 855
Pure CIPs MRF	70 wt. %	30 wt. %	none	none
CIPs/Claytone MRF	70 wt. %	28 wt. %	1 wt. %	1wt.%

3.2.2 Fabrication of MR Damper

Figure.3.4 shows a monotube MR damper of shear mode type without accumulator damper, which was fabricated to test against sedimentation of MRFs for low force applications. Fig.3.4(a) shows the schematic view of the proposed MR coil piston, and the 3D model view of the MR damper with copper coil winding, MRF, seals, housing cylinder, bearing, and the piston rod is shown in Fig.3.4(b). As the piston of the MR valve moves, the MRFs flow from the top to the bottom reservoir through the annular flow gap between the MR piston and the inner cylinder of the MR damper. Fig. 3.4(c) shows the fabricated MR damper to assess the damping performance of the prepared MRFs. Table 3.3 shows the dimensions of the MR piston which is used damper

Table 3.3 Geometric dimensions of the MR damper

Parameters	Dimensions in mm
Outer cylinder diameter (D_1)	42
Inside cylinder diameter (D_2)	41
Length of the piston ($2L_1+L_2$)	40
The diameter of the MR piston (D)	40
Length of the coil (L_2)	20
Annular flow channel gap (h)	1
The diameter of the piston rod (D_p)	12
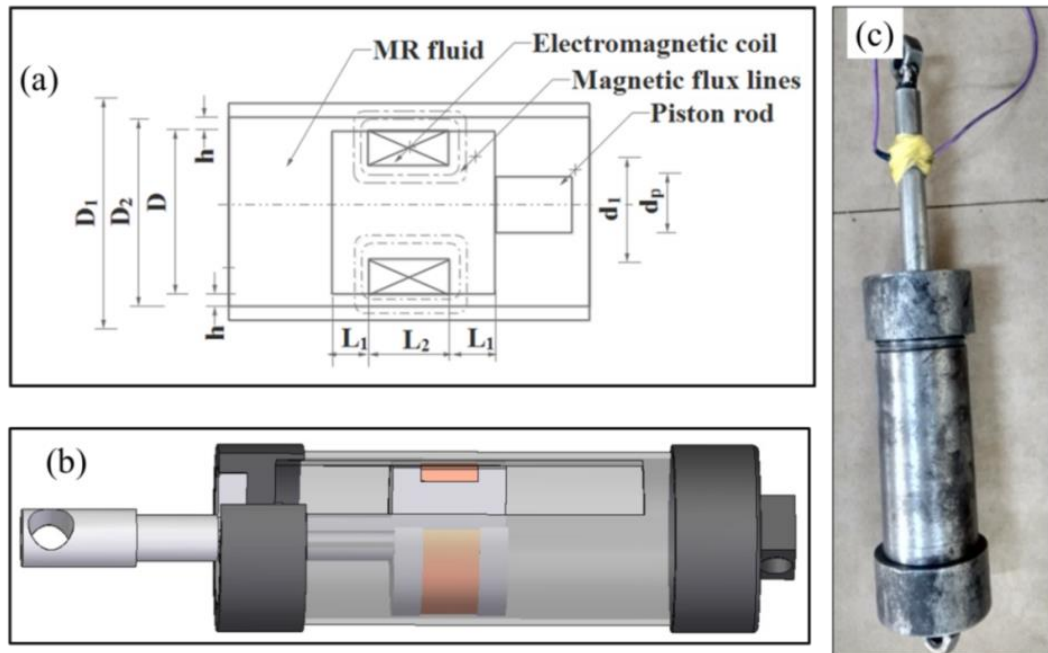
Fig.3.4 MR damper (a) schematic drawing of MR piston, (b) 3D model view, and (c) fabricated and tested MR damper

3.3 Preparation of carbonyl iron-based MRF with fumed silica additives

The flow chart depicting the preparation of MRFs with different types of hydrophobic and hydrophilic fumed silica surface area with CIPs and silicone oil is shown in Fig 3.5. The MRFs were well homogenized using Cowles Dissolver at different stirring speeds from the mechanical stirrer. The MRFs were formulated using CIPs (CN grade) obtained from BASF. The carrier fluid used was silicone oil purchased from (Spectrum Reagents and Chemicals Pvt. Ltd.) with a dynamic viscosity of (μ=0.01

Pa.s). The solid loading of CIPs, fixed at 80 wt. % concentration was added to all MRF samples.
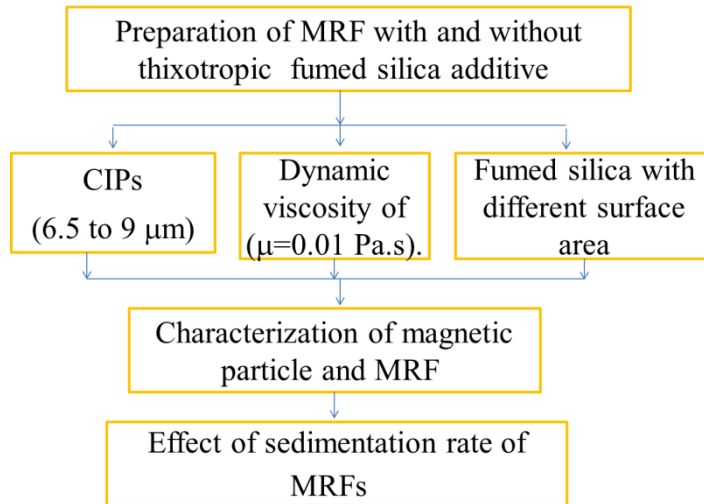
Fig.3.5 Flow chart preparation MRF with different types of additive

Table 3.4 Characteristics of fumed silica used for MRFs preparation

Sl. No.	Silica type	BET Surface area m^2/g	Magnetic particle	Particle size in µm	Material category
MRF1	NA	NA	CIPs	6-8	NA
MRF2	Cab-O-Sil® TS-720	115 m^2/g	CIPs	0.04-0.13	hydrophobic
MRF3	Cab-O-Sil® TS-610	125m^2/g	CIPs	0.07-0.3	hydrophobic
MRF4	Hi-Sil 233	135m^2/g	CIPs	1-3	hydrophilic
MRF5	Sigma-Aldrich (S5505)	200m^2/g	CIPs	0.2 - 0.3	hydrophilic

The commercially available fumed silica (FS) with different grades and different surface areas used are listed in Table 3.4. For the present work, Cab-O-Sil® TS-720 and TS-610 (Cabot Sanmar Ltd.), and Hi-Sil 233 (PPG Industries, Inc) were provided free of cost. The fumed silica-S5505 (200 m^2/g) grade which was aggregated in the form, was purchased from (Sigma-Aldrich). The prepared MRF was named MRF1 which contained silicone oil and CIPs. Also, MRF 2, 3, 4, and 5 samples contained CIPs, silicone oil, and 3wt.% of fumed silica additive concentrations.
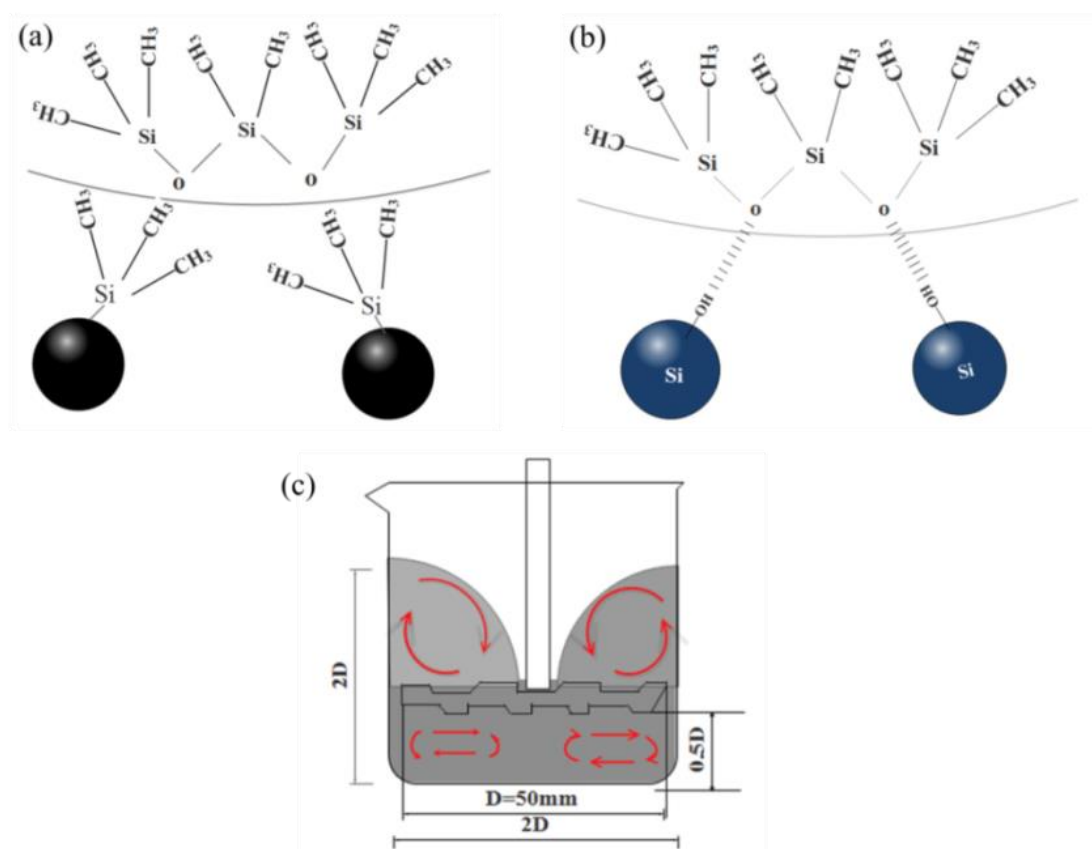
Fig.3.6   Mechanism showing (a) hydrophobic surface with weak interaction, (b) hydrophilic surface with strong interaction, and (c)fumed silica of dispersion mechanism

Commercially available silicon oils have less solubility and hence solubilization of these required either altering structural chemistry by introducing hydrophilic side groups or adding a solvent to the oil phase. Fig. 3.6(a) shows the structure, which indicates weak hydrogen bonding contact between the particles of the hydrophobic

65

fumed silica layer. Fig.3.6 (b) shows a strong interaction between the hydrophilic fumed silica particles, which form a three-dimensional network, containing the silanol groups (Si-OH) on the surface. The oligomeric and polymeric hydride of siloxanes included Si-O-Si linkage, in which pair of silicon atoms separated by one polar oxygen atom. These siloxanes form the backbone of silicones. In general, silicones are inherently hydrophobic and flexible, and further, they can be structurally modified to contain hydrophilic groups. The partial intermolecular bonding interaction between electron-rich donor atoms and electron-poor atoms results in hydrogen bond formation. The tetrahedrally substituted Si-O bonds of siloxanes have relatively high Lewis basicity and are hence expected to form strong hydrogen bonding. The polar and hydroxylic silanes are hydrophilic (MRF4, MRF5) and alkyl-substituted silanes are hydrophobic (MRF2, MRF3). The preparation of MRF is simple and requires care, but is not complicated.

To mix the constituents of MRFs suspension such as carbonyl iron particles, silicone oil, and fumed silica as a thixotropic agent a mechanical stirrer of specific design supplied by the manufacturer was used as shown in Fig.3.6(c) and the design parameter are listed in Table 3.5. The preparation consisted of the following steps. Initially, the fumed silica and silicone oil were mixed at a low level of stirring and form a gel, which might be due to the fumed silica particles forming a thixotropic network structure. Then, CIPs were added to the silicone oil gel and stirred at 1000 rpm for 1 hour using the mechanical stirrer (Remi-RQG-121D).

During stirring, the MRFs suspension shows with a doughnut-like shape as shown in. Fig.3.6(c). Flow pattern was observed and using Cowles dissolver effective mixing of MRFs was obtained. The initial dispersion was rapid. If the dispersion mixed for too long, the result will be an irreversible decrease in viscosity. The dispersions often have thixotropic properties, i.e., a viscosity that varies with the rate of stirring. For liquids with minimal hydrogen bonding, small amounts of fumed silica would increase the viscosity.

Addition from 1 to 3 % by weight usually suffices to cause the liquid to form a gel. More energy was generally required to disperse the fumed silica as the surface area

66

increases. Finally, the MRFs sample was immersed in an ultrasonicator for five minutes to ensure homogeneity and to remove the bubbles from the samples. The calculation of tip speed (peripheral speed) is given by the general formula.

$$\text{Tip speed} \left(\frac{\text{m}}{\text{s}}\right) = \frac{\text{D} \times \pi \times \text{RPM}}{60} \qquad (3.1)$$

Table 3.5 Impellor and vessel dimensions provided by the supplier

Sl. No.	Parameters	Dimensions (mm)
1.	Disk diameter(D)	50
2.	Jar diameter (2D)	100
3	Filling height (2D)	100
4.	Height of stirring dissolver the bottom	25

3.4 Preparation of manganese-zinc ferrite particle-based MRF

MRF was prepared with as received Mn-Zn ferrites particles supplied as a free of cost sample from KIP Chemicals Pvt. Ltd and silicone oil purchased from (Sigma Aldrich; ν=10 cSt; $\rho = 0.96$ g/cc^{-1}), where ν is kinematic viscosity, and ρ is the density of carrier fluid medium was added. The MRF was stirred using a mechanical stirrer at 100 rpm. The stearic acid (Sigma Aldrich) additive was added with 1 vol. % of into the MRF suspensions to inhibit the sedimentation of particles. The MRFs were homogenized by mechanical mixing at 1000 rpm for 1 hour and followed by ultrasonication for 15 minutes at room temperature. The MRFs were labelled as MRF#20, MRF#25, and MRF#30, respectively, and the volume fraction of each constituent is listed in Table 3.6

Table 3.6 The composition of MRF

Samples	(Mn-Zn ferrites) vol. %	(Silicone oil) vol. %	(stearic acid) vol. %
MRF#20	20%	79%	1%
MRF#25	25%	74%	1%
MRF#30	30%	69%	1%

67

The preparation steps of Mn-Zn ferrite parties based MRFs shown in Fig.3.7. Initially particles are added with different volume fraction were added in silicone oil. In order to reduce the settling of particles stearic acid was used as stabilizer and stirred wit 350 Rpm using mechanical stirrer for complete homogeneity of the MRF samples
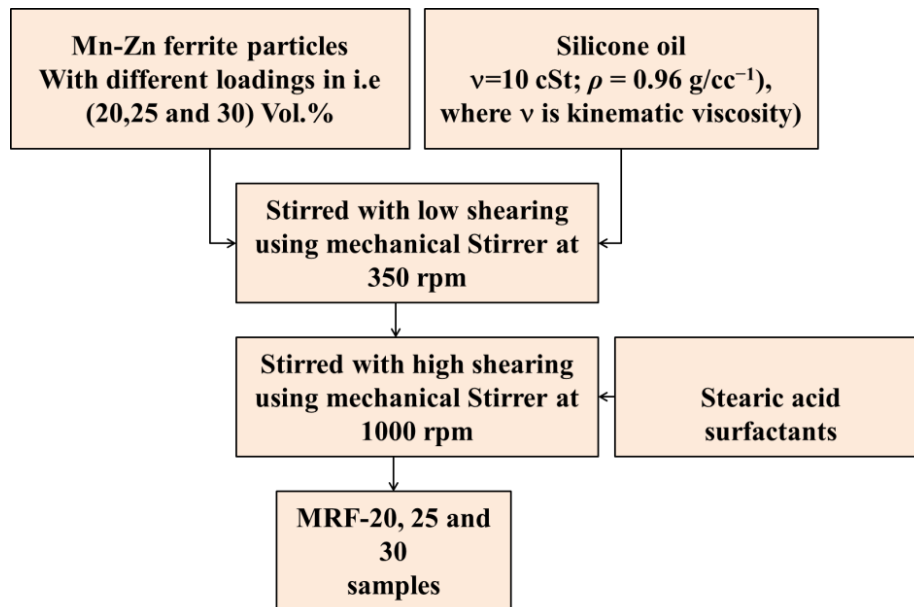
Fig 3.7 Flow chart preparation of Mn-Zn ferrite particles

3.5 Preparation of MRFs with a different carrier liquid

3.5.1 Materials

The constituents required for the purpose of stabilization in MR fluid i.e. fumed silica (0.2-0.3) μm surface area $200 m^2/g \pm 25$ m^2/g (aggregate) (Sigma Aldrich) were mixed using homogenizer stirred for about 15 min in silicone oil (Sigma Aldrich), light paraffin oil (Spectrum chem. Pvt. Ltd) and Poly-alpha-olefin oil (Chemtura Corporation) with a Specific Gravity of (0.96, 0.83 and 0.84 g/cm^3) and viscosity range of (5, 30 and 400 cSt.) respectively until a homogeneous solution was obtained. Afterwards, carbonyl iron powder particles density: 7.86×10^3 kg/ m^3, CN grade, Avg. particle size (1-9) microns from (Vimal intertrade Pvt. Ltd, India) were mixed in the gel using a mechanical stirrer at 900 rpm for about 12 hours. In the present work, the 3 types of MRF samples are designated by MRF-1, MRF-2, and MRF-3 in Table 3.7

Table 3.7 Properties of prepared samples composition

ID	Type of based fluid (cSt)	CIPs (Volume %)	Carrier liquid (Volume %)	Fumed silica (Volume %)
MRF-1	Silicone oil (5)	25	72	3
MRF-2	Light paraffin oil (30)	25	72	3
MRF-3	Poly-alpha-olefin oil (400)	25	72	3

The preparation steps of different viscosity bases oil based MRFs shown in Fig.3.7. Initially CIPs particles of 6 to 9 μm are added with different volume fraction were added in silicone oil. In order to reduce the settling of particles fumed silica was used as stabilizer and stirred wit 350 Rpm using mechanical stirrer for complete homogeneity of the MRF samples.
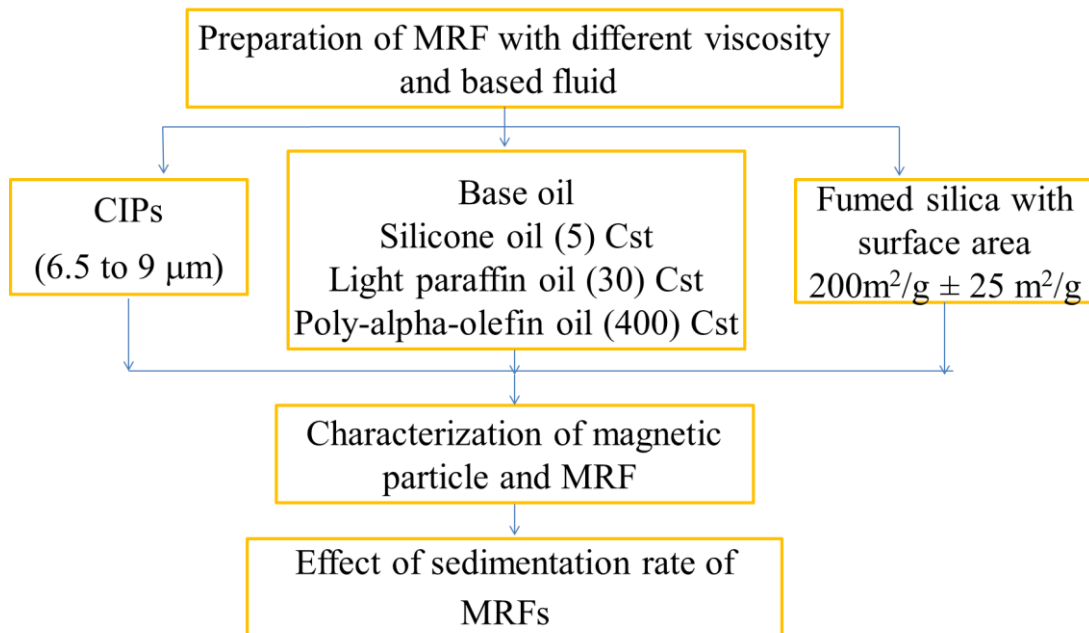
Fig.3.8 Flow chart preparation of MRFs with different base liquid

3.6 Characterization of MRFs

To study the crystal structure, chemical composition, morphology of materials, and additives characterization tools used are discussed below. Materials used for the

synthesis of MRF and MRFs were characterized using various techniques such as XRD, SEM, EDS, contact angle, FTIR were discussed to evaluate the material's physical properties. Magnetic saturation properties of magnetic particles and MRFs were studied using VSM and SQUID. Also, since MRFs sample in the liquid state these properties were tested using a standard samples liquid holder using VSM. The damping force characteristics prepared MRFs were identified using the dynamic testing machine. The prepared MRFs rheological flow curve properties such as shear stress as a function of shear rate and viscosity as a function shear rate were measured using a rheometer. In addition, surface tension characteristics were evaluated using the pendent drop method to determine the difference in the contact angle properties.

3.6.1 X-Ray Diffraction (XRD)

X-ray powder diffraction (XRD) is a rapid analytical method primarily used for the phase identification of a crystalline material which can provide information on cell unit dimensions. The X-ray diffractometer consists of three basic elements, an X-ray tube, a sample holder, and an X-ray detector. X-rays are generated in a cathode ray tube by heating a filament to produce electrons, accelerating electrons to the target by applying a voltage, and bombarding the target material with electrons. Constructive interference of a monochromatic beam of X-rays scattered at specific angles from each set of lattice planes in a sample produces XRD peaks. The atomic positions within the lattice planes determine the peak intensities. The phase of particles was estimated by an X-ray diffractometer (Malvern panalytical Seris-3) using Cu K-radiation wavelength $\lambda=1.154$ (Å), and the scan step size was 0.02 deg/min with 0.02 steps per degree. Bragg's law, which relates the wavelength of the X-rays to the interatomic spacing, describes the diffraction of X-rays by a crystal and is given by the following equation:

$$2dsin\theta = n\lambda \tag{3.2}$$

Where, d denotes the perpendicular distance between adjacent planes, θ is the angle of incidence or Bragg angle, λ is the wavelength of the beam, and n denotes an integer number known as the order of reflection and is the path difference in terms of wavelength between waves scattered by adjacent planes of atoms. The standard

database for XRD patterns (JCPDS database) is used for phase identification of a wide range of crystalline phases in samples.

3.6.2 Scanning Electron Microscopy (SEM) and EDS

The morphology of the magnetic particle, additives, and after adding the additive was observed by Scanning Electron Microscopy (SEM) (JEOL-63807A) with an accelerating voltage of 15 kV. SEM images provide topographical, morphological, and compositional makes features invaluable in a variety of scientific and industrial applications. The chemical compositions were investigated using Energy Dispersive X-Ray Analysis *(EDX)* attached to the SEM.

3.6.3 Magnetorheometer

Rheological responses of the MR fluids were measured using a commercial rheometer (MCR 300, Anton Paar, Germany) with a controlled magnetic field supported by an MR device (MRD 180) as shown in Fig.3.9. While a lower plate is stationary, an upper plate rotates at the same time a torque is measured. The magnetic field applied is perpendicular to the flow field which is parallel to the rotating axis. A controlled shear rate (CSR) mode over a shear rate range of 0.01–200 1/s is applied for all tests under different magnetic field strengths.
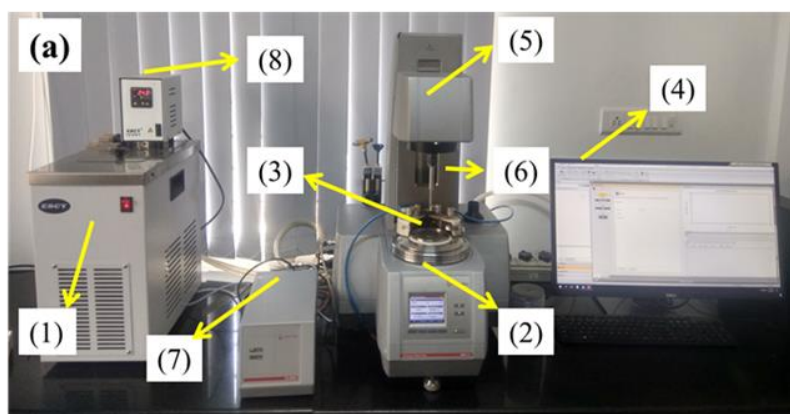
Fig.3.9 Magnetorheometer

To control temperature, a water circulator was adopted to the MRD 180. The coil current and magnetic field strength were tuned via the software using a separate

control unit. The RheoPlus software controls the magnetic field strength across the plates holding the MR sample by adjusting the electric current through the coil. Magnetic field was applied perpendicular to the parallel plate system. Therefore, the magnetic field in the gap between two plates is a function of electric current passed through the coil. The volume of MR fluid in the gap was taken primarily as 0.3 mL. It can be noted that the use of parallel-plate geometry has the advantage of easier operation and cleaning procedures when compared to concentric cylindrical geometry. The temperature was set as 25° C throughout the measurements.

3.6.4 Dynamic Testing Machine

The experimental setup of the Dynamic Testing machine (GEOTRAN) consisted of a load cell, LVDT, DAQ, and Signal Generator, as indicated in Fig 3.10. The frequencies, peak to peak displacement, and sedimentation testing of the MRF in the MR damper were set at 1.5 Hz of 5mm at 0hr, 24hr, and 72hr. The applied current was changed from 0 and 0.4 A. The saturation of the applied current to the MR piston coil was limited to 0.4A.
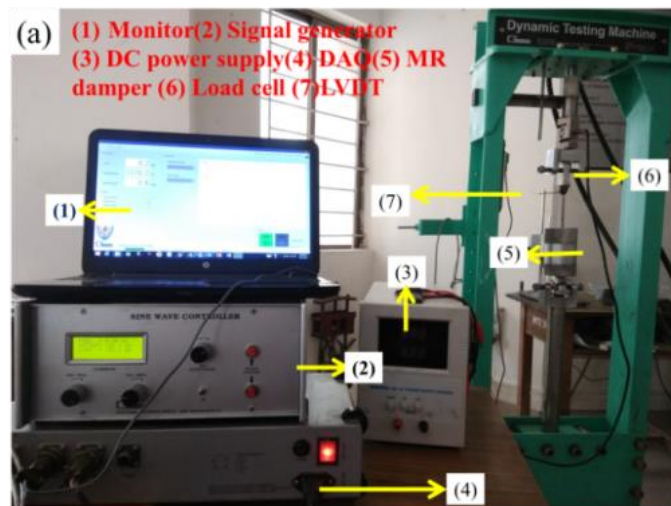
Fig.3.10 Dynamic Testing Machine

3.6.5VibratingSampleMagnetometer

Saturation properties, magnetization versus magnetic field strength (M-H) curve were measured at room temperature with a standard commercially available liquid sample holder (i.e., No- 730935 Kel-F®) from (Lakeshore, USA, Model 7407). Fig.3.11(a)

and (b) show a schematic representation of VSM measurements and dimensions of the liquid holder. The MR fluid was poured inside the holder in such a way to minimize the small air bubbles and filling into the bottom cup completely to avoid the slushing of the liquid due to sample vibration. Then, the MRF sample was positioned with a plastic straw in the horizontal X-Y and vertical Z-axis planes, and the sample was vibrated vertically about the center point of the coil.
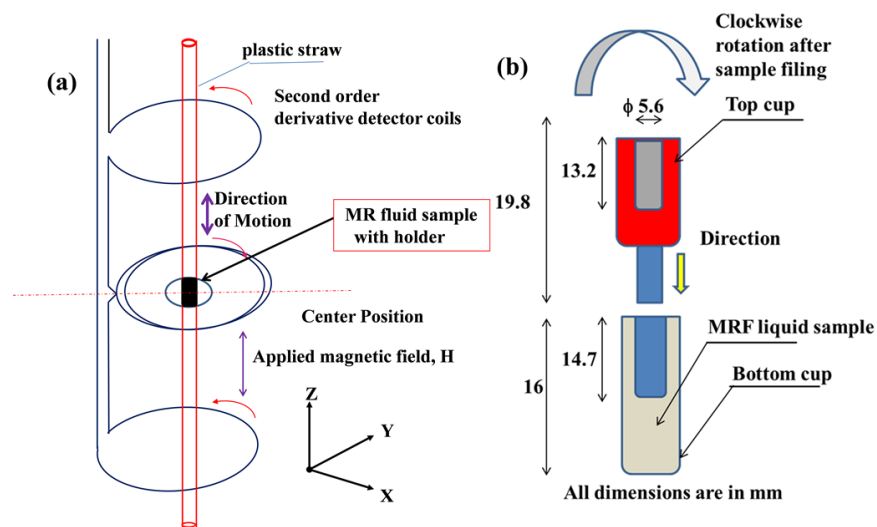
Fig.3.11 (a) Pic up coil geometry (b) Standard liquid sample holder for MRF (permission from Lakeshore cryotronics)

The voltage is induced across the pick-up coil, and is proportional to the magnetic moment of the MR fluid material. A hysteresis loop shows the relationship between the induced magnetic flux density (B) and the magnetizing force (H). It is often referred to as the B-H loop. Magnetic permeability is used to describe the capability of materials to be magnetized when placed in a magnetic field. Materials with higher relative permeability, for example, ferromagnetic materials, can present higher magnetization under a magnetic field. Based on the susceptibility (χ_m) of each sample measured from VSM, the relative magnetic permeability (μ_r) can be calculated by the definition

$$\mu_r = 1 + \chi_m \ldots \ldots \ldots \quad (3.3)$$

where μ_r is the relative magnetic permeability of the material. The relative magnetic permeability μ_r, is the ratio of the magnetic permeability of a specific material to that of free space. The magnetic permeability of the free space is defined as the permeability constant, $\mu_0 = 4\pi \times 10^{-7}$ H/m $^{-1}$. The magnetic characteristics of the magnetic particles were examined by vibrating sample magnetometer (VSM) (Model 7407, Lakeshore, U.S.A.) in the powder state. The measurements were carried out at room temperature.

3.6.6 Visual Inspection Sedimentation

MR suspensions tend to settle due to the density difference between the particles and fluid Visual inspection consists of a comparison of heights (H_d) of the dispersed phase and settled phase along different time intervals to give an idea about the rate of settling of iron particles in the as shown in Fig. 3.12. The sedimentation ratio can be evaluated using the formula

$$\text{Sedimentation ratio } (\%) = \frac{\text{Volume of Supernatant Fluid}}{\text{volume of Total Suspension}} \times 100 \qquad (3.4)$$
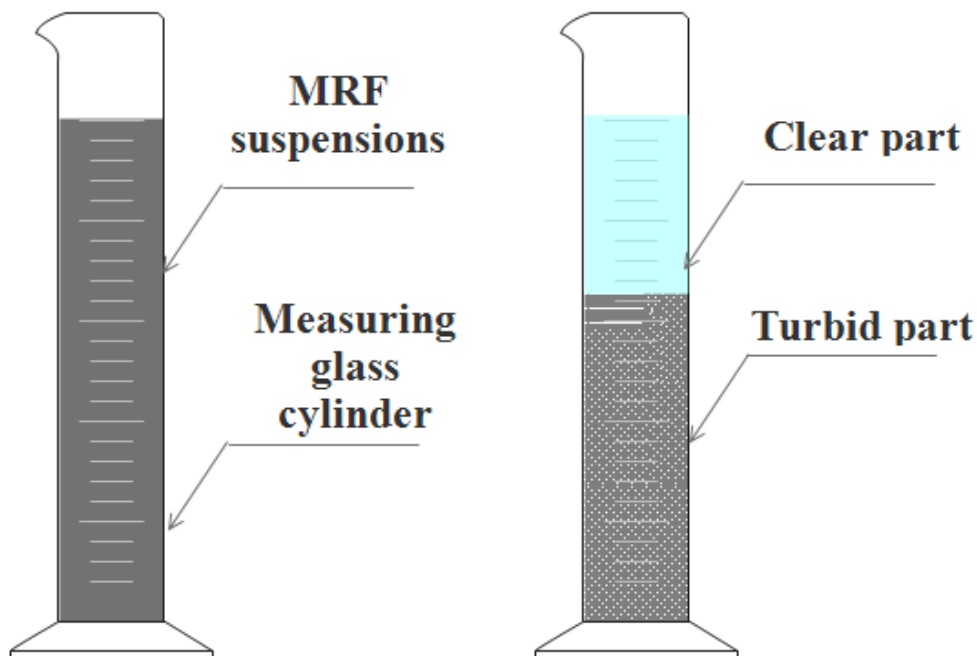
Fig.3.12 Visual sedimentation observation

3.6.7 Surface tension investigations
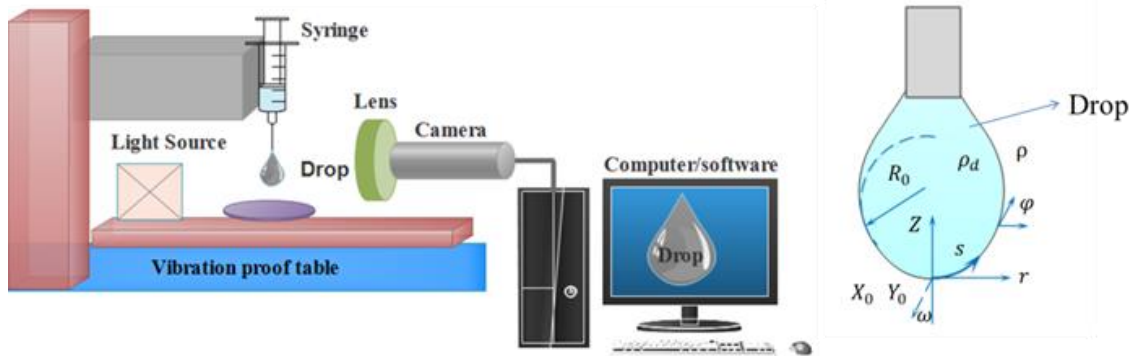
Fig.3.13 Schematic setup for the pendant drop method to measure the surface tension

The basic experimental set-up of the pendant drop method is shown in Fig.3.13 which consists of the needle with the syringe, a camera, and a source of light (Kruss drop shape analyser DS-100). Here, needles with diameters of either 0.8 mm or 0.5 mm were used. All measurements were made in a transparent glass substrate with dimensions of 20 mm× 20 mm × 10 mm mounted in a base table. As can be seen from the figure, camera was used to capture an image of a liquid drop that hangs on a dosing needle and subsequently analyze it with the kruss advance software module. In the pendant drop method, surface tension was calculated from the shadow image of a pendant drop using shape analysis of drop. A pendant drop at equilibrium obeys the Young–Laplace equation (3.5), which relates the Laplace pressure across an interface with the curvature of the interface and the interfacial tension γ.

$$r\left(\frac{1}{R_1} + \frac{1}{R_2}\right) = \Delta p = \Delta p_0 - \Delta \rho g Z \tag{3.5}$$

where R_1 and R_2 represent the principal radii of curvature: $\Delta p = p_{in} - p_{out}$ is the Laplace pressure across the interface: $\Delta \rho = \rho_d - \rho$ is the density difference (see Fig. 3.13) and ρ_d , ρ are the drop phase density and continuous phase density respectively.

CHAPTER-4

EFFECT OF ADDITIVES ON RHEOLOGICAL AND SEDIMENTATION PROPERTIES OF CIPs BASED MRF

Magnetorheological (MR) fluid is one of the major constituent elements in structural suspensions and damping characteristics in automobile applications. The major drawback is sedimentation in MR fluids. In the present study an attempt has been done to address the sedimentation issue. The synthesis and characterization of MR fluid in combination with clay and additives leads to improvement in sedimentation rate. The cost-effective MRFp-3 showed better results compared to commercially available MR fluid concerning off/on state shear stress and viscosity. It was also observed that in-house prepared MRFp-3 has better sedimentation than commercially available (LORD-132DG) up to 700 h.

4.1 Introduction

In this study, MR fluid was prepared using carbonyl iron powder mixed with poly-alpha-olefin oil. The detailed composition of MRFs is enlisted in chapter-3 section 3.1. These particular clay additives are known to be used in fluid compositions and act as anti-settling agents, thickening agents, and rheology modifiers. The magneto-rheological activity, sedimentation stability were evaluated and compared with commercially available LORDMRF132DG fluid.

4.2 Results and Discussions

4.2.1 Scanning electron microscopy (SEM) analysis

Fig. 4.1(a)-(e) show the surface morphology, the particle size distribution of raw CIPs and clay additives. As can be seen from the Fig.4.1(a) shows the pure CIPs are spherical and have a smooth surface with a 2-9 μm particle size distribution.Fig.4.1(b) shows the particles size distribution of CIPs varying between 2 to 9 micron. The size and morphology of the MRF additive components can remarkably affect the MRF suspensions in which will connect the CIPs particles for improving dispersion stability. It can be seen in Fig.4.1(c) that the layered, ribbon-like structure

morphology is typically observed in garamite 1958 organo-clay. Similarly, claytone APA and baragell 10 additive particles look like large and small scales in the form of sheet aggregates morphology which can be observed from figure 4.1 (d) and (e), respectively (Keyoonwong et al. 2012).
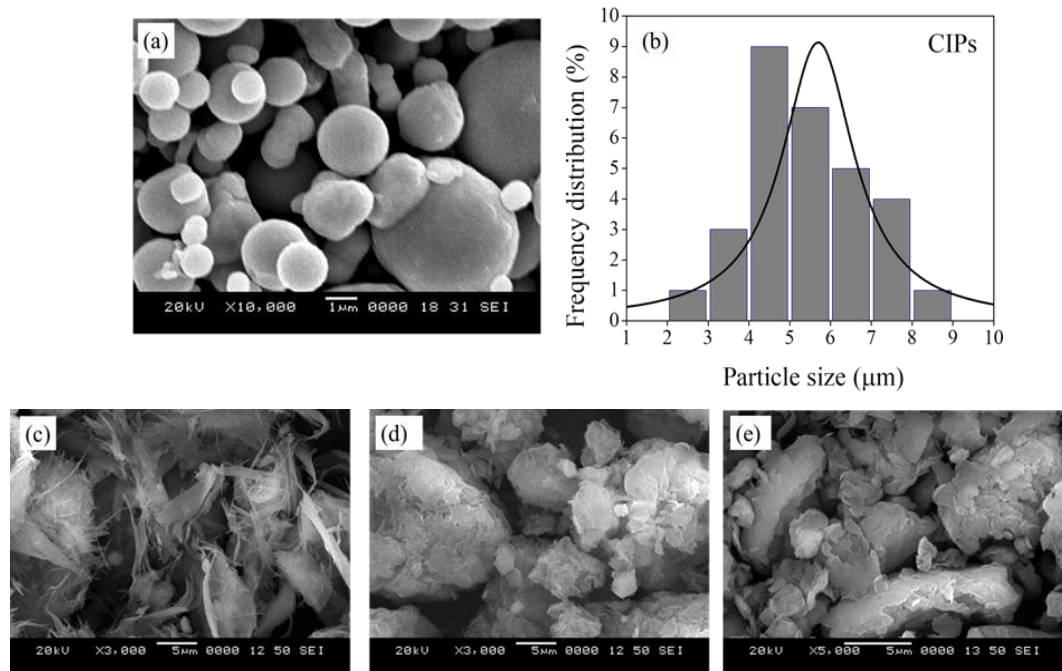
Fig.4.1 SEM micrographs (a) pristine CIPs, (b)particle size distribution curve (c) Garamite 1958,(d Claytone APA, and Baragell (e) 10

4.2.2 X-ray Diffraction (XRD) analysis

The crystalline structures of the as-received carbonyl iron particles were studied by X-ray diffraction (XRD). It can be seen from Fig. 4.2 that CIPs demonstrated by the strong peaks at 2θ values 44.6°, 64.9°, and 82.3°, respectively were assigned to (110), (200), and (211) lattice planes, respectively of the body-centered cubic (bcc) iron (JCPDS card no 65-4899) (Guo et al. 2018a). BCC(α-phase) Fe exhibits phase soft magnetic behaviour which is needed for MR fluid.
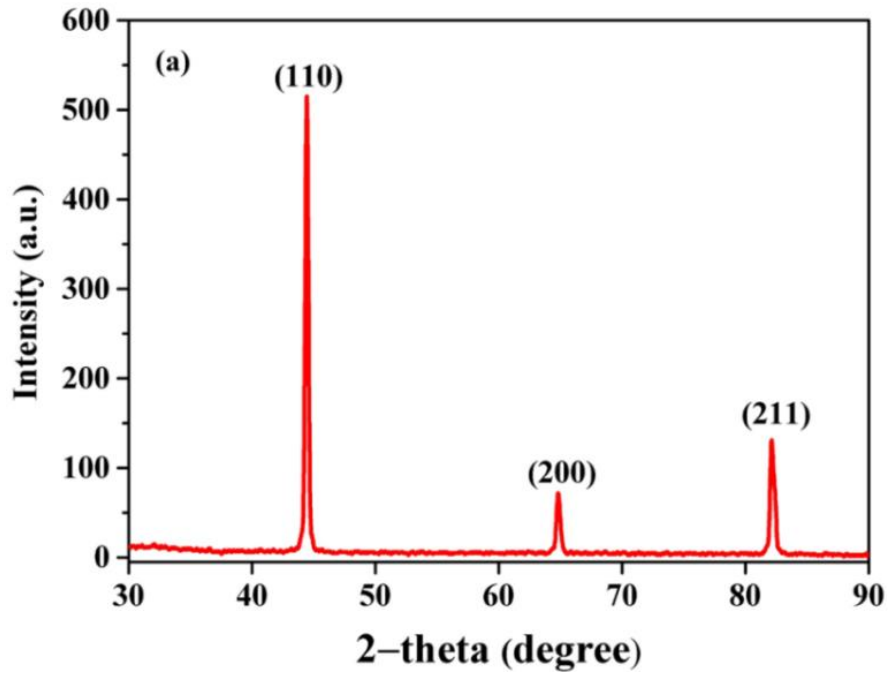
Fig.4.2 XRD pattern of Carbonyl iron powders

4.2.3 Superconducting Quantum Interface Device (SQUID) analysis
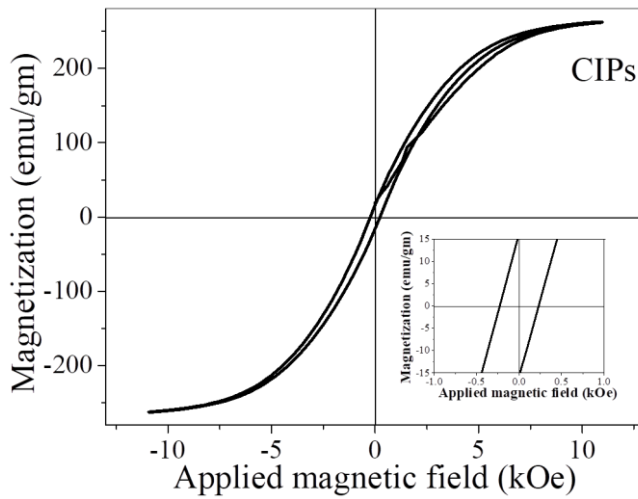
Fig.4.3 Magnetic hysteresis loops of CIPs

Magneto-static properties were evaluated in the field range, from −10 kOe to 10 kOe by SQUID and the resulting hysteresis loop of CIPs as shown in Fig. 4.3, is very narrow indicating that the particles possess soft-magnetic property. The specific

saturation magnetization (σ_s) was about 250 emu/g for the CIPs which is an important crucial factor. This is desirable for improving the properties of MRFs and the coercivity (H_c) of the particles was found to be 0.5kOe(Zhou et al. 2012).

4.3 Rheology flow curves

4.3.1 Off-state rheology
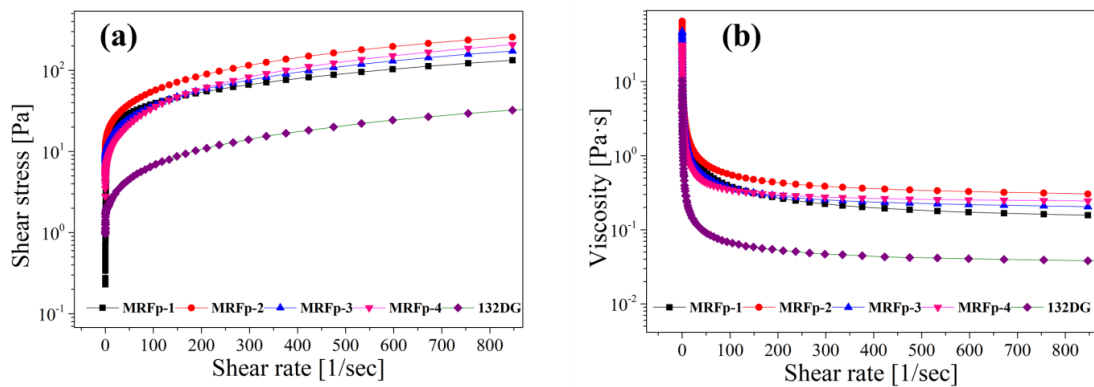
Fig.4.4 At zero magnetic field applied (a) shear rate flow curve (b) shear viscosity

The rheological measurements at temperature 25°C are shown in Fig. 4.4(a) and (b). Variation of off-state shear rate v/s shear stress and shear rate v/s viscosity with the shear rate varying from 0.1 to 800s^{-1} for MRF samples without any applied magnetic field shows Newtonian fluid behaviour, where the viscosity decreases with increasing shear rate,exhibiting shear thinning behaviour (Choi et al. 2006). From Fig.4.4(a), it is observed that the value of shear stress obtained for Lord-132DG is relatively low. In the case of MRFp-2, MRFp-3 and MRFp-4, shear stress is relatively higher, This behaviour is due to presence of additives in the base oil. In the case of MRFp-1, it is found that shear stress is comparatively low, which suggests the absence of additives in the base fluid. The value of off-state viscosity obtained for Lord-132DG is relatively low. In the case of MRFp-2, MRFp-3 and MRFp-4, off-state viscosity is relatively higher, and it was found that it is based on the presence of additives in the base oil. In the case of MRFp-1, it was found that viscosity was comparatively low, which suggested the absence of additives in the base fluid as shown in Fig.4.4(b)
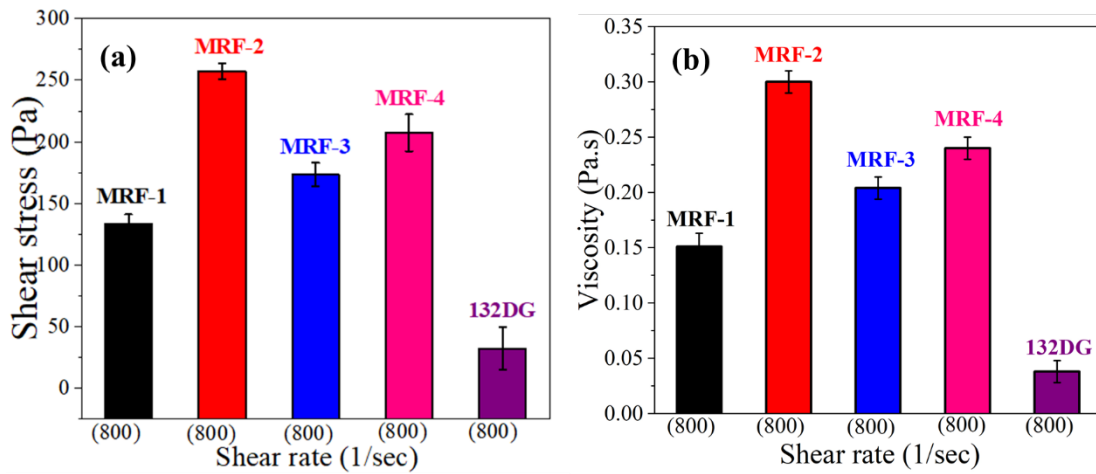
Fig.4.5 Bar graph of (a) Shear stress flow curve and (b) shear viscosity at zero magnetic field applied

Fig. 4.5 (a) and (b), show bar graph of shear rate v/s shear stress and shear rate v/s shear viscosity in terms of shear rate which varied from 0-800(1/sec) for each of the MR fluids. From the graph, it is observed that the minimum shear stress value seen from Lord-132 DG is 25 Pa which is very low compared to MRFp-1, MRFp-2, MRFp-3, and MRFp-4 which is (127, 252, 172, and 210) Pa, respectively. It is also evident that by increasing shear rate, the shear stress increases and viscosity decreases, and viscosity obtained from Lord-132DG is 0.025 Pa-s which is much lower than MRFp-1, MRFp-2, MRFp-3, and MRFp-4 which is (0.15,0.31,0.20, and 0.225) Pa, respectively. From bar graphs 4.5 (a) and (b) it is observed that off-state shear stress and viscosity values are found to be lower in commercially (Lord-132DG) MRFs when compared with MRFp-1, 2, 3, and 4. Hence, the MR fluids with added additives increase the off-state shear stress and viscosity.

4.3.2 On-state Rheology

Fig. 4.6(a) and 4.6(b) show the variation of magnetic flux density v/s shear stress and magnetic flux density v/s viscosity for synthesized MR fluids under constant shear rate (100 sec^{-1}). The values of shear stress under the definite condition are similar for all the MR fluid samples. The differences in the shear stress values are appeared when the magnetic flux density was larger than 0.2T. The highest level of shear stress plots was obtained for MRFp-1, which suggests low off-state viscosity and high saturation

magnetization. From Fig 4.6 (b), it is observed that the range of shear viscosity values under the specified condition are similar for all the fluids. The difference in the viscosity values was observed when the magnetic flux density was greater than 0.2T. The highest level of viscosity plots was obtained for MRFp-1, which suggests comparatively higher viscosity and high saturation magnetization. Fig. 4.6(b) shows the magneto-rheological viscous effect of synthesized MRFs in which on–state shear viscosity increases by increasing the magnetic field density from 0 to 0.7 Tesla.
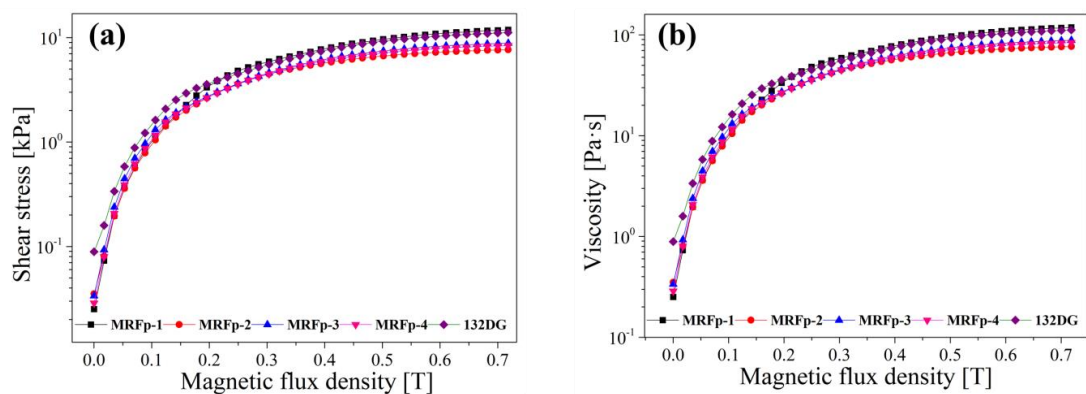
Fig.4.6 Magnetic field sweep (a) Shear stress (b)Viscosity

Due to the magnetic field, the particles become polarized and thereby organized into chains of magnetic particles within the fluid. The action of the chain of particles increases the apparent viscosity or flow resistance of the MR fluid. The magnetic CIPs dipole interaction-moment of a particle is given by the equation $\mu = VxB$, where $V = \pi d^3/6$, where V is the volume of the particle, and d, x and B represent the diameter, magnetic saturation of the CIPs and applied magnetic field from 0 to 0.7 Tesla, respectively.

Fig. 4.7(a) and (b), a show bar graph of magnetic flux density v/s shear stress and magnetic flux density v/s viscosity at a constant shear rate of 100 (1/sec) for each of the MR fluids. From Fig. 4.7(a) it is observed that the maximum shear stress obtained from MRFp-1 is 12kPa which is greater than the the values obtained for MRFp-2, MRFp-3, MRFp-4, and Lord 132 DG which are (7.8, 8.4, 8.2, and 11.7) kPa, respectively. It is also evident that, shear stress increases, and viscosity increases as

the magnetic flux density increases. Viscosity obtained from MRFp-1 is 120.12 Pa-s which is relatively higher than the viscosities obtained from MRFp-2, MRFp-3, MRFp-4 and Lord-132DG which are (79.2, 89.7, 81.3 and 111.2) Pa-s, respectively.
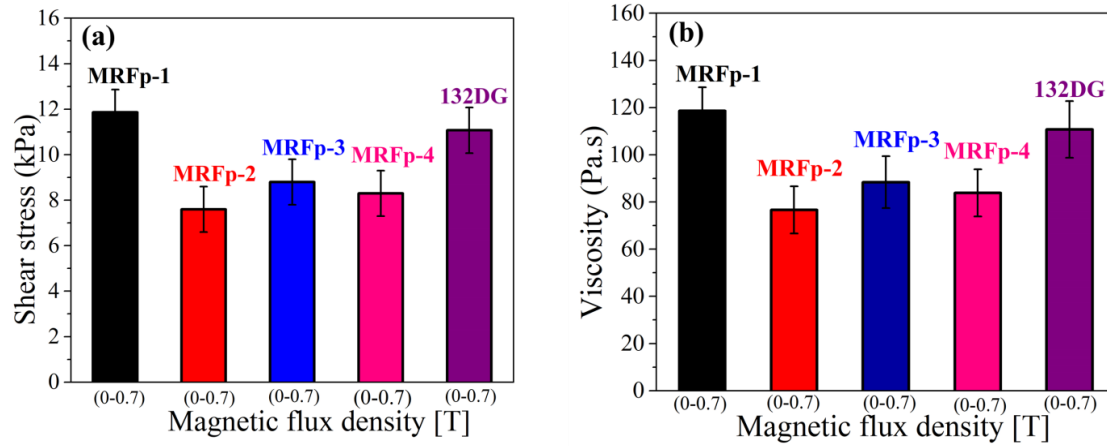
Fig.4.7 Bar graph of (a) magnetic flux density v/s shear stress and (b) magnetic flux density v/s viscosity

From Fig. 4.7 (a) and (b), it is found that on-state shear stress and viscosity values of MRFp-1 are very close to that of Lord-132DG fluid rather than MRFp-2, MRFp-3, and MRFp-4. Hence, the MRF fluids with added additives decrease the on-state shear stress and viscosity.

The rheological flow curves was done for the shear stress versus shear rate were measured using rheometer for fitting Bingham plastic [BP] constitutive model, which is a frequently used model in MRF suspensions because of the development which is organized into chains of CIPs magnetic particles within the fluid. The yield stress of Bingham plastic [BP] constitutive is governed by the general equation.

$$\tau = \tau_y + \eta\dot{\gamma} \ \ \tau \geq \tau_y \tag{4.1}$$

$$\dot{\gamma} = 0 \ \ \ \tau < \tau_y \tag{4.2}$$

The parameters of the BP model are as follows: τ is shear stress, τ_y represents yield stress and is a function of magnetic field intensity [H] η which denotes shear viscosity and $\dot{\gamma}$ is the shear rate.

4.4 Sedimentation analysis
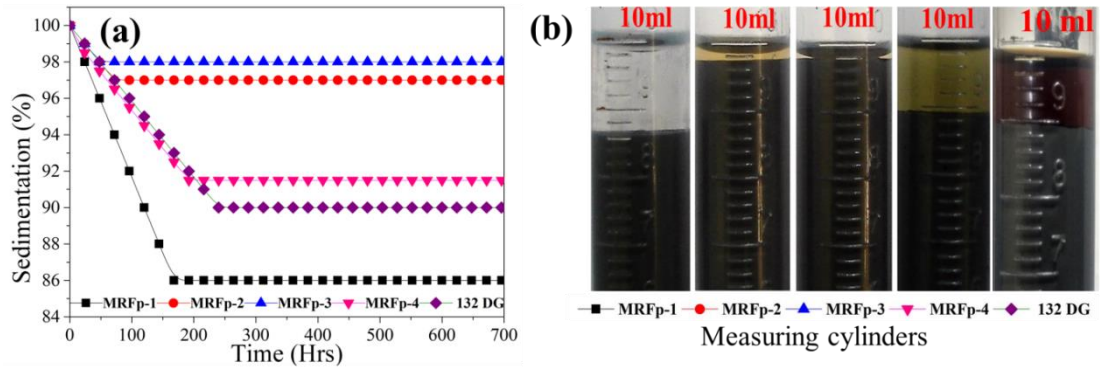
Fig.4.8 Visual inspection (a)sedimentation (%) v/s Time (hrs) (b) settling layer

Fig. 4.8(a) and (b), show the sedimentation stability curves of prepared MR fluids. The MRFp-1 based fluid exhibited a quicker sedimentation rate than the MRFp-2, MRFp-3, MRFp- 4, and Lord-132DG based suspension, which suggests that the sedimentation dispersion stability of the MRFp-1 has pure CI-based suspension. In the case of MRFp-2, MRFp-3 and MRFp-4, additives of claytone APA, garamite 1958, and baragel are present in the suspension, respectively, which creates a light gel in PAO oil limits the settling of iron particles and improves the anti-settling stability of prepared fluids. From Fig.4.8(a), it is evident that the MRFp-2, MRFp-3, MRFp-4, and Lord-132DG has a sedimentation ratio of 97, 98, 92, and 90(%), respectively, and have relatively low settling rate of particles during static settling test compared to MRFp-1(86%) which was observed during approximately 700 hrs (29 days) of sedimentation tests under static storage of synthesized MR fluid without disturbance. The general equation for sedimentation velocity was estimated by Stoke's law given by (C Berg 2010)

$$v_\infty = d^2(\rho_p - \rho)g/(18\mu) \quad (4.3)$$

Where v_∞ is the terminal velocity, ρ_p represents particle density, ρ denotes the carrier liquid density, d represents the particle diameter, μ represents the viscosity of the medium and g is the gravitational acceleration. Sedimentation ratio can be determined by placing cylindrical measuring cylinders at 27°C given by the general

83

equation, Sedimentation (%) = $\nabla B/B \times 100$ where, ∇B is the length of the turbid part and B is the total length of the MR fluid. The synthesized MRFs of 10 ml was transferred to a 10 ml graduated measuring cylinder and placed in static storage without any disturbance (Chuah et al. 2015). It was found that a clear layer was formed between the carrier medium and magnetic particles for a period of 29 days as shown in Fig.4.8(b).

4.5 Summary

The advantage of producing low-cost MR fluids systems makes them ideal substitutes for commercially available MRFs. As can be observed the MRFp-2, 3, and 4 have slightly low shear rate v/s shear stress and shear rate v/s viscosity at the applied magnetic field (0 to 0.7 Tesla) when compared to LORD 132 DG. The results reveal that as the three different clay additives, including claytone APA, baragell, garamite 1958, and friction reducers are decreases the particles settling which can improve the sedimentation stability. The dynamic yield stress of MRF was found to increase with applied magnetic field strength due to interaction among the particles, which depends on the saturation magnetization of the magnetic particles. Thus, the present study highlights the importance of the additives and their concentration in the fluid in evaluating the cost effective of MRFs.

CHAPTER-5

SEDIMENTATION, RHEOLOGICAL, AND DAMPING FORCE CHARACTERISTICS OF CIPs BASED MRF WITH/WITHOUT ADDITIVES

In this chapter, description regarding how the MRF samples were prepared using pure carbonyl iron particles (CIPs), CIPs/claytone APA/molyvan 855 additive, and friction reducer is dispersed in Poly-Alpha-Olefin (PAO) oil is given. The scanning electron microscopy (SEM) revealed that the claytone additive morphology looks like a surface abundant in small-folds, which connect the gaps between the spherical pure CIPs and prevent sedimentation in the MRF. The magnetic saturation properties were investigated through the vibrating sample magnetometer (VSM). The pure CIPs MRF showed (M_s) value as 146.12 emu/g and the CIPs/claytone APA/molyvan indicates (M_s) as 55.12 emu/g. The magnetorheological flow curves, such as shear stress and viscosity as a function of shear rate, were investigated for the MRF samples through the magneto-rheometer.The sedimentation analysis of the MRF was observed by visual inspection and it was seen that the CIPs/claytone APA/molyvan improved the sedimentation rate more than the pure CIPs MRF. Finally,the experimental characterization of the prototype mono-tube MR damper was carried out using the hydraulic dynamic testing machine at 1.5Hz frequency for damper peak-peak displacement length of $\pm$ 5 mm at three intervals of 0hr, 24hr, and 72hr in damper to assess the effect on damping force for the prepared MRF samples against the sedimentation rate.

5.1 Introduction

A large density difference between a non-magnetic carrier medium and a dispersed magnetic phase causes the sedimentation problem. For this reason, the addition of additives to MRF suspensions is an effective method to reduce the sedimentation stability rate. Most of the studies reported on MRF preparation had less focus on MR damper performance against the settling of the MRF.

In the present chapter the effect on sedimentation stability, magnetic saturation, and magneto-rheological properties of pure CIPs, CIPs/claytone/molyvan 855 additive, and friction reducer MRF are examined. The detailed composition are enlisted in the preparation of MRFs with and without additives and shown in table 3.2 chapter 3. Besides, the MR damping performance was investigated and compared at three-time intervals (0, 24, and 72 hours) without disturbance of both the MRFs using a mono-tube MR damper.

5.2 Materials and their chemical structures

Poly-alpha-olefin (PAO) oils are hydrogenated olefin oligomers/synthetic hydrocarbon, which are synthesized by catalytic polymerization of linear alpha-olefins. PAO fluid commonly called spectrasyn poly-alpha-olefin fluid was purchased from (Exxon Mobil Chemical Co.) as a base fluid. Synthesis involved mainly two steps. In the first step, the synthesis of a mixture of oligomers that are polymers of relatively low molecular weight was done.

Further, after the catalytic process, in the second step involves hydrogenation of unsaturated oligomers. The molecular structure as depicted in Fig.5.1 (a) is a very uniform comb-like structure. Various properties such as high viscosity index, lower pour point, better thermal, and oxidation stability are superior when compared with mineral-based oils. The commercially available Molyvan 855 was received from the Vanderbilt Chemicals, LLC, as a free sample for our research work.

The molyvan 855 is an excellent oil-soluble molybdenum, each component works as a friction modifier/frictional reducer with better anti-wear and anti-oxidant properties, does not contain sulfur or phosphorus elements, and used in lubricants. Fig. 5.1(b) shows the chemical structure of Molyyan 855, having four components, and the MO group is responsible for the adequate friction-reducing agent. BYK Additives and Instruments provided the free sample of claytone APA for our present work, and the chemical structure is shown in Fig.5.1(c). Claytone APA is modified montmorillonite used as a rheology modifier additive generating excellent properties such as soft sediment and anti-settling agents. The recommended application of this clay in paints,

inks, and adhesives. Claytone APA is self-activating and readily dispersible for low to high polarity systems which includes alcohols, esters, and glycols.
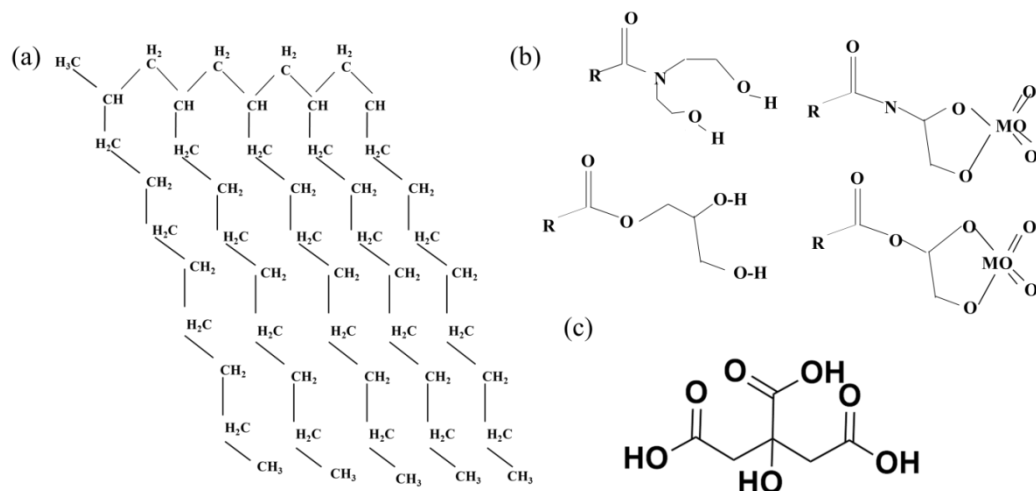
Fig.5.1 Chemical structure of (a) poly-alpha-olefin oil (Exxon Mobil Chemical Co) (b) molyvan 855 (R.T.Vanderbilt chemicals) (c) claytone APA

5.3 Results and Discussion
5.3.1 SEM and EDS Analysis

Element	Weight %	Atomic %
O K	0.99	3.38
Fe K	99.01	96.62
Totals	100.00	
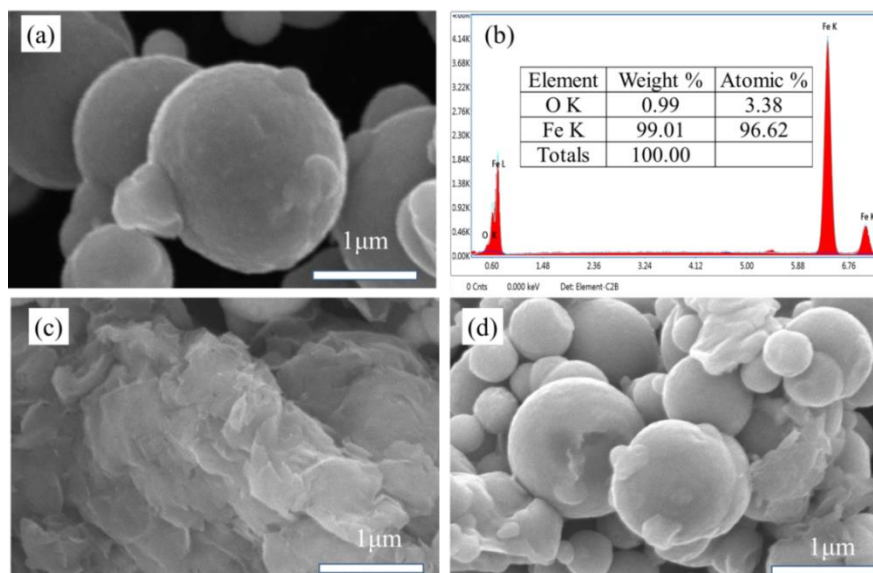
Fig.5.2 Micrographs of (a) pure CIPs, (b) EDS analysis, (c) claytone APA, and (d) CIPs/claytone APA

Fig. 5.2(a) represents the morphology of the CIPs, which possess smooth surfaces and are spherical in shape. The energy dispersive spectroscopy of the pure CIPs shows that they have Fe (99.02 %) and O (0.11 wt %) present with strong intensities. Fig. 5.2(b) confirms that the CIPs are soft magnetic. Fig. 5.3(c) of the raw claytone APA shows an agglomerated structure with a surface abundant in folds. Fig. 5.2(d) shows that claytone APA occupies the interspaces between the CIPs or is attached to the CIPs, which reduces the sedimentation rate of the claytone APA- based MRFs.

5.3.2 VSM Analysis
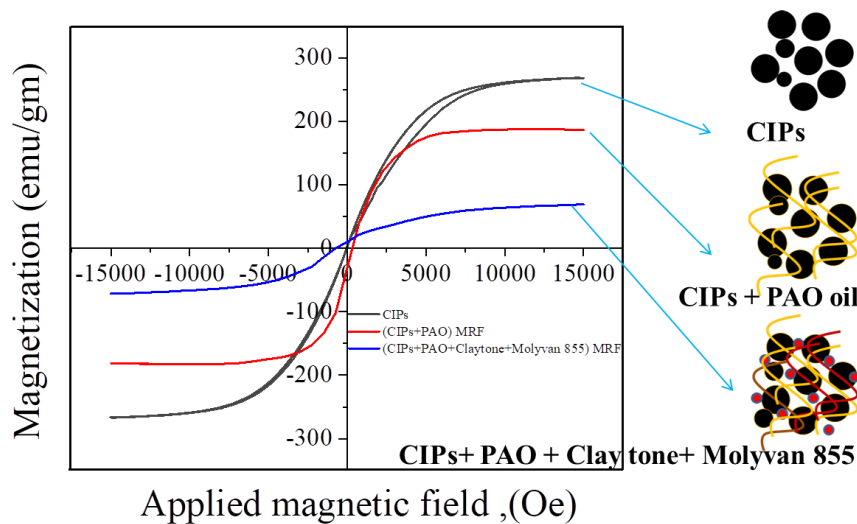
Fig.5.3 Hysteresis loop of liquid samples from the VSM measurements

Fig. 5.3 shows the plot magnetization versus applied magnetic field (M vs. H) curve of the CIPs and CIPs/claytone APA-based MRFs, which were measured using the vibrating sample magnetometer in the applied magnetic field varying from −15000 to 15000 (Oe) at room temperature. The magnetic saturation (M_s) of the pure CIPs MRF was found to be 146.53 emu/g higher than that of CIPs/claytone APA (55 emu/g). The M vs. H curves indicate a big difference in saturation magnetization. Due to the presence of claytone APA additive, possess weak MR effect due to reduction in saturation magnetization compared with pure CIPs based MRF (Sidpara et al. 2009b). In the case of additives added based MRFs, the effect of 1wt.% of Claytone APA and

1 wt.% Molyvan 855 additive are added while preparing MRFs suspension. On the other hand, these magnetic saturation differences are related to differences in the densities of magnetic CIPs in the samples. The density of CIPs in the liquid samples was less than for the bare CIPs because they are dispersed in a liquid suspension. In other words, the actual mass of CIPs in the liquid samples was smaller than (CIPs+PAO+claytone APA), so the calculated saturation magnetizations (emu/gm) are reduced. Table 5.1 shows the properties of both the MRF samples by VSM analysis.

Table 5.1 Magnetic Properties of the Prepared MR Fluid Samples

Parameters	CIPs-based MRF	CIPs/claytone APA MRF
Coercivity (emu/g)	386.46	351.14
Magnetic saturation (emu/gm)	146.12	55.24
Maximum field (oe)	15,000	15,000
Retentivity (emu/gm)	0.10795	0.001417

5.4 Rheology Analysis

Fig.5.4 (a) represents shear stress versus shear rate ranging from 0.01 to 500 [1/sec] on a log-log scale for pure CIPs (closed symbols) and CIPs/claytone APA (open symbols)- based MRFs subjected to different magnetic field strength (0 to 255 kA/m) measured by a rotational twin drive MCR-701 Rheometer. It was found that in absence of magnetic field strength, the shear stress of the CIPs and CIPs/claytone APA MRFs exhibited a non-linear relationship and increases with shear rate which exhibits typical of non-Newtonian fluid behaviour. This might be due to the high particle concentration and residual magnetization of CIPs. With increasing magnetic field strength, the shear stress of the both pure CIPs and CIPs/claytone APA MRF also increased. Fig. 5.4(a) indicates that at (255kA/m) magnetic field strength is imposed, the shear stress values were about 15,100 Pa and 10,200 Pa for pure CIPs and CIPs/claytone APA MRF samples at a maximum shear rate of $500s^{-1}$, respectively. Both the MRF samples represented typical Bingham plastic model fluid behaviour when the magnetic field strength was applied as given by Eq. (5.1). This

was due to the formation of a robust column particle structure because of the dipole-dipole interaction between the adjacent magnetic particles under the application of the magnetic field (Kwon et al. 2013).

$$\tau = \tau_y + \eta_p \dot{\gamma}, \ \tau \geq \tau_y, \qquad \dot{\gamma} = 0, \ \ \tau \leq \tau_y. \tag{5.1}$$

Where τ_y represents the dynamic yield stress $\dot{\gamma}$ given by shear rate, τ represents the shear stress, and η_p is the plastic viscosity.
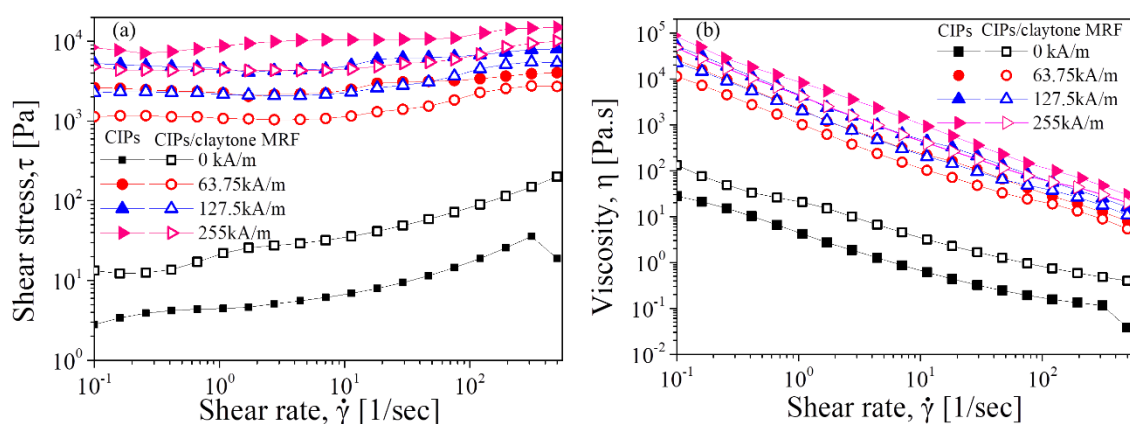
Fig.5.4 Rheology flow curves (a) shear stress (b) viscosity as a function of shear rate

Fig. 5.4(b) clearly shows that the viscosity of the pure CIP MRFs is slightly lower than that of the CI/claytone APA MRF at zero magnetic field strength. The viscosity decreasesd due to the change in the internal structure under shear deformation. It was due to the shear-thinning behavior effect for both the MRF samples. When the magnetic field was further increased, the free rotation of the magnetic particles was restricted, which increased the shear viscosity of the MRF samples due to the formation of chain-like structure.

The relationship between the field-dependent dynamic yield stress and the strength of the magnetic field was fitted by the third-order polynomial equation and depicted in Fig. 5.5(a). A polynomial equation was extracted from this graph to evaluate the yield stress for any arbitrary value of magnetic flux strength between 0 and 255 KA/m. Equation (5.2) was obtained from the least square curve fitting method, wherein the

third-order model provided accurate values with the adj-R^2 values fit method. Particularly at zero magnetic field strength, the yield stress values are positive values as observed from Table 5.2

$$\tau_y = a + bH + cH^2 + dH^3 \qquad (5.2)$$

Where, τ_y is field-dependent yield stress (Pa), H is magnetic field strength in kA/m, and a, b, c, and d are the fit constants.

Table 5.2 Optimal parameters of CIPs and CIPs/claytone APA MRF

Sample name	a	b	c	d	adj-R^2
CIPs MRF	37.388	60.128	0.03793	-1.74162×10^{-4}	0.99
CIPs/claytone APA MRF	199.108	35.48	0.06656	-2.19589×10^{-4}	0.99

A time-dependent field-induced shear stress measurement was performed for pure CIPs and CIPs/claytone APA MRF, as shown in Fig. 5.5, (b) as a Region I for off-state, Region II for on- state, and Region III for off- state. From interval-I / Region I, it can be observed that the magnetic field is in off-state condition, and the exhibited value of the pure CIPs MRF shear stress was to be found to be lower than that of CIPs/claytone APA MRF.
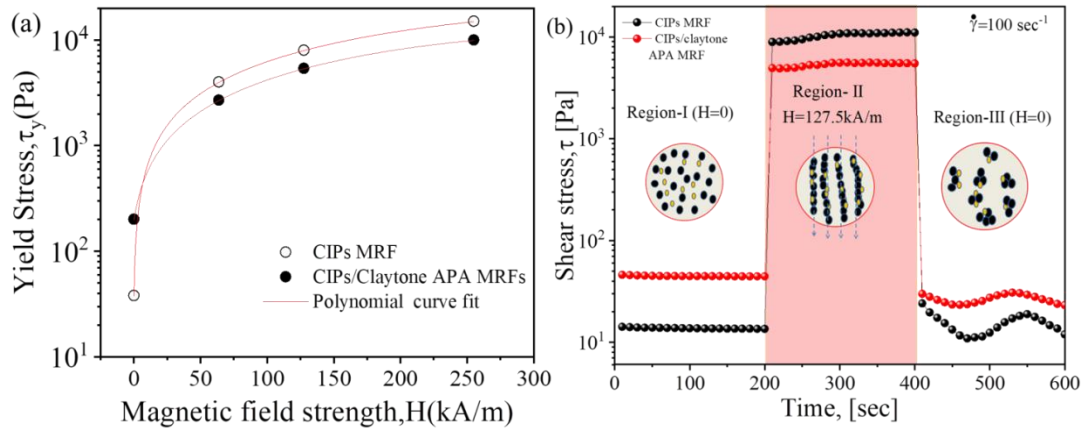
Fig.5.5 (a)Dynamic yield stress as a function of magnetic field strength (H), and (b) shear stress versus time at a constant shear rate γ =100s^{-1}.The MRF of shear stress versus time in three different regions.

In Region II, the magnetic field present was in on-state condition, i.e., 127.5kA/m, and the value of the pure CIPs shear stress was higher than that of CIPs/claytone APA MRFs. The shear stress increased rapidly due to the polarization force of the dipole-dipole interaction of the magnetic particles, which build robust column structures for both the MRFs. It can be seen from region III after the magnetic field was removed in the time 400s to 600s, Since the time scale of the data acquisition was much faster than relaxation time after the magnetic field was turned off, it was observed that there an immediate decline of shear stress curve CIPs MRFs was sinusoidal when compound is the CIPs/claytone APA MRFs. The decrease of shear stress with time was thought to be related to the effect of remanent magnetization, when the magnetic field was at off condition. As a result, column structures formed have not been broken, or the new aggregates might have formed, which indicates the high concentration of CIPs in the MR fluid (Yang et al. 2018). This phenomenon also demonstrated in the inset figure the reversible transformation of microstructure formation of MRFs at off/on/off regions

5.5 Sedimentation Analysis
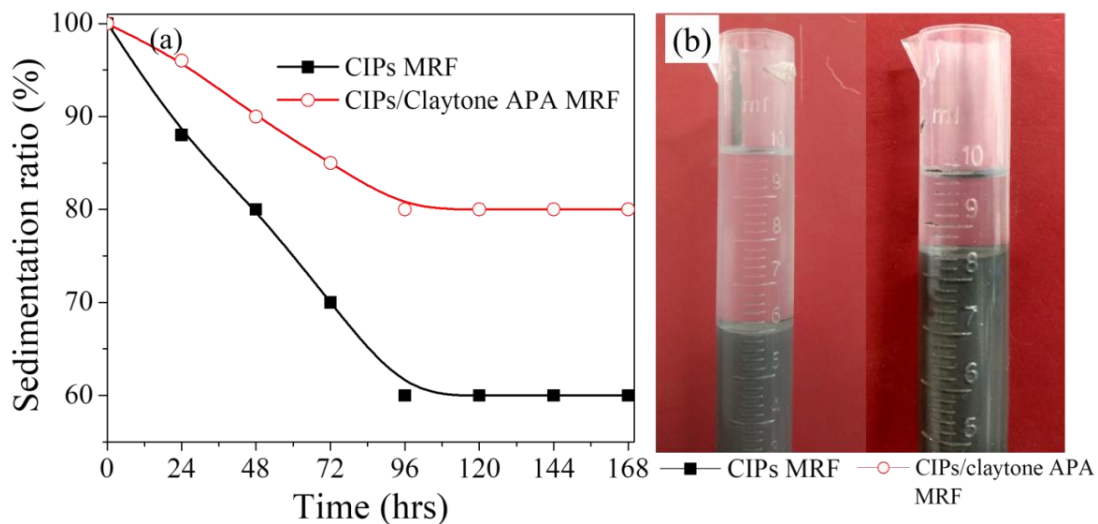
Fig.5.6 (a) Sedimentation versus time in (hrs), and (b) MRF poured after complete settling of pure CIPs and CIPs MRF

Fig.5.6 (a) shows the sedimentation rate of the two types of MR fluids inspected visually. Both the prepared MRFs were poured into a 10 ml cylinder, as seen in Fig. 5.6(b), which shows the complete settlement of the MRFs in 7 days. The CIPs MRF settled down rapidly during the initial period and finally reached a stable value of 60.5%. Subsequently, the sedimentation ratio of the CI/claytone APA MRF became slow due to the presence of additives and the friction reducer, which in turn slowed down the settling velocity of the CIPs, and the sedimentation ratio gradually reached a stable value at 82%. On the other hand, the CI/claytone APA MRF demonstrated a better sedimentation ratio than the pure CIPs MRF until 168 hrs. To find the sedimentation ratio, the equation commonly applied for MRFs is given by Eq. (5.3).

$$R\% = (A/A + B) * 100) \qquad (5.3)$$

Where, R represents the sedimentation ratio, b is the height of the sedimentation MRF, and (A+B) represents the total height of the MRF.

5.6 MR Damper Performance of CIPs filled MRF

Fig. 5.7 shows the damping force phenomenon of the CIPs filled MRF for the first time with a peak-peak displacement of 5 mm and a frequency of 1.5 Hz. Fig. 5.7(a) indicates that on the first day, the MR damper performance showed off-state conditions, and the rebound and compression phase values of the damping force properties were +104.48 N and −114.16 N, respectively. At on-state conditions of 0.4 A, the rebound and compression damping forces increased to +133.64 N and −144.59 N, respectively. Fig. 5.7(b) shows that after 24 hours, the CIPs MRF sedimentation in the MR damper performance showed off-state (absence of magnetic field I=0A) conditions, and the rebound and compression values of the damping force were +89.37 N and −102.12 N, respectively. In on-state (presence of magnetic field I=0.4 A) condition, the rebound, and compression damping forces increased to +117.59 N and −132.34 N, respectively.

From Fig. 5.7(c), it was found that after 72 hours, the CIPs MRF sedimentation in the MR damper performance showed off-state conditions, and the rebound and compression damping force values were +72.25 N and −87.92 N, respectively. At on-state condition of 0.4 A, the rebound and compression damping forces increased to

+107.43 N and −111.18 N, respectively. These results suggest that variation in damping force, as listed in Table 6.3, is higher than the reported values when the applied current was increased from 0 to 0.4 A. It should be noted that the rebound and compression damping force reduces largely as the number of sedimentation days was increased in the CIPs filled MRF
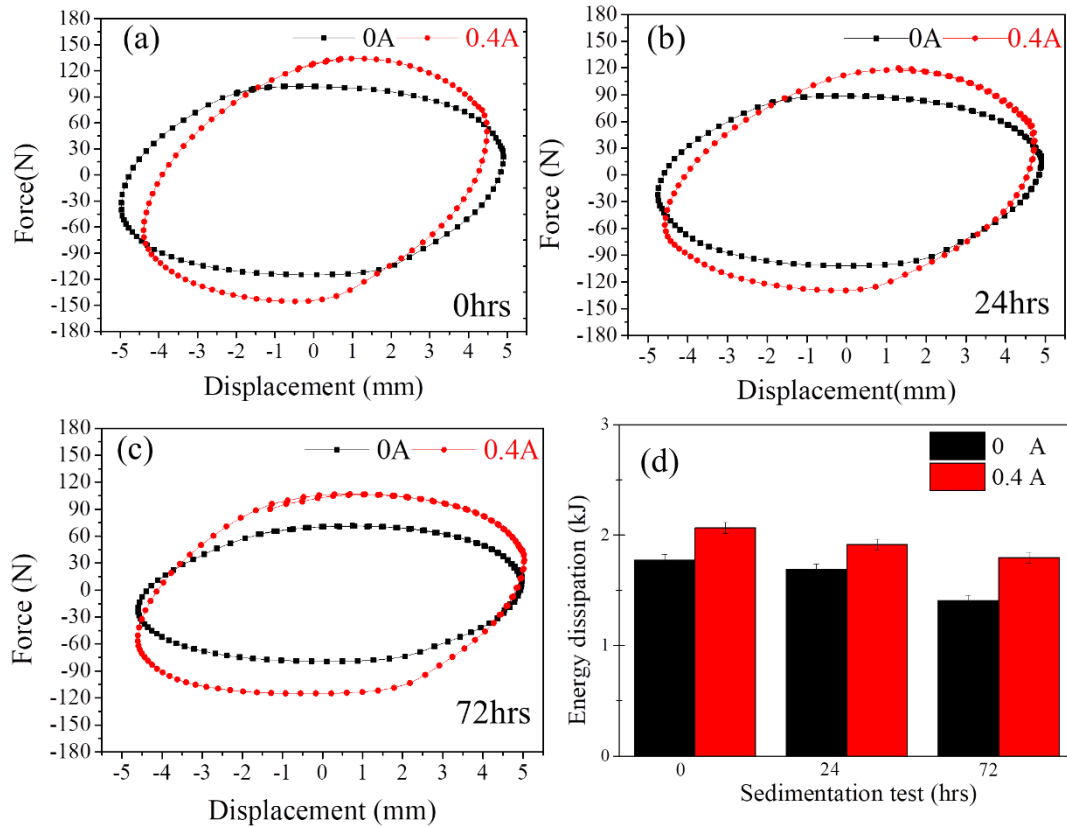
Fig.5.7 Experimental damping force versus displacement of CIPs MRF (a) 0, (b) 24, (c) 72 hours, and (d) energy dissipation for 0 and 0.4A at different sedimentation days

The energy dissipation (E_d) values can be calculated using the area enclosed under force vs. displacement loop. It dissipate more energy as applied current increases, as shown in Fig. 5.7(d) and equivalent damping coefficient (C_e) is given by Eq. (5.4) and (5.5) (Snyder et al. 2001). Also, the energy dissipation decreases as the period of the MRFs in the damper increases due to the effect of the gravitational settling of the CIPs in the MRFs (Hemanth et al. 2017).

$$E_d = \int f(t)\,du \qquad (5.4)$$

$$C_e = \frac{E_d}{\pi f A^2} \tag{5.5}$$

Where A represents amplitude in (m), f is given by frequency (Hz), and F is the damping force (N).

Table 5.3 Damping characteristics of MR Damper CIPs based MRF for Different settling times

Rebound Damping Force (0A) F_{Re}(N)	Compression Damping Force (0A) F_{Co} (N)	Rebound Damping Force (0.4 A) F_{Re}(N)	Compression Damping Force (0.4 A) F_{Co}(N)	Frequency Range (Hz)	Sedimentation Time (Hours)
104.48	114.16	133.64	144.39	1.5	0
89.37	102.12	117.59	132.34	1.5	24
72.25	77.92	107.43	111.18	1.5	72

5.7 MR Damper Performance of CIPs/claytone APA- filled MRF

Fig.5.8 shows the damping force phenomenon of the displacement loop behaviour properties of the CIPs/claytone APA MRF for the first time by filling in a damper with peak-peak displacement amplitude of 5 mm and frequency of 1.5 Hz. Fig. 5.8(a) indicates that on the first day, the MRF damper performance showed off-state conditions (0A), and the rebound and compression damping force values were +97.22N and −134.76 N, respectively.

At on-state conditions (0.4 A), the rebound and compression phase damping forces increased to +116.88N and −144.59 N, respectively. Fig. 5.8(b) shows that after 24 hours, the MRF sedimentation in the MR damper performance showed off-state conditions, and the rebound and compression values of the damping force were +94.21N and −99.26 N, respectively. At the on-state condition of 0.4 A, the rebound and compression damping forces increased to +108.55 N and −115.12 N, respectively. Fig. 5.8(c) indicates that after 72 hours, the MRF sedimentation in the MR damper performance showed off-state conditions, and the rebound and compression values of

the damping force were +80.57 N and −82.61 N, respectively. At the on-state condition of 0.4 A, the rebound and compression damping forces increased to +88.90 N and −94.74 N, respectively. Fig.5.8(d) indicates that the energy dissipation bar graph can be calculated using Eqs. (10) and (11). The CIPs/claytone APA-based MRF in the damper energy dissipated less, damping force was slightly lower as the number of sedimentation days increased than the CIPs based MRF damper. Table 5.4 indicates that the damping force of rebound and the compression strokes of the CIPs/claytone APA MRF-based damper at different sedimentation against time intervals was higher than the reported value.
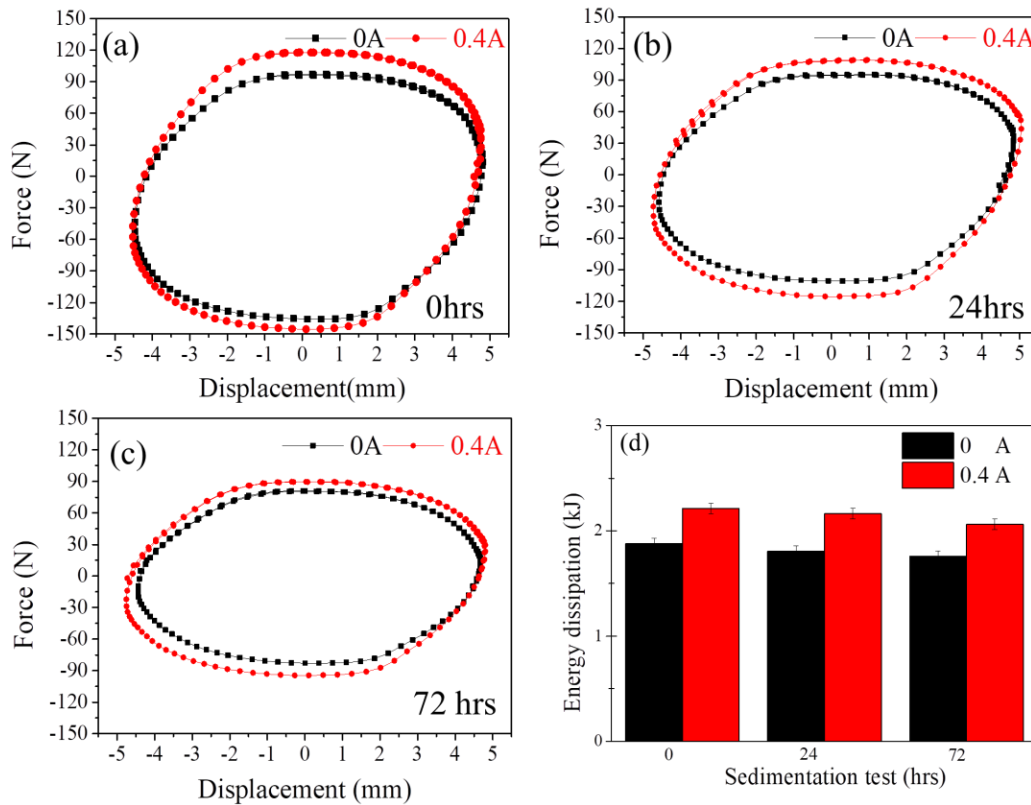
Fig.5.8 Experimental damping force vs. displacement loop of CIPs/claytone APA MRFs (a) 0, (b) 24, (c) 72 hours, and (d) energy dissipation for 0 and 0.4A at different currents

Table 5.4 Damping characteristics of MR Damper CIPs/claytone APA MRF for different settling times

Rebound Damping Force (0A) $F_{Re}(N)$	Compression Damping Force (0A) $F_{Co}(N)$	Rebound Damping Force (0.4 A) $F_{Re}(N)$	Compression Damping Force (0.4 A) $F_{Co}(N)$	Frequency Range (Hz)	Sedimentation Time (Hours)
97.22	134.76	116.88	144.29	1.5	0
94.21	99.26	108.55	115.12	1.5	24
80.57	82.61	88.90	94.74	1.5	72

5.8 Summary

In this work, a new MRF based on claytone APA was proposed to reduce sedimentation problems and its properties were validated using a shear mode MR damper. The damping force of the MR fluid using the claytone APA particles, which was measured as a function of time, displacement and velocity, respectively, was lower than that of the MR fluid using the pure CIPs. At the same applied magnetic field strength, the damping characteristics of the two MR fluids were found to be directly related to their yield stresses obtained. The applied magnetic field strength varied from 0 to 255 kA/m and rheological measurements were obtained for the proposed MRF, the shear stress values were about 15,100 Pa and 10,200 Pa for pure CIPs and CIPs/claytone APA MRF samples at a maximum shear rate of $500s^{-1}$, respectively. The CIPs MRF settled down rapidly during the initial period and finally reached a stable value of 60.5%. Subsequently, the sedimentation ratio of the CI/claytone APA MRF became slow due to the presence of additives and the friction reducer, which in turn slowed down the settling velocity of the CIPs, and the sedimentation ratio gradually reached a stable value at 82%.

CHAPTER-6

INFLUENCE OF DIFFERENT FUMED SILICA BASED MRF FOR SEDIMENTATION EFFECTS

This chapter deals with the influence of varying specific of surface area particles of fumed silica. Hydrophobic, and hydrophilic fumed silica mixed in silicone oil as a thixotropic additive on carbonyl particles based magnetorheological fluids (MRFs) were prepared. Scanning electron microscopy analysis confirmed the fumed silica particles attached to the surfaces of CIPs. The vibrating sample magnetometer result showed that the MRF4 and 5 have a better magnetic saturation value of 30.12 emu/gm and 40.12 emu/gm, respectively. The experimental rheological flow curve behaviours were investigated using the magnetorheometer. The Herschel–Bulkley rheological model was found to be in good agreement with the experimental curves and suggested shear thinning property was observed. The results showed that the hydrophilic silica with larger surface area type presented (i.e.MRF 4 and 5) better magnetorheological fluid characteristics in terms of shear stress, with a high value of dynamic yield stress, and have much-improved sedimentation ratio up to seven days.

6.1 Introduction

A previous literature survey suggests that is an important additives fumed silica, which acts as a hydrogen bonding thixotropic additive which stabilize the MRFs longer time. Firstly, Lim et al. (2004) studied about 80 wt.% of CIPs with 3 wt.% fumed silica suspended in mineral oil-based MRF and proved that the sedimentation ratio greatly improved to about 99% up to 800 hours. M. Kciuk et al. (2009) studied MRFs prepared with different types of carrier fluid viscosity mixed with different proportions of CIPs and 1 wt. % fumed silica as a stabilizer. Jinhuan Xu et al. (2018) showed the effect of varying concentrations of fumed silica on rheological and polishing characteristics of carbonyl-based MRFs. J. de Vicente et al. (2003) discussed CIPs based MRFs and silica nanoparticles as a stabilizer that prevented the aggregation between the particles . S. Alves et al. (2009) discussed the effect of various types of fumed silica in which MRF with 0.80 wt.% of additive and 79.36

wt.% of CIPs was dispersed in 19.84 wt.% of nujol oil, and its rheological properties at off and on-state conditions were discussed. In another work, all these previous studies showed that fumed silica is a promising thixotropic additive and plays important role in slowing down the particle settling in MR fluids. However, the effect of hydrophobic and hydrophilic fumed silica on the silicone oil-based magneto rheological fluids behaviour has not been studied. In the present work, additives-free MRFs and additive mixed MRFs containing with the four different grades surface areas of fumed silica, varying particle size, hydrophobic, and hydrophilic surface nature of silica particles mixed in silicone oil along with carbonyl particles were stduied. Also, the rheological, magnetic saturation and sedimentation properties were compared with the additive-free MRF sample. The experimental flow curves of the prepared MRFs were fitted using the Herschel–Bulkley (H-B), Bingham-Plastic (B-P), and Casson rheological models.

6.2 Results and Discussions

6.2.1 Particle morphology using SEM analysis

Fig. 6.1 depicts the SEM images of pure CIPs and different grades of fumed silica mixtures with CIPs. Fig.6.1(a) shows that pure CIPs have a smooth surface and a spherical shape with particle size varying from 6 to 8 microns. On the other hand, Fig.6.1(b)-(e) illustrates the surface images of a mixture of FS-CIPs, showing that the particle appeared as gel-like surface. In this case, fumed silica additive particles coated and the CIPs and all the fumed silica particles occupied the interspaces among the CIPs due to relatively smaller size, so that they act as one component. In this way, the added FS particles restrained the direct contact of the CIPs and evenly distributed over the surface of the CIPs. This additive coating prevented the particles from agglomerating and reduced the apparent density of the CIPs, thereby reducing the sedimentation rate (Liu et al. 2013). As shown in Fig.6.1(c) the particle size distribution curve was obtained from Image J analysis. The particle size of the fumed silica was approximately three times less than the CIPs so that it maintained better CIPs to additive size ratio and increased the affinity on the surface of the CIPs
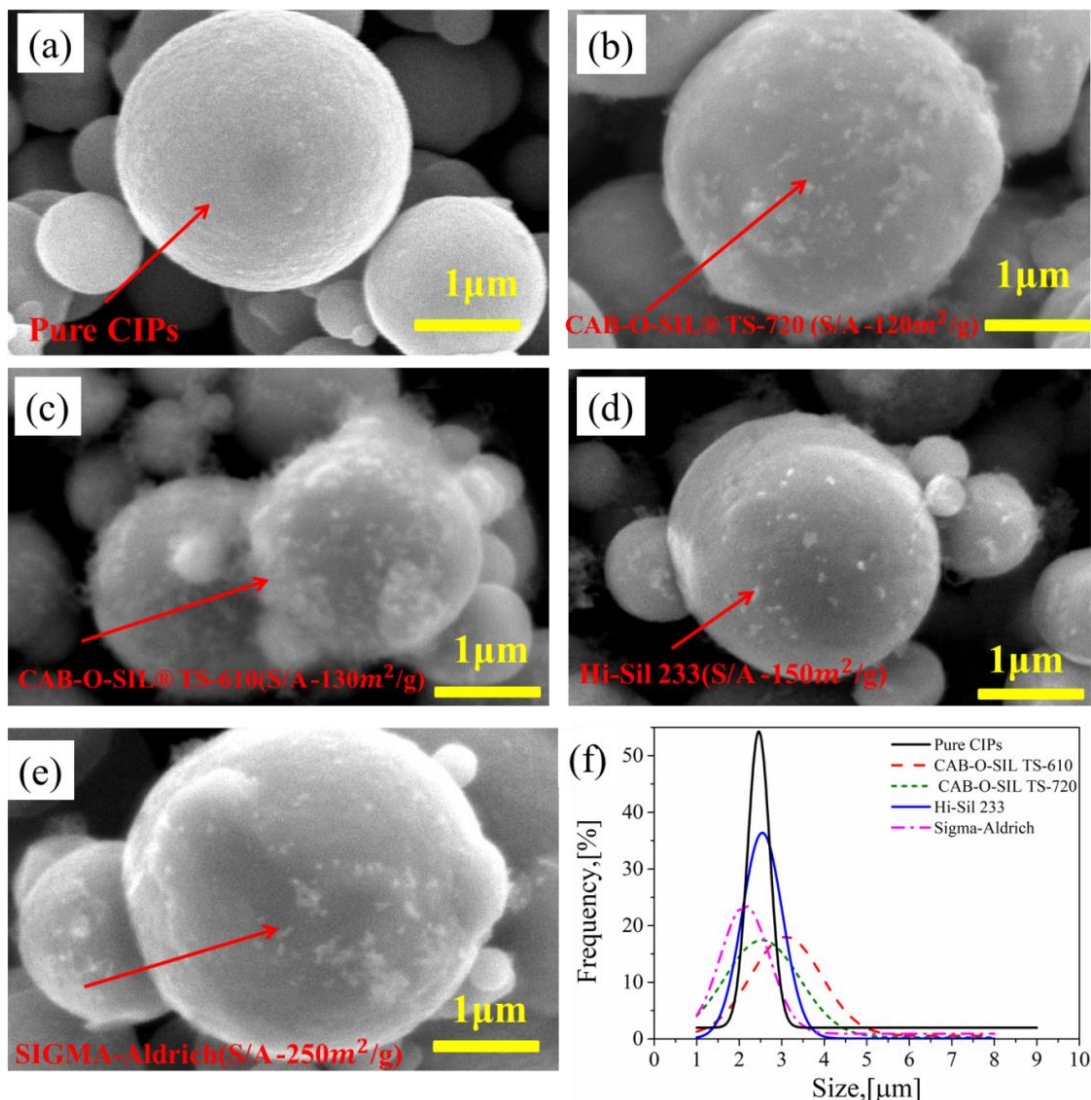
Fig.6.1 Micrographs using Scanning Electron Microscope - (a) Pure CIPs, (b) CAB-O-SIL® TS-720/CIPs, (c) TS-610/CIPs, (d) Hi-Sil 233/CIPs silica, and (e) Sigma-Aldrich/CIPs mixtures Note- (S/A) Surface Area (m²/g)

6.3.1 Fourier-transform infrared spectroscopy FTIR (Analysis)

Fig. 6.2 displays the FT-IR spectra of MRF1 (a), MRF2 (b) MRF3 (c) MRF4(d), and MRF5 (e) samples to analyze their chemical structure in the wavenumber range of 500–4000 cm^{-1}. All individual samples were mixed to make pellets with KBr. Fig. 6.2 (a) (b), (c) (d), and (e), show one large band at 3425 cm^{-1} which is assigned to O–H stretching vibration from hydroxyl groups (Ni et al. 2010). As can be seen from Fig.6.2(a), the stretching vibration of C–H is corresponds to two broad bands, which

are located at 2926 and 2851 cm^{-1}. The peak at 1632 cm^{-1} is attributed to the adsorbed water and structural hydroxyl groups, which is the characteristic of the bending vibration of (H–O–H). As shown in Fig.6.2(b), (c) (d), and (e), strong bands were observed at approximately 1104 cm^{-1}, attributed to asymmetric stretching of Si–O–Si and symmetric stretching of Si–O–Si bonds (Chae et al. 2012). Therefore, the characteristic peaks of both CIPs and SiO were present in the spectrum for the MRF2, 3, 4, and 5 samples which indicates the successful presence of the silica on the surface of the CIPs.
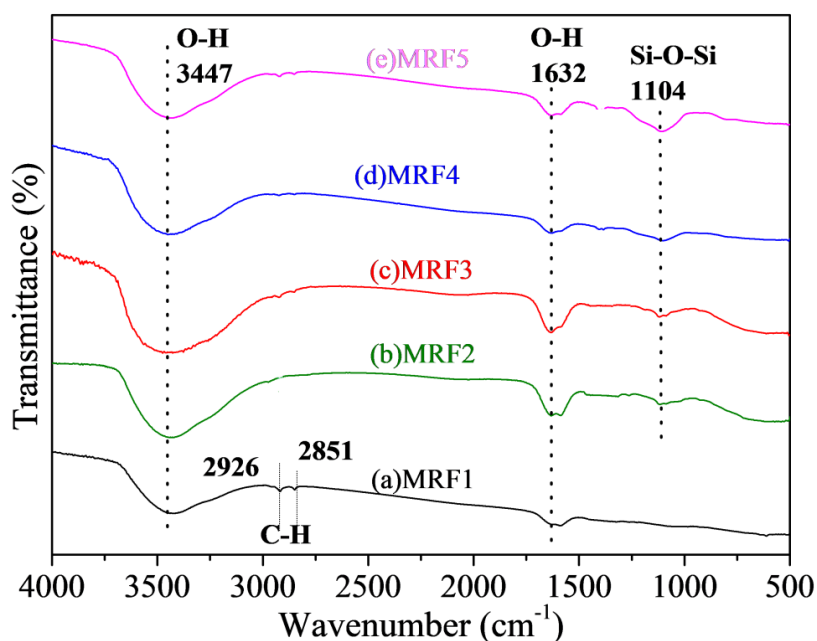
Fig.6.2 FT-IR spectra of MRF1 (a), MRF2 (b) MRF3 (c) MRF4 (d), and MRF5 (e) samples

6.3.2 Energy dispersive spectroscopy (EDS) analysis

Fig.6.3 depicts the chemical compositions of CIPs after adding different fumed silica concentrations which are characterized by EDS. Fig.6.3(a) shows that the EDS study suggested a high with strong peak intensities of Fe ion content of pure CIPs (97.85 wt.%). As shown in Fig.6.3.(b). (c),(d) and (e), peaks of Fe ion content peak intensities are reduced slightly in MRF2,3,4, and 5 samples to 95.03 wt.%, 95.10 wt.%, 92.67 wt.%, and 93.17 wt.% respectively. In our analysis, an increase of carbon content in MRF2,3,4 and 5 samples 2.02 wt.%,2.12 wt.%, 3.10 wt.%, and 2.91

wt.%, respectively was seen. These increased content of carbon indicates the presence of the fumed silica on the surface of CIPs. On the other hand, the CIPs/fumed silica particles based MRFs contained a small content of Si ions along with Fe ions due to surface modification of fumed silica coating on the CIPs surface(Park et al. 2009)
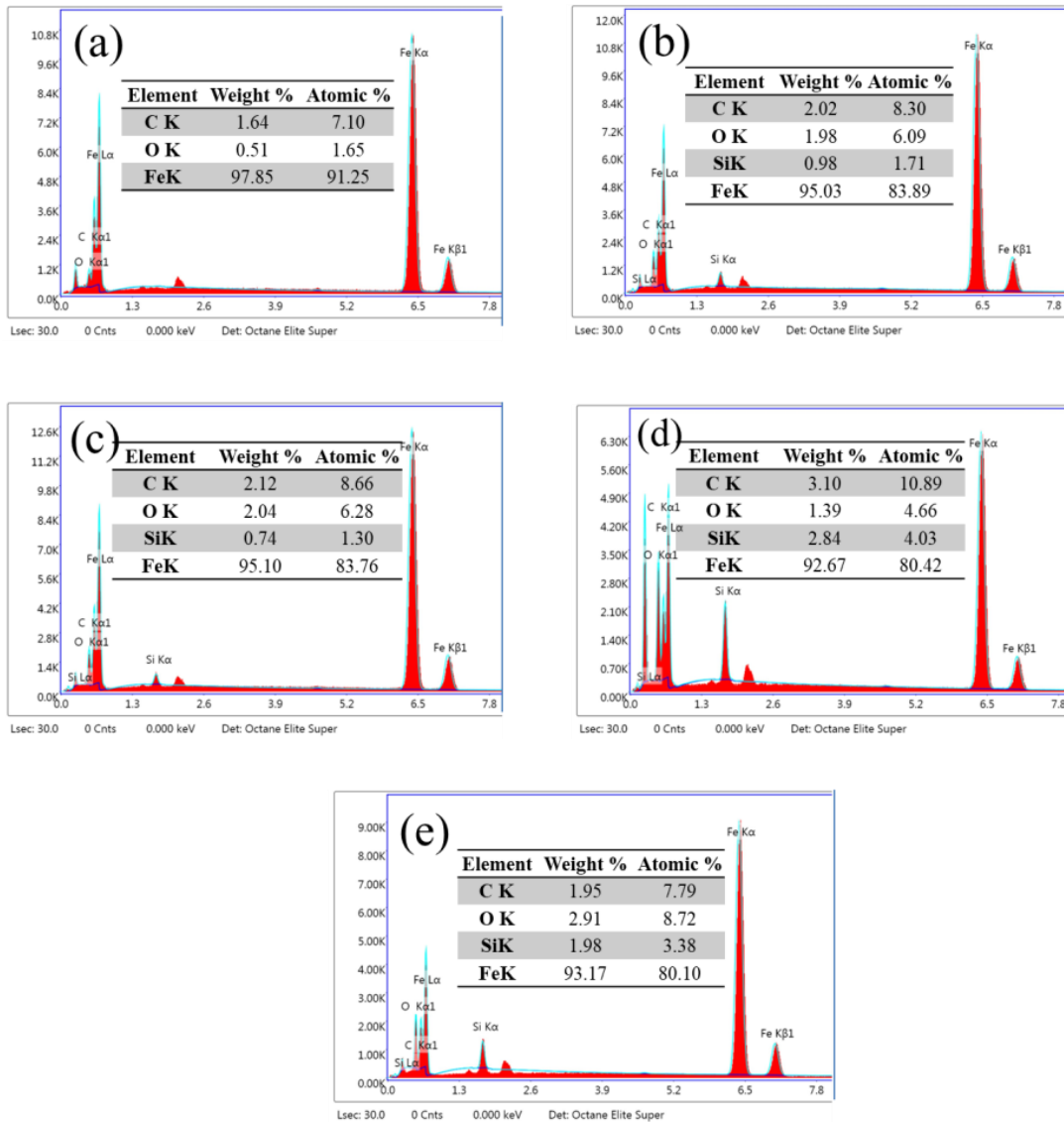
Fig.6.3 EDS spectra (a) Pure CIPs, (b) CAB-O-SIL® TS-720/CIPs, (c) TS-610/CIPs, (d) Hi-Sil 233/CIPs silica, and (e) Sigma-Aldrich/CIPs mixtures

.

6.2.4 VSM analysis
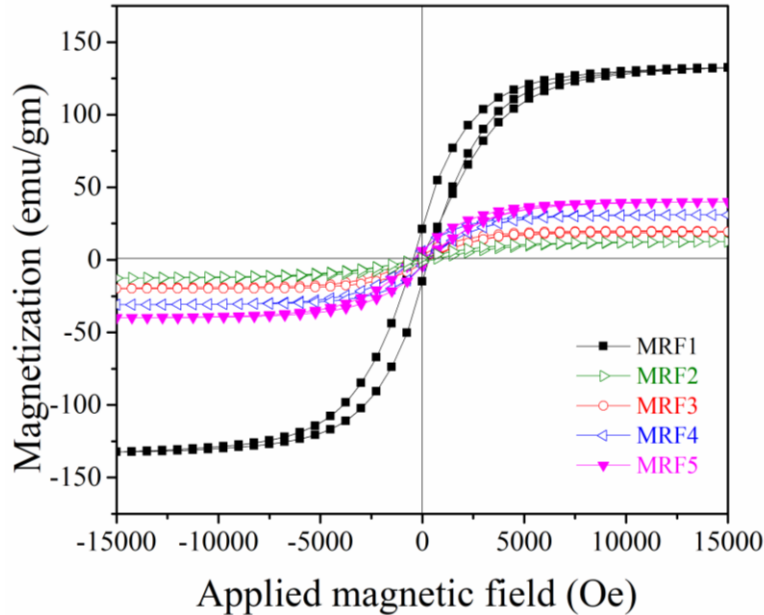
Fig,6.4 VSM hysteresis curve

The magnetization hysteresis curves of MRF1, 2, 3, 4, and 5 samples in the liquid state were measured via VSM at room temperature in a magnetic field range of -15,000 Oe to 15,000 Oe as shown in Fig. 6.4. The saturation magnetization (M_s) value of MRF1 is 132.42 emu/gm, and the coercivity and retentivity values are 382.95 emu/gm and 0.6173Oe, respectively. The M_s values of MRF2, 3, 4, and 5 are smaller than that of MRF1 because of the presence of fumed silica, residual magnetization, and density of CIPs in the liquid was reduced which decreased the saturation magnetization value. Also, while the fumed silica surface area is less then the M_s value decreases largely in the case of MRF2 and 3, whereas high surface area fumed silica MRF 4 and 5 exhibited better M_s. Also, it is probable that a more uniform particle size distribution led to homogeneous mixing and strong structure in the MR fluid when the magnetic field was applied. This behaviour could be explained that greater magnetostatic interaction between the larger surface area particles. Increasing the specific surface area dimension and bigger particle size of silica particles contributed to the enhancement of the magnetic saturation of the MRF4 and 5 samples in the applied magnetic field range. The coercivity, retentivity, and magnetic

saturation of MRF1, 2, 3, 4, and 5 samples are shown in Table 6.1 (Chand et al. 2013).

Table 6.1 Magnetic characteristics of prepared MRFs

Parameters/unit	MRF1	MRF2	MRF3	MRF4	MRF5
Coercivity (H_c) (Oe)	382.95	419.21	371.42	385.93	370.44
Magnetic saturation (M_s)	132.42	12.597	19.9480	30.966	40.006
Retentivity (M_r) (T)	0.61713	0.00713	0.10717	0.28992	0.3314

6.2.5 Surface tension and contact angle investigations
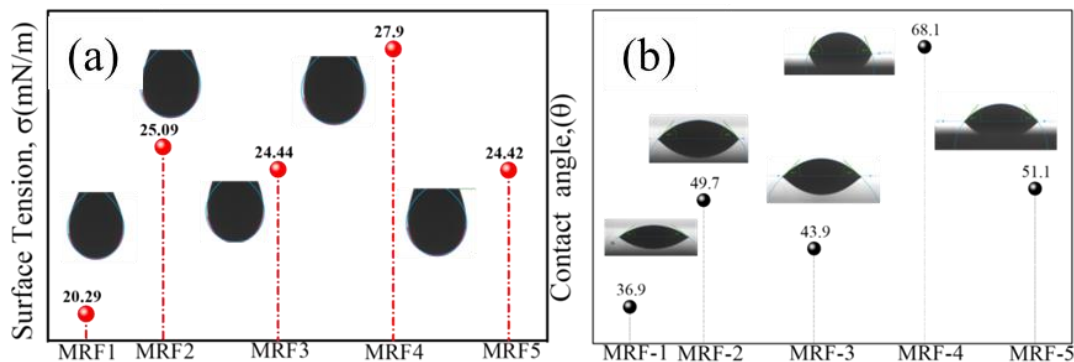
Fig.6.5 Pendent drop method (a) surface tension, (b) contact angle

Fig.6.5(b) and (c) show the surface tension and contact angle values of MRF samples. However, the main difference was observed in MRF2, 3, 4, and 5 samples with surface tension and contact angle values more than the MRF1 samples. In contrast, it is due to the fumed silica added along with silicone oil which increased the viscosity of the MRFs. On the other hand, the dispersive component became dominant after the fumed silica was added, resulting in better wetting of particles with silicone oil(Sedlacik and Pavlinek 2014). In addition to that the hydrophilic and hydrophobic fumed silica particles with lower surface area gaves higher surface tension i.e. (MRF2 25.09 mN/m) (MRF4 27.9 mN/m), and contact angle values i.e. (MRF2 49.79°) (MRF4 68.1°) higher than the larger surface area of fumed silica particles i.e. (MRF3 24.44 mN/m) (MRF5 24.42 mN/m) (i.e. MRF3 43.9°), and (MRF5 51.1°). Nevertheless, hydrophobic and hydrophilic silica with low surface area particles has become more interactive in silicone oil and it provides better compatibility of MRFs.

6.2.6 Viscosity flow curve analysis
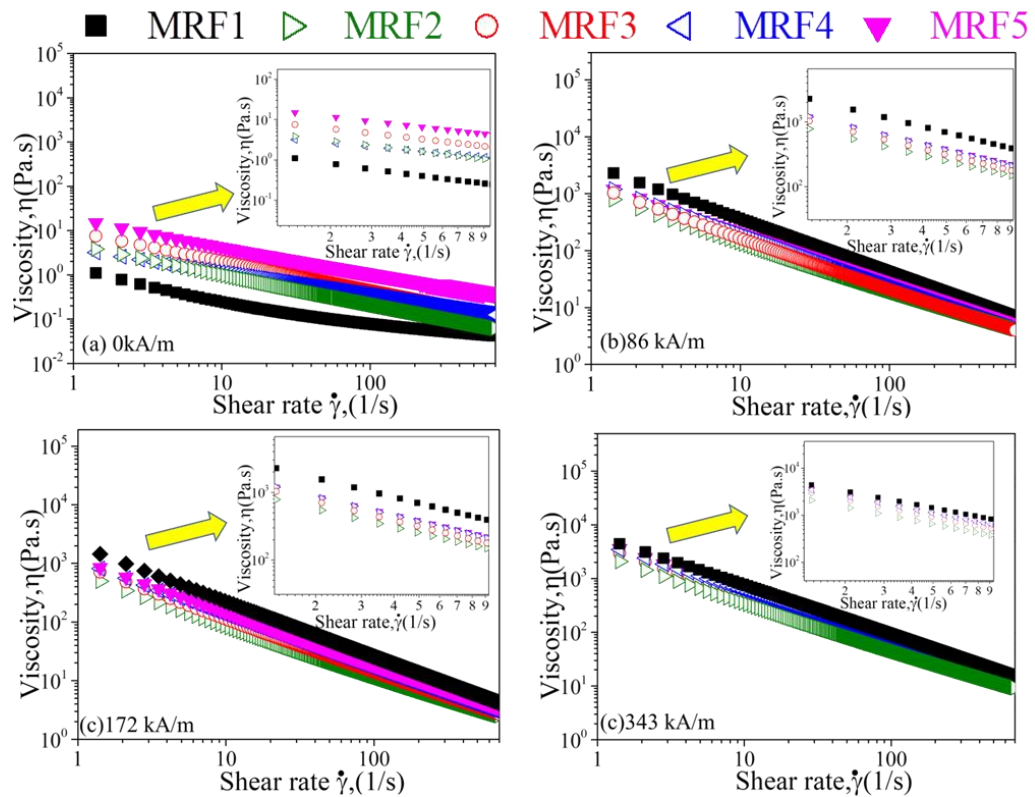
Fig.6.6 Flow curve experiments of viscosity dependence on shear rate (a) 0kA/m, (b) 86kA/m, (c) 172kA/m, and (d) 343kA/m at four magnetic fields applied.

Fig.6.6 shows viscosity curves under different magnetic field strengths applied as a function of the shear rate ranging between 0.01 to 700 (1/s) for MRF1, 2, 3, 4, and 5 samples. It shows that with the increase in magnetic field strength the viscosity of the samples also increased. It becomes evident that CIPs in the MR fluid form strong column-like structure because of dipole interactions near the particle with an applied magnetic field. As shown in Fig.6.6 (a), at zero magnetic field strength (i.e.,0 kA/m), the viscosity of MRF2, 3, 4, and 5 samples exhibit a higher value than the MRF1. It is a known fact that due to the addition of the fumed silica (FS) additive particles helps to make MRFs polydisperse and impacts on the off-state viscosity. Different magnetic fields applied as shown in Fig.6.6 (b)-(d), the MRF2 and 3 containing hydrophobic fumed silica show smaller values of viscosity values than the hydrophilic type silica-

based MRF4 and 5 samples. These silica particles have lower hydrogen bonding sites due to the lower surface area, and smaller particle size, which reduced the hydroxyl population, lessened the ability to form inter-aggregate hydrogen bonds and hindered the particles in the MR suspension, resulting in the reduction of viscosity. Furthermore, a decrease in viscosity observed in all the prepared MRF samples emphasized the shear thinning behavior, as typically observed in a non-Newtonian fluid (Kwon et al. 2018). The shear-thinning phenomenon was attributed to the changes in the internal structure under a robust column structure under shear deformation (Ginder et al. 1996).

6.2.7 Shear stress flow curve analysis

Fig. 6.7 shows the experimental shear stress flow curves at different magnetic field strengths (i.e. 0,86,172, and 343 kA/m) applied using a rotational type rheometer of about 0.01-700 s^{-1} shear range. All the MRFs samples signify plateau behavior of shear stress over the entire range of applied shear rate. As shown in Fig 6.7.(a), the MRF1, 2, 3, 4, and 5 samples exhibited a typical non-Newtonian type fluid at zero magnetic field applied due to the dense volume concentration of CIPs. In contrast, Fig.6.7 (b)-(d) indicates that by applying magnetic fields, the shear stress of MRF2, 3, 4, and 5 samples increases with increasing magnetic field strength because of attractive force between the particles, and it can be seen that shear stress curves of the additive added samples (i.e. MRF2, 3, 4 and 5) are lower than the additive-free sample (i.e. MRF1) at all the magnetic field strength (i.e.86, 172, and 343 kA/m). These results could be explained by the presence of specific interactions of non-magnetic fumed silica particles interacting with the CIPs. As the silica particles adsorbed on the surface of CIPs filled the gaps which avoid direct interaction between neighbouring CIPs, it decreased bulk magnetic property, thus the shear stress was reduced (Kim et al. 2011). In particular, MRF4 and 5 samples containing the hydrophilic fumed silica-base with larger surface area that showed higher shear stress than the hydrophobic type i.e. MRF 2 and 3. In contrast, it was due to the cross-linking network formed by the silica particles via strong hydrogen bonding and the bigger size of the particles. On the other hand, due to dipole-dipole interaction

between the CIPs, a robust chain-like structure in the MRFs was established (Kim et al. 2012a).
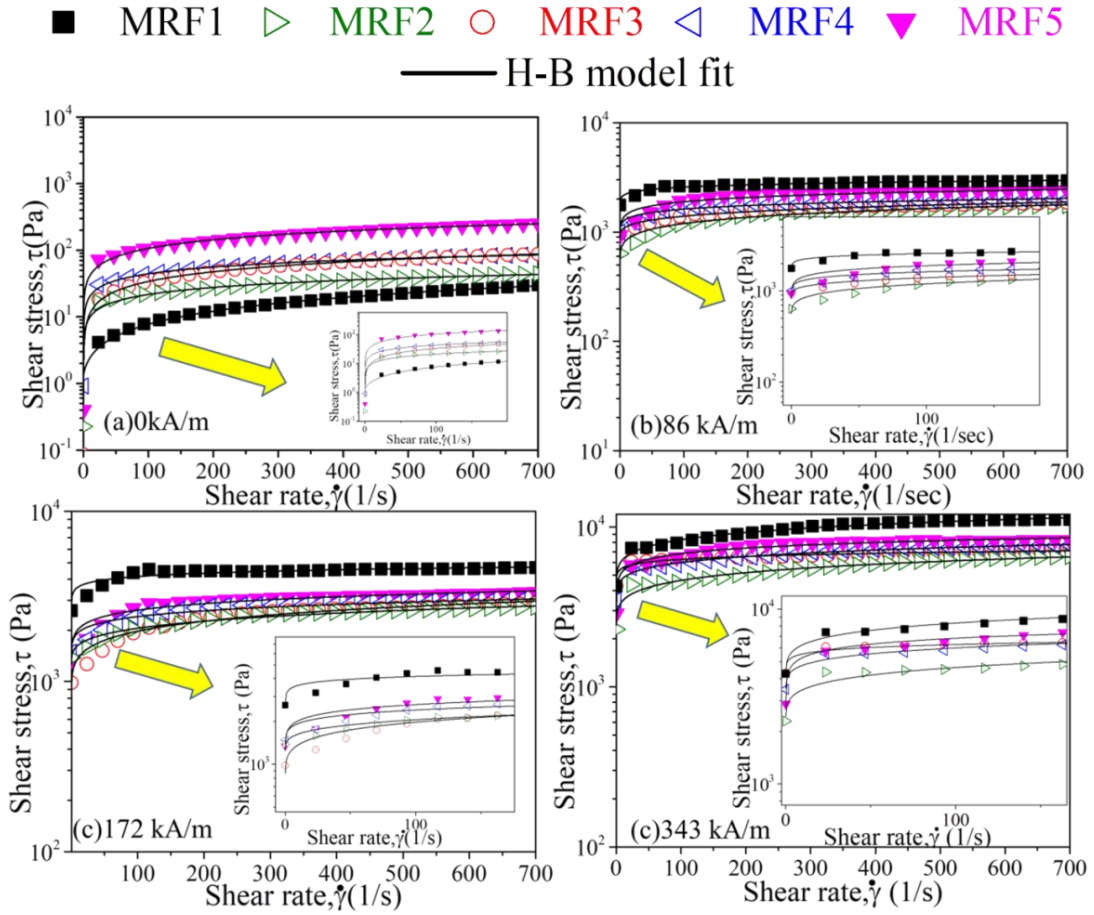
Fig.6.7 Experimental flow curves at different magnetic field strengths of (a) 0, (b) 86, (c) 172, and (d) 343 kA/m.

Three constituent rheological models were initially selected to assess the yield stress of the MRFs. The Bingham fluid model is widely used in MR fluids. The two major parameters, i.e., the shear stress τ and η_0 represent the shear viscosity used to assess the yield stress of the MRFs as given by Eq. (6.1).

$$\tau = \tau_y + \eta_o\dot\gamma \quad \tau > \tau_y \quad \dot\gamma = 0 \quad \tau < \tau_y \tag{6.1}$$

where, τ_y represents yield stress associated with an applied magnetic field, n_o defines shear plastic viscosity, and $\dot\gamma$ designates shear rate. The experimental flow curves

fitted using this model values are inconsistent with slight variation of Adj-R^2 values, and the constant plastic viscosity statement is invalid as observed in Table 6.2.

On the other hand, since the curves are non-linear as shown in Fig 6.6.(b)-(d), the Herschel-Bulkley model as given by Equation (6.2) was used to analyze the flow of the MR fluids, particularly at which flow behaviour index parameter measures the degree to which the MR fluid shear thickening (i.e., n>1) or shear thinning (i.e., n<1) was observed.

$$\tau = \tau_y + k\dot{\gamma}^n. \tag{6.2}$$

Where τ implies shear stress, τ_y indicates the yield stress associated with the magnetic field applied, and k and n are the consistency coefficient and flow behavior index, respectively. According to Table 4, it can be observed that all the prepared MRF samples suggest shear thinning behavior due to n value is less than 1.

The Casson model, was fitted and mainly used to explain the curve of the shear stress flow curve as shown in Equation (6.3) (Gabriel and Laun 2009)

$$\sqrt{\tau} = \sqrt{\tau_y} + \sqrt{\eta_\infty}\sqrt{\dot{\gamma}}. \tag{6.3}$$

Where, η_∞ defines shear viscosity at an infinite rate of shearing. The experimental flow curves are in good agreement with the Herschel-Bulkley, rather than the Bingham and Casson models, regarding Adj. R^2 values shown in Table 6.2

From Fig.6.7(a), it can be observed that the shear stress values of MRF1,2, 3, 4, and 5 samples dramatically increased at different magnetic field strengths (i.e., 0, 86, 173, and 343 kA/m). There was a magnitude of the difference of the shear stress in MRF1 compared with MRF2, 3, 4, and 5 samples at zero magnetic applied strength (i.e.,0 kA/m).

Table 6.2 Optimal parameters of MRF1, 2, 3, 4, and 5 samples using different rheological fluid models

Sample	MFS kA/m	Herschel-Bulkley				Bingham model			Casson model		
		τ_0	k	n	R^2	τ_0	η	R^2	τ_0	η_∞	R^2
MRF1	0	1.29	0.20	0.75	**0.99**	3.96	0.03	0.98	1.47	0.02	0.99
	86	1502.9	503.31	0.16	**0.96**	2419.39	0.92	0.60	2193.5	0.09	0.79
	171	1530.1	1628.7	0.10	**0.86**	3900.22	1.37	0.41	3520.7	0.15	0.61
	343	3914.7	1246.8	0.27	**0.98**	7405.84	6.59	0.77	6128.4	1.30	0.91
MRF2	0	1.16	3.74	0.36	**0.98**	16.117	0.04	0.88	10.45	0.01	0.95
	86	533.03	148.77	0.32	**0.96**	1049.83	1.17	0.76	833.68	0.27	0.90
	171	799.12	278.8	0.31	**0.95**	1726.88	2.00	0.75	1359.3	0.48	0.89
	343	2292.12	583.6	0.30	**0.97**	4084.50	3.98	0.83	3359.9	0.81	0.93
MRF3	0	0.27	3.57	0.48	**0.99**	22.70	0.10	0.93	12.48	0.05	0.98
	86	895.50	100.49	0.34	**0.97**	1276.72	0.96	0.8	1086.2	0.16	0.93
	171	1273.63	278.18	0.31	**0.95**	1877.7	1.45	0.79	1589.4	0.25	0.92
	343	3286.19	815.66	0.26	**0.98**	5436.91	3.80	0.78	4657.6	0.64	0.91
MRF4	0	0.11	9.935	0.33	**0.99**	33.361	0.08	0.86	22.04	0.03	0.94
	86	865.25	268.65	0.22	**0.95**	1490.68	0.88	0.66	1293.0	0.13	0.83
	171	1259.62	399.53	0.22	**0.91**	2220.08	1.36	0.62	1911.0	0.21	0.80
	343	3591.2	1417.0	0.13	**0.96**	5877.85	2.13	0.66	5180.7	0.71	0.74
MRF5	0	6.81	12.28	0.45	**0.99**	74.88	0.27	0.92	44.12	0.12	0.93
	86	652.36	507.83	0.19	**0.96**	1711.16	0.92	0.60	2193.5	0.09	0.79
	171	1007.18	639.98	0.20	**0.91**	2379.64	1.69	0.60	2003.4	0.30	0.78
	343	1276.3	2904.0	0.13	**0.96**	6125.48	4.07	0.55	5396.1	0.20	0.80
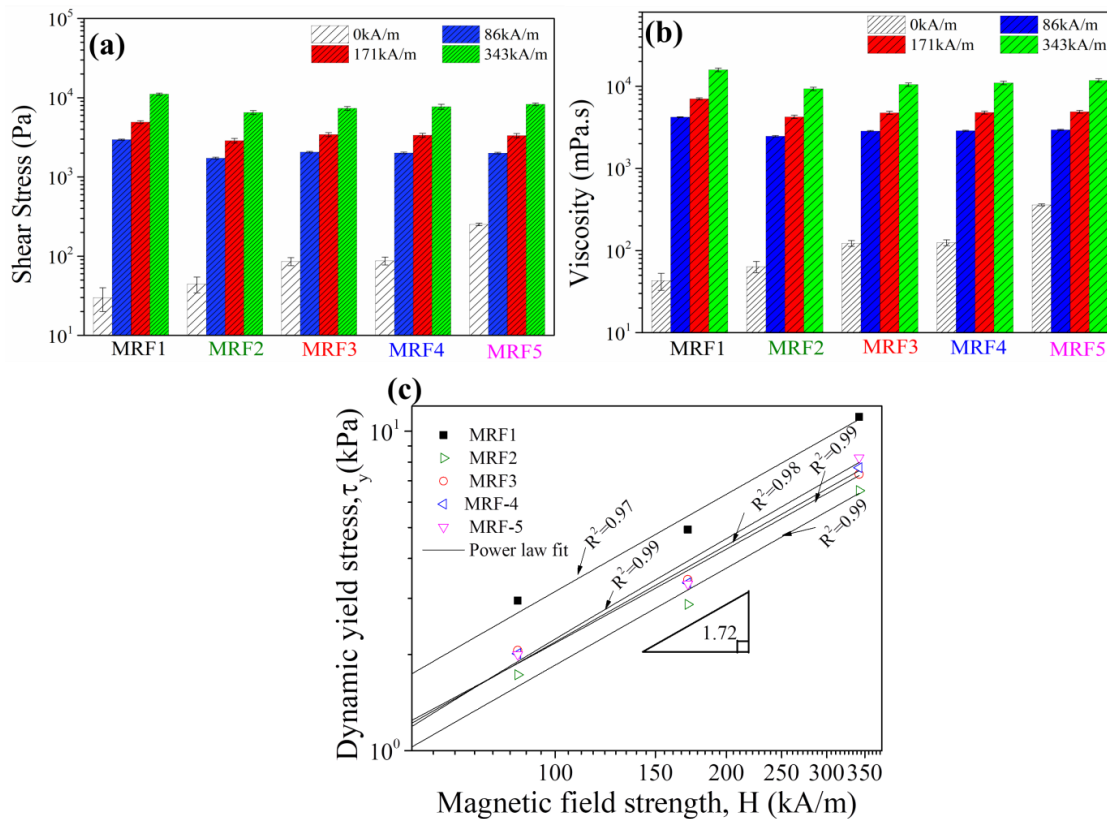
Fig.6.7 Bar graph showing the comparison of (a) shear stress, (b) viscosity at a maximum shear rate of 700 (per sec), and (c) Dynamic yield stress as a function of different magnetic field strengths

This is due to the addition of fumed silica particles, which create thixotropic silica gel, causing collision between the moving fumed silica particles freely in the carrier liquid, and the field-induced between the CIPs. Fig. 6.7(b) shows that the viscosity of the MRF2, 3, 4, and 5 samples at zero magnetic field strength (i.e.,0 kA/m) was higher than that of the MRF1 sample, due to the improved loading distance of the FS (fumed silica) particles related to the repellent forces between the CIPs. Due to the fumed silica surface with large surfaces of hydroxyl silicone, hydrogen bonds between these hydroxyls groups of fumed silica were formed, when fully dispersed in silicone oil, then the formed strong silica network structure. The dynamic yield stress as a function of the magnetic field strengths applied, on a log-log scale of the MRF1, 2, 3,4, and 5 samples were obtained from the flow curves at the various magnetic field

110

strengths applied, as shown in Fig. 6.7. In general, the relationship between the magnetic fields and yield stress is represented by the power-law relationship as given in the following equation (6.4). It is well known that the τ_y developed in the MRFs increases with increasing applied magnetic field strength.

$$\tau_y \alpha \, H^m \tag{6.4}$$

Where, τ_y represents yield stress, H is magnetic field strength and the slope m of the dynamic yield stress line is 1.72 for all the MRFs.

$$\tau_y \alpha \, H^{1.72} \tag{6.5}$$

The slope of this dependence indicates the mechanism of the column-like structure formation of magnetic particles. In addition to that slope values close to 1.72 is considered the intrinsic magnetic property and high-volume concentration of CIPs. On the other hand, MRFs properties are strongly affected by the saturation magnetization mechanism of CIPs and internal structure formation that takes place in the MRFs samples.

6.2.8 Sedimentation analysis

Fig.6.8 shows the sedimentation experiments conducted on MRF1, 2, 3, 4, and 5 samples. The MRFs were transferred into a 10 ml graduated cylinder to study the sedimentation by observing through naked eye and left to settle. The filled MRF samples having fixed CIPs 80 wt. % concentration and 3wt.% fumed silica along with silicone oil were placed under the static condition without disturbance. Using the fumed silica, the MRFs samples form a gel-like structure which limits the settling of iron particles in silicone oil. From Fig. 6.8(a), it can be seen that the MRF1 sample has a sedimentation ratio (86%), which decreases quickly during the first 24 hours. It may be due to the absence of the fumed silica additive. On the other hand, MRF2 and 3 samples contain hydrophobic fumed silica particle have a lower surface area. The sedimentation slightly improved about 88%, and 97%, respectively. In the case of hydrophilic type, MRF 4 and 5 samples typically consist of larger surface area, and even after 166 hours sedimentation improved greatly by about 98% and 99%. It was duet this reason that the larger surface area of fumed silica provided maximum hydrogen bonding sites for three-dimensional network formations than the smaller

surface area fumed silica particle. The fumed silica particles surround the spherical CIPs, ensuring protection against the sedimentation in MR fluids. The probable cause leading to lower sedimentation ratio was that fumed silica is that sub-sized particles filled the gap between the particles reduced the apparent density of CIPs as confirmed by the SEM analysis. Fig.6.8(b) shows the final image of the MRFs samples for which sedimentation was completely settled after 166 hours. The MRF sedimentation ratio can be evaluated by using Equation (6.6) as follows.

$$R(\%) = \frac{A}{A+B} * 100 \quad (6.6)$$

Where, A represents the length of clear MRFs and B implies the length of the turbid part. Table 6.3 shows the compared values of the sedimentation ratio of the prepared MRFs samples.
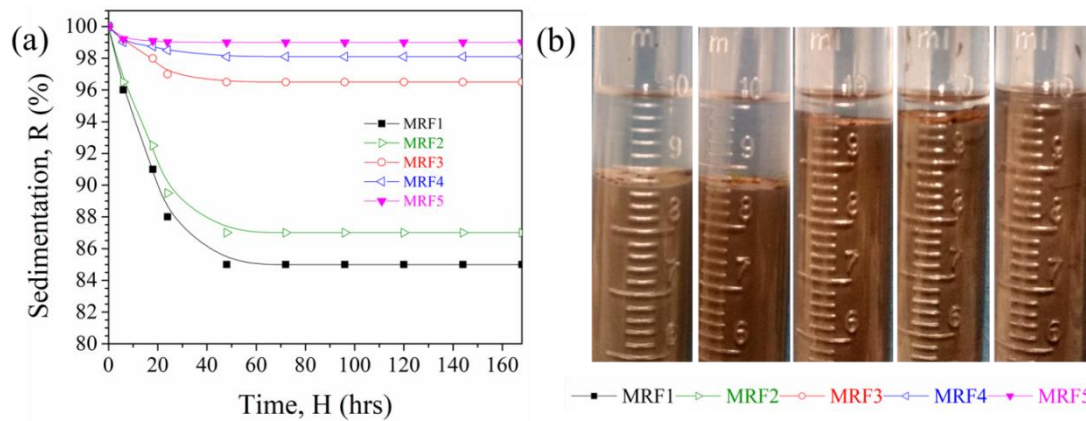
Fig.6.8 Visual observation method (a) changes of sedimentation ratio with time,(b) final result of sedimentation MRF under static conditions

Table 6.3 Sedimentation ratio of MRF samples by visual inspection

MRFs samples	MRF1	MRF2	MRF3	MRF4	MRF5
Sedimentation, R（%）	86%	88%	97%	98%	99%

6.3 Summary

The magnetorheological fluid (MRF) was prepared in the laboratory, and CIPs were mixed with silicone oil using different surface areas of hydrophobic and hydrophilic fumed silica (i.e., 120,130,150, and 250m^2/g). The off-state viscosity of MR fluid can also be controlled by the amount of fumed silica in the system. The stability of the MR fluid was greatly improved by the addition of different fumed silica. On the other hand, from the test of the sedimentation rate of MR fluid samples, it is found that the sedimentation rate can be reduced using the proposed fumed silica different surface area fumed silica types. The results indicate that the MRF2 and 3 containing hydrophobic fumed silica show smaller values of viscosity values than the hydrophilic type silica-based MRF4 and 5 samples. In the case of hydrophilic type, MRF 4 and 5 samples typically consist of larger surface area, and even after 166 hours sedimentation improved greatly by about 98% and 99%. One of the main technical contributions of this work is to find suitable specific surface area of the additives to achieve both the enhancement of the shear stress and the reduction of the sedimentation rate simultaneously.

CHAPTER-7

SEDIMENTATION AND RHEOLOGICAL PROPERTIES USING DIFFERENT CARRIER FlUIDS

The present chapter focuses on the preparation of MR fluid samples with three types of carrier fluids such as silicone, light paraffin and Poly-alpha-olefin (5, 30, and 400 cSt) viscosity oils with 25% volume fraction of carbonyl iron particles and 3% fumed silica as a thixotropic agent to improve sedimentation of the MR fluid. The morphology, magnetic saturation, and phase of the carbonyl iron particles were investigated using Field Emission Scanning Electron Microscopy (FESEM), Superconducting Quantum Interference Device (SQUID), and X-ray diffraction (XRD) respectively. The obtained powder particles were spherical having a high magnetic saturation of 270 emu/gm. The prepared MR fluids rheological properties were tested using Anton Paar MCR702 Twin drive rheometer fitted with a magneto-rheological module. Sedimentation stability was examined by direct observation.

7.1 Introduction

In this chapter, preparation of MR fluid sample was done with three different carrier liquids like Silicone (5cst), light paraffin (30cst), Poly-alpha-olefin 400 (cst) oil of different viscosities with 25% volume fraction of carbonyl iron particles was done. The previous study suggests that 3% fumed silica as a thixotropic agent forms a network through hydrogen bonding for improving stabilization of the MR fluid. These specific relative volume fractions of the MR fluid fumed silica particles, and carbonyl iron particles were preferred due to their high sedimentation stability, as demonstrated in literature.

7.2.Experimental

7.2.1 Preparation of MR fluid

The constituents required for preparation of the MR fluid are: fumed silica (0.2-0.3) μm surface area $200m^2/g \pm 25$ m^2/g (aggregate) (Sigma Aldrich) mixed using homogenizer and stirring for about 15 min in silicone oil (Sigma Aldrich), light paraffin oil (Spectrum chem. Pvt. Ltd) and Poly-alpha-olefin oil (Chemtura

Corporation) with a Specific Gravity of (0.96, 0.83 and 0.84 g/cm^3) and viscosity range of (5, 30 and 400 cst.) respectively at until a homogeneous mixture is obtained. Thereafter, carbonyl iron powder particles with density, ρ=7.86 ×10^3 kg/ m^3, CN grade, Avg particle size (2-9) microns are mixed in the oil solution using mechanical stirrer at 900 rpm for about 12 hours. In the present work, the 3 types of MRF samples are designated by MRF-1, MRF-2, and MRF-3 and their properties are shown in table 7.1

Table 7.1. Properties of prepared samples composition

ID	CIPs (vol. %)	Carrier liquid (vol. %)	Fumed silica (vol.%)
MRF-1	25	Silicone oil (5 cst) 72	3
MRF-2	25	Light paraffin oil (30 cst) 72	3
MRF-3	25	Poly-alpha-olefin oil 400 (cst)	3

7.3 Characterization

The morphology of the carbonyl iron particles was examined by field emission scanning electron microscopy (FESEM, ZEISS ULTRA55,). The magnetic properties of carbonyl iron were studied through a superconducting quantum interference device (SQUID, MPMSXL5) magnetometer at room temperature with the applied magnetic field of 15kOe. The crystal structure of raw carbonyl iron particles was observed by X-ray diffractometer (XRD) (D max, Rigaku) with Cu/K-α radiation source (1.5418 Å). The magnetorheological fluid properties were investigated by twin drive rotational rheometer (MCR702, Twin drive Anton Paar, India) connected with a magneto–cell (PS-MRD 180/1.2T, Anton Paar India) which produces a homogeneous magnetic field. A parallel plate measuring device dia 20 mm was   used   with a gap of 0.3 mm at 40^{0}C.The suspension stability of CI/fumed silica based MR fluids was studied by direct observation method.

7.4.Results and Discussions

7.4.Rheology flow curves

The Rheometer MCR 702 Twin Drive consists of the stationary bottom plate and rotating top parallel plate with dia 20 mm with MRD cell (70/1T). The fluid sample was placed in the gap between the plates. Shear stress, viscosity for three different compositions like MRF-1, MRF-2, and MRF-3 were determined in the following manner. Fig.7.1 (a) and 7.1(b) represent the shear stress versus shear rate 1/sec) graphs and Shear stress versus the applied magnetic field in the range 0 to 0.9 Tesla at 40^0c. The experiment was conducted with a magnetic field and without a magnetic field (i.e. off-state and on-state). Fig. 7.1 (a) shows a linear increase in shear stress with an increasing shear rate. When there is no magnetic field, the characteristics of the MR fluid become that of Newtonian fluid. The range of shear rate tested was from 0 to 200 (γ = 1/sec). The results found that the shear stress obtained for MRF-1 and MRF-2 was relatively low, which inicates the low viscosity of the carrier base fluid. In the case of MRF-3, a shear stress limit was very high due to the high viscosity of the base fluid. When a magnetic field was applied, a different consequence appeared in Fig.7.1 (b). The shear stress increased with increasing applied magnetic field (i.e 0 to 0.9T) for all three samples. The prepared MRF-1 shows higher shear stress 15000 (Pa) as compared to that other MRF-2 12000 (Pa) and MRF-3 9000 (Pa) at a magnetic field of 0.9 Tesla. MR performances may be affected due to particle size and the surface morphology of MR particles. The MR fluids exhibited the Bingham plastic a minimum yield stress is needed for fluid flow behaviour shear stress under applied magnetic field strength, representing the stable chain structures of magnetized particles. The tables 7.3 and 7.4 show results found by the MR effect..

Table 7.3 Properties of investigated MR fluids off-state rheology

ID	Shear stress (Pa)	Shear rate (1/sec)	Temperature ^{0}c
MRF-1	60	0-200	40
MRF-2	125	0-200	40
MRF-3	1400	0-200	40
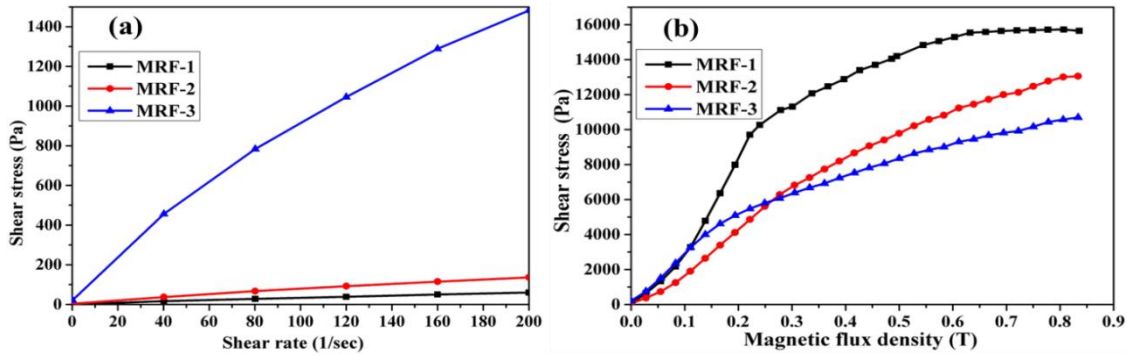
Fig.7.1 Shear stress versus shear rate at different magnetic field strength (b)The response of the shear stress v/s magnetic flux density at 40^0C and a constant shear rate of 100 (1/sec)

Table 7.4 Properties of investigated MR fluids on-state rheology

ID	Shear stress (Pa)	Shear rate (1/sec)	Magnetic flux density (Tesla)	Temperature^{0}c
MRF-1	15000	100	0-0.9	40
MRF-2	12000	100	0-0.9	40
MRF-3	9000	100	0-0.9	40

7.4.5 Sedimentation stability of MR fluids

To investigate the effect of sedimentation of MR with three different carrier liquids Sedimentary ratio (*R*) can be determined by pouring the magnetorheological fluid in 10 ml of measuring cylinder without disturbance at room temperature. To evalute the sedimentation dispersion stability, the experiment was performed placing the MR fluid samples ideal for 750 h, and sedimentation rate of particles in MR suspension was taken at a regular interval. Sedimentation ratio can be defined as

$$\text{Sedimentation ratio (\%)} = \frac{\text{Volume of a supernatant fluid}}{\text{Total volume of MR fluid}} \times 100$$
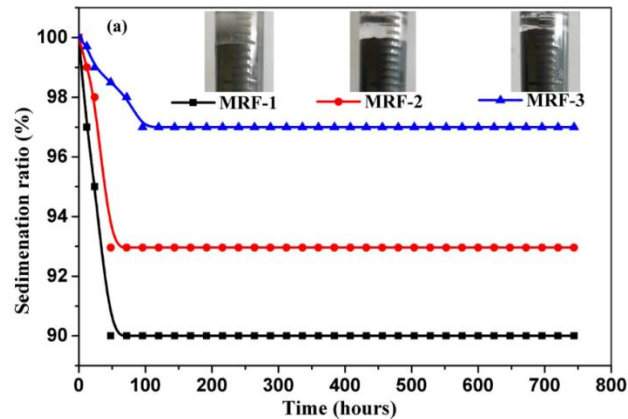
Fig.7.2 Sedimentation ratio curves three different carriers based MRFs

Fig.7.2 shows the sedimentation curves of three different carrier-based MR fluids samples that were used for the examination of dispersion stability varying in treatment time (i.e. MRF-1, MRF-2, and MRF-3). It is clear from Fig.7.2 that the MRF-3 based fluid lowest sedimentation ratio of 97% compared to MRF-1 and MRF-2 due to the high viscosity of the base oil. The inset figure shows the final results of the sedimentation after 800 h for MRF based suspensions

7.5 Summary

Three distinct carrier liquid loadings and viscosities (5, 30, and 400 Cst) were prepared using magnetic CIPs-based magnetorheological (MR) fluids. Rotational flow curves were used to measure the MR properties, which revealed non-Newtonian behaviour for all of the samples studied. The shear stress of silicone oil with 5 cSt was greatly improved in higher magnetic fields, according to experimental data. Under applied magnetic field strength, fluid with 3 vol.% fumed silica particle composition shows an exceptionally good response in all aspects of analysis, and the flow curve values match well with the Bingham plastic model. The sedimentation ratio was also explored to confirm the influence of various low viscosity-based fluids and fumed silica particles on MRF.

CHAPTER-8

CHARACTERIZATION OF MANGANESE-ZINC FERRITE PARTICLE-BASED MAGNETORHELOGICAL FLUID AND THEIR SEDIMENTATION CHARACTERISTICS

In this present study, three samples of magnetorheological fluid were prepared at three different volume concentrations of (i.e. ϕ_1=20, ϕ_2=25, and ϕ_3=30 vol.%). Manganese-zinc (Mn-Zn) ferrites were used as magnetic phase dispersed in silicone oil along with stearic acid as a stabilizer to reduce the sedimentation of particles. The characterization methods like Scanning Electron Microscopy (SEM), Energy Dispersive Spectroscopy (EDS), X-ray (XRD) diffraction, and Vibrating Sample Magnetometer (VSM) were used to study morphology, crystal structure, and magnetic saturation properties. It was found that Mn-Zn ferrite showed the plate-like shape, presence of small aggregation, and spinel structure in phase. The magnetic measurement showed the saturation magnetization (M_s) of 77.12 emu/gm at room temperature. To understand the MR behaviour, experimental flow curves shear stress (τ), viscosity (η), as a function of shear rate and frequency sweeps were measured at different magnetic field strengths applied (H) using a magnetorheometer with parallel plate arrangement. Furthermore, the yield stress could be well predicted under a magnetic field using the Herschel Bulkley, Bingham, and Casson fluid models. The MRF#20, #25, and #30 samples of suspensions were observed by visual observation, the sedimentation ratio was significantly improved by the stearic acid from the carboxyl group mixing in silicone oil, which forms a gel-like structure that hinders the fast settling of Mn-Zn ferrites.

8.1 Introduction

In recent decades, magnetorheological fluid technology has improved and increased its demand in the research area of smart fluids materials due to its low driving magnetic fields, broad working temperature, and controllable properties. Typically, carbonyl iron particle (CIPs) based MRFs can demonstrate yield stresses in the range of 10-100 kPa under applied magnetic field flux density of the order of magnitude 1T. However, the frequent problem of CIPs based MR fluid is the tendency to settle down

over some time due to the high-density difference between particles (ρ=7.86g/cm^3) and carrier fluids (ρ=0.91g/cm^3) which causes sedimentation and form a dense cake impossible to disperse which limits the use in major applications. To rectify these issues, significant attempts have been adopted by the researchers to avoid sedimentation, such as using surfactants, additives, inorganic/organic coatings, nanoparticles, and using viscoelastic carrier fluids. Spinel ferrites were used as good alternatives CIPs particle materials because of low density (4.3–4.8 g/cm^3) of particles and unique magnetic behaviour which is an essential parameter for the preparation of stable MRFs. Some important studies have been made on high stable MRF than the iron particles-based MRFs that use the ferrite powder as reported by researchers such as calcium ferrite, zinc ferrite nanoclusters, and Ni–Zn ferrite powder(Patel et al. 2017). Manganese zinc ferrites (Mn–Zn) as a typical example of spinel ferrites are preferred in many areas due to their high initial permeability, moderate saturation magnetization, as well as low losses, and relatively high curie temperature. It finds applications in magnetic sensors, transformer cores, inductors, and spintronic devices (Wang et al. 2017b).

The present work deals with the preparation of MRFs and the effect of the varying particle volume concentration (ϕ) of Mn-Zn ferrite particles and stearic acid used as a stabilizer. Before carrying out the magnetorheological characteristics of the ferrite particles, structural and magnetic properties were investigated using scanning electron microscopy, vibrating sample magnetometer, and X-ray diffraction characterization techniques. Magnetorheometer was employed to investigate the relationship between shear stress, shear viscosity, and frequency sweep under different applied magnetic field strengths. The experimental results were fitted with the Bingham, Hershel Bulkley, and Casson model to obtain the shear yield stress under the equivalent applied magnetic field strengths. Finally, sedimentation experiments were conducted for prepared MRF samples at three different volume fractions and observations were made concerning time.

8.2 Experimental

8.2.1 Materials and Preparation of MRF

MRF was prepared as received Mn-Zn ferrites particles provided as a free of cost sample from (KIP Chemicals Pvt. Ltd is adding in silicone oil purchased from (Sigma Aldrich; $\nu=10$ cSt; $\rho = 0.96$ g/cc^{-1}), where ν is kinematic viscosity, and ρ is the density of carrier fluid medium. The stearic acid (Sigma Aldrich) additive was added with 1 vol. % of into the MRF suspensions to inhabit the sedimentation of particles. MRFs were homogenized by mechanical mixing at 1000 rpm for 1 hour and followed by ultrasonication for 15 minutes at room temperature.MRFs were labeled as MRF#20, MRF#25, and MRF#30, respectively, and will be referred to by the same Table 8.1 nomenclature henceforth.

Table.8.1 The composition of MRF

Samples	Base magnetic particle (Mn-Zn ferrites) vol. %	Carrier fluid (Silicone oil) vol. %	Stabilizer (stearic acid) vol. %
MRF#20	20%	79%	1%
MRF#25	25%	74%	1%
MRF#30	30%	69%	1%

8.4 Results and Discussions

Fig 8.1. (a) shows a scanning electron microscope micrograph of as received Mn–Zn ferrite sample. It can be seen that large and small particles attached with irregular shapes, as well as elongated plate-like shape, with the existence of soft agglomeration (Wu et al. 2012). Fig. 8.2.(b) shows the EDS spectra with sharp intensities of elements present like manganese, zinc, carbon, iron, and oxygen, and the absence of any impurities elements is observed from Mn–Zn ferrite powder (Anupama et al. 2018). Also, the inset pie chart was drawn showing the atomic weight percentages of *Mn-Zn ferrite* samples.Fig.8.1. (c) shows a particle size distribution histogram

curve obtained from statistical analysis software Image J used to determine average particle size mean length calculated to be between 0.5 to 6 microns.

8.4.1 SEM and EDS analysis
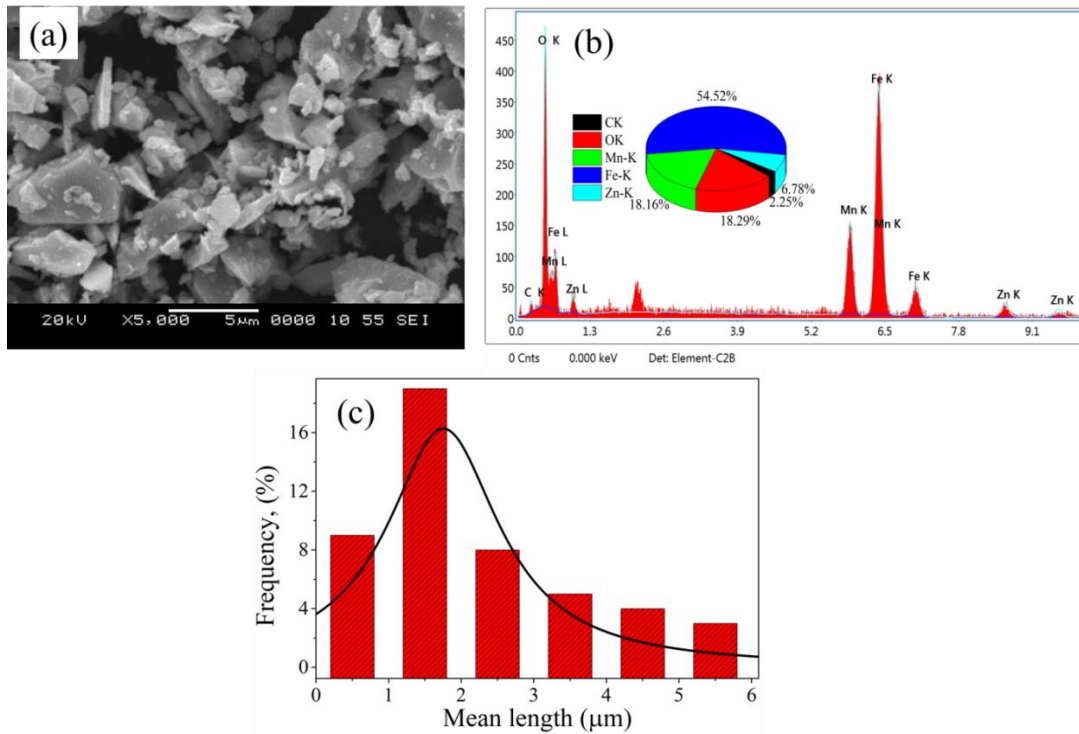
Fig.8.1 Micrograph of Mn-Zn ferrites (a) SEM (b) EDS analysis(c) histogram curve

8.4.2 XRD analysis

Fig. 8.2 represents the diffractogram of the Mn-Zn ferrite sample. The XRD pattern shows that the Mn-Zn ferrite sample has a pure spinel structure in phase. Characteristic diffraction lines peaks are indexed to planes of (2 2 0), (3 1 1), (4 0 0), (5 11) and (4 4 0) assigned to corresponding 2θ values of 29.17°, 35.1°, 43.1°, 56.1°, and 62.12°, respectively. Also, the crystal structure contributions were found to be in good agreement with those reported for the Mn-Zn ferrite in JCPDS card# (74-2401). The mean crystallite size was 36.128 nm for Mn-Zn ferrite and was calculated using the Scherer formula(Holzwarth and Gibson 2011).

$$d = \frac{K\lambda}{\beta \cos\theta} \tag{8.1}$$

Where, d represents crystallite size, K is a dimension factor equal to unity, and β represents half-width of the relevant diffraction reflection, λ represents the X-ray wavelength of Cu-Kα (λ-1.5406 Å) radiation and θ is the Bragg diffraction angle. The XRD pattern of Mn-Zn shown in Figure has been analysed employing profile refinement technique with the help of High Score Plus software suite. The Figure shows the experimental, calculated and residual XRD profiles for the Mn-Zn ferrite particles. The low value of χ^2 (goodness of fit) equal to 1.231 and R$_{wp}$ of 4.5234 % was achieved, which may be considered to be good for estimations.
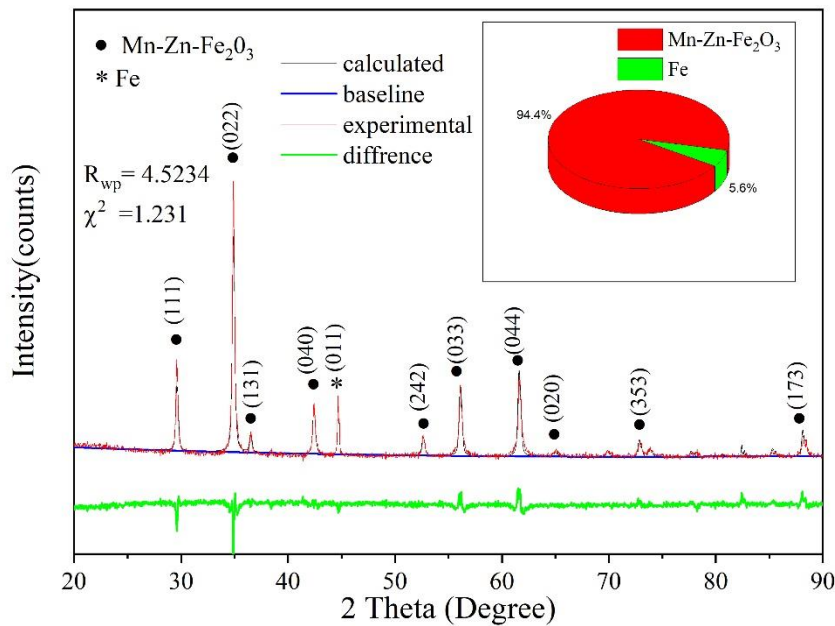
Fig.8.2 XRD pattern of Mn-Zn ferrites

8.4.3 Mn-Zn ferrite magnetic properties using VSM

The room temperature magnetization curve of the as-received Mn–Zn soft ferrite particles was measured using a vibrating sample magnetometer in the magnetic field range of 15000 Oe to -15000 Oe. The hysteresis loops did not show any magnetic saturation up to the maximum applied magnetic field of 2500 Oe resulting in a narrow hysteresis loop (low coercivity H$_C$ ≈ 58.12 Oe. The magnetic saturation value of Mn-Zn ferrite particle reached (M$_s$) 77.98 emu/g at 10,000 Oe magnetic fields. As per the XRD results, there were some Fe and few cubic spinel phases in the sample, resulting

in weak magnetic properties. Therefore these samples exhibited poor ferromagnetic behaviour (Xu et al. 2019). The saturation results in Mn-Zn ferrites from VSM analysis indicated that they showed a good response to an external magnetic field, which could be potentially be useful for MRF.
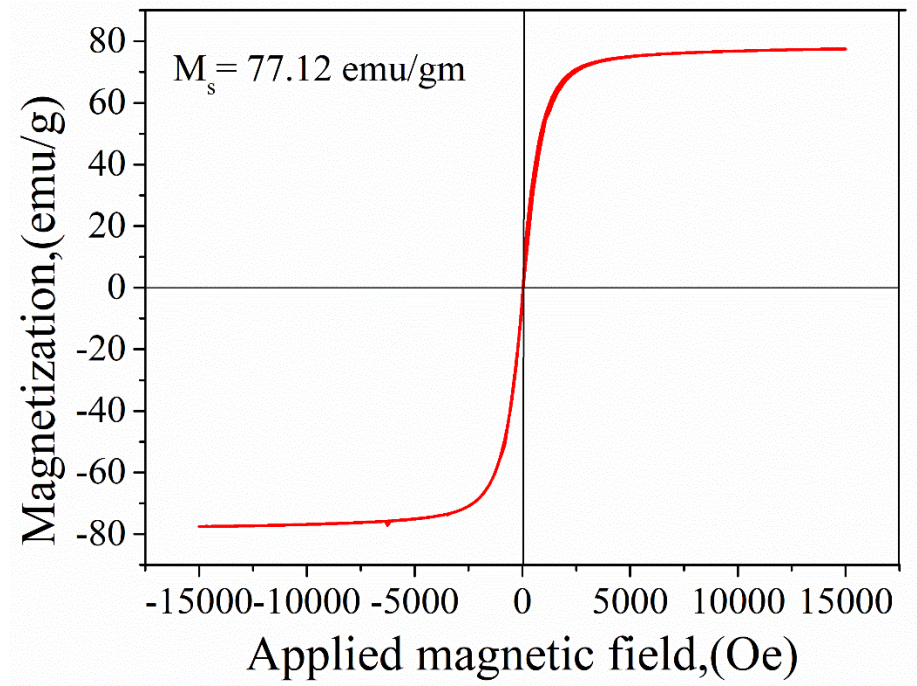
Fig.8.3 Magnetic hysteresis loop curve of Mn-Zn ferrite particles

8.5 Rheological properties analysis

8.5.1 Flow curves of shear stress

Plot of shear rate versus shear stress for three MRFs samples was measured at three different magnetic fields (0 kA/m, 86 kA/m, and 343 kA/m) using magnetorheometer while the shear rate was varied between from 0.1 to 500 s^{-1} (as shown in Fig. 5). At zero magnetic field strength, the MRFs flow curve show that shear stress increases almost linearly, suggesting a typical Newtonian behaviour (see Fig. 5.a). The application of the magnetic field induces dipole-dipole interactions between magnetic particles, and causes formation of a chain-like structure in the MR fluid. On the other hand, as the Mn-Zn ferrite volume concentration increases, shear stress (τ) also increases for a particular magnetic field strength (H). (Fig. 8.4.b and c).
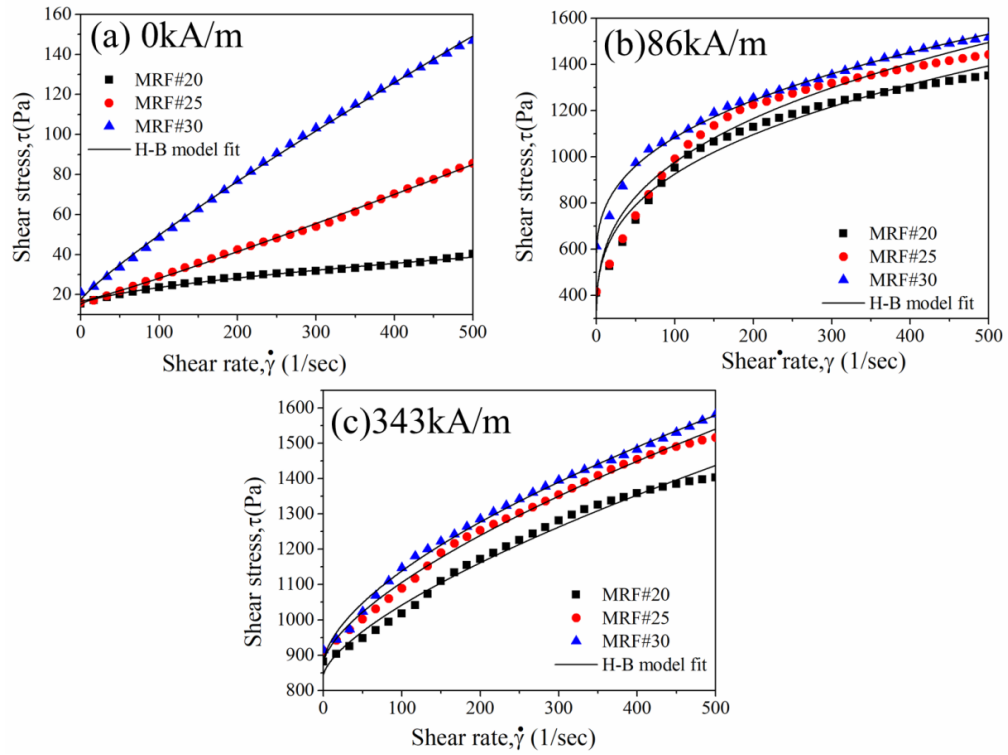
Fig.8.4 Dependence of shear stress, (τ) on the shear rate ($\dot{\gamma}$) at different magnetic field strengths (a) 0kA/m (b) 86kA/m and (c) 343 kA/m for MRF#20

Consequently, in MRF#30 sample the Mn-Zn ferrite concentration was high, these particle align a thick column and stronger chain-like structure leading to larger yield stress when compared to low concentration MRF#20 and 25 samples. It could be mentioned that the values of shear stress of Mn-Zn ferrite-based MRFs are minimum due to the low saturation magnetization (77.18 emu/g). This is clearly observed from the VSM analysis. To determine the optimal parameters for the MRF samples, three different constitutive rheological model parameters were chosen. In this contrast, the most applied model to MRFs is a Bingham fluid model parameter given in Equation (1). Yield stress can be found by extrapolating the shear stress at zero shear rate, also defined as the lowest yield stress required for liquid flow. For example, the yield stress was calculated to be 998.12 Pa for MRF#30 at 343 kA/m.

$$\tau = \tau_y + n_o\dot{\gamma} \qquad \tau > \tau_y \qquad \dot{\gamma} = 0 \qquad \tau < \tau_y, \tag{8.1}$$

Where, τ indicates shear stress: τ_y implies yield stress, which is a function of applied magnetic field, $\dot{\gamma}$ denotes the shear rate, η_o refers shear viscosity at a high shear rate.

Table 8.2 indicates the optimal parameter values obtained from the model. It can be seen from the table that the Adj-R^2 values are not consistent for all the MRF samples at different magnetic field strengths.

Table 8.2. Optimal parameters of MRF#20, MRF#25, and MRF#30 fluids using Bingham fluid

samples name	$\tau = \tau_y + \eta_o \dot{\gamma}$	0 kA/m	86 kA/m	343kA/m
	τ_y	18.73	727.063	923.03
MRF#20	η_0	0.048	1.49	1.08
	R^2	**0.92**	**0.81**	**0.96**
	τ_y	14.48	758.082	973.35
MRF#25	η_0	0.13	1.65	1.20
	R^2	**0.91**	**0.80**	**0.96**
	τ_y	23.168	973.75	998.12
	η_0	0.257	1.20	1.24
MRF#30	R^2	**0.86**	**0.96**	**0.96**

Since the flow curves are non-linear, the constitutive equation of the Herschel-Bulkley fitted with the experimental curves from (Fig. 8.4a, b, and c) was employed to determine the shear yield stress values which can be calculated using the Eq. (8.2)

$$\tau = \tau_y + k\dot{\gamma}^n \tag{8.2}$$

Where, k denotes the consistency coefficient and n designates the shear-thinning exponent, respectively. Table 3 shows the fitting parameters for the Herschel- Bulkley model that achieves the best fits which were reasonably good concerning the Adj-R^2 values for three MRFs.

With increasing magnetic field strength, the k and n parameters values of MRF samples increase and decrease, respectively. The n values define the degree to which a material is shear thickening. The value is greater than one (n > 1) or shear-thinning less than one (n < 1). The MRFs 20, 25, and 30 suspension values shown are lower than 1 which indicates the shear thinning behaviour suspensions as given in Table 8.3.

Table 8.3 Parameters values of MRF#20, MRF#25, and MRF#30 H-B model

Samples name	$\tau = \tau_y + k\dot{\gamma}^n$	0 kA/m	86kA/m	343kA/m
MRF#20	τ_0	14.89	284.18	843.48
	K	0.47	133.39	8.674
	n	0.62	0.34	0.68
	R^2	0.99	0.97	0.98
MRF#25	τ_0	16.56	267.96	877.70
	K	17.21	146.91	10.82
	n	0.2	0.341	0.662
	R^2	0.99	0.96	0.99
MRF#30	τ_0	17.21	543.76	878.11
	K	0.58	96.040	15.22
	n	0.87	0.37	0.61
	R^2	0.99	0.99	0.99

Also, even though the flow curves look from the BP and HB model, the Casson model parameter fit with the experimental flow curves, which can be written mathematically describing the shear stress given in Eq. (8.3)

$$\sqrt{\tau} = \sqrt{\tau_y} + \sqrt{n_\infty}\sqrt{\dot{\gamma}} \qquad (8.3)$$

Where, n_∞ refers Casson shear viscosity at the infinite shear rate, τ_y designates yield stress, τ indicates shear stress, and $\dot{\gamma}$ denotes the shear rate. Experimental flow curves well fitted by the Casson model regarding Adj. R^2 values and detailed rheological parameters obtained by this model are summarized in Table 4

Table 8.4 Optimal parameters of MRF#20, MRF#25, and MRF#30 fluids of Casson

Samples name	$\sqrt{\tau} = \sqrt{\tau_y} + \sqrt{n_\infty}\sqrt{\dot{\gamma}}$	0 kA/m	86kA/m	343kA/m
MRF#20	τ_y	2.84	541.39	790.46
	η_∞	0.02	0.42	0.18
	R^2	0.99	0.92	0.98
MRF#25	τ_y	5.85	562.81	827.016
	η_∞	0.08	0.48	0.21
	R^2	0.99	0.91	0.98
MRF#30	τ_y	8.96	663.16	845.24
	η_∞	0.16	0.21	0.22
	R^2	0.99	0.98	0.97

8.5.2 Flow curves of viscosity
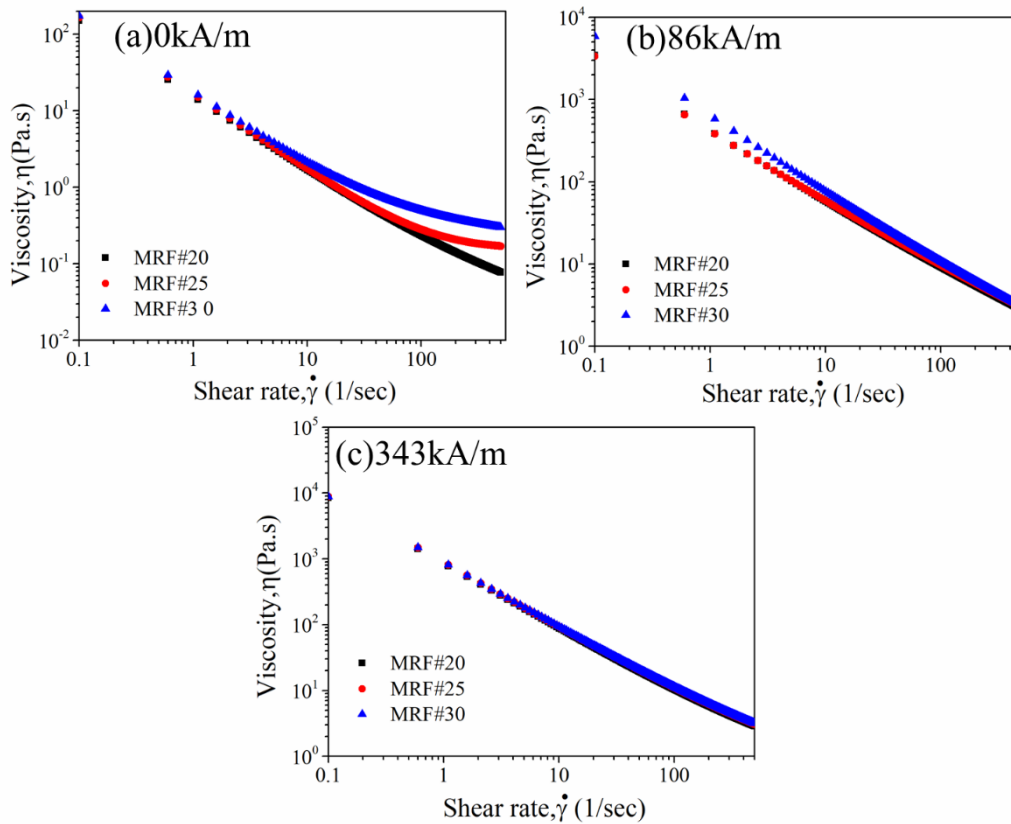
Fig.8.5 Viscosity of MRFs, as a function of (η) on the shear rate ($\dot{\gamma}$) at three various magnetic field strengths (a) 0kA/m (b) 86kA/m and (c) 343 kA/m for MRF#20 (block symbols), MRF#25 (red symbol), and MRF#30 (green symbol) samples

Fig 8.5 (a-c) shows the measured shear viscosity (η) versus shear rate ($\dot{\gamma}$) for MRF#20, MRF#25, and MRF#30 samples at the various magnetic fields, i.e. (0 kA/m, 86 kA/m, and 343 kA/m) for a range of 0.01 to 500 s^{-1}. As can be seen from the figure, shear viscosity dramatically decreased in the higher shear rate region, suggesting MR fluids having a shear-thinning behaviour due to the variations in the disruption in internal structure under shear deformation. On the other hand, shear viscosity increased with increasing the magnetic field strength applied and particle volume fraction. Meanwhile, higher shear viscosity obtained from the MRF#30 sample when compared to MRF#20 and 25 is clearly observed in Fig.8.5(a)-(c). This was due to a higher volume fraction of magnetic particle present in the MRF. It increased both off-state and on-state viscosity, however forms a stronger column-

like structure formation was made in the direction of the magnetic field, and hinderedthe free rotation of particles and made the MRF suspensions more viscous in the MRF#30 sample(Jung et al. 2016).

8.5.3 Effect of Mn-Zn ferrites on shear stress, viscosity, and yield stress.

Figure 8.6 (a) and (b) show bar graphs comparing the shear stress and viscosity with a maximum shear rate of $500s^{-1}$. For all prepared MRF samples, the shear stress and viscosity values increased with the applied magnetic field strength and the magnetic particle volume fraction of the MR fluid. In Fig.8.6(b),the viscosity values in the absence of magnetic field of MRF#20,25 and 30 are 0.076,0.169 and 0.29 Pa.s respectively. It was due to the low mass density of Mn-Zn ferrite particles which occupy the large volume fractions of particles in the carrier fluid. This results in increased viscosity of the MRF#30 sample. Also, Fig.8.6 (c) shows the trend in field-dependent yield stress as a function of magnetic field strength, and which is an important parameter for MRFs. It was determined by fitting experimental data at nonzero shear rate levels with viscoplastic constitutive models, such as the Bingham, Herschel–Bulkley, and Casson equations. On the other hand, at a given magnetic field strength, yield stress increased as the volume fraction of Mn-Zn ferrite particles was increased. The yield stress of MRF#30 was higher than that of MRF#25 and 20, which indicated that the Mn-Zn ferrite volume fraction little effect on the achievable yield stress. Increase of magnetic field, causes the formation of magnetic particle alignment, and builds a strong chain-like structure, as a result, prepared MRFs attribute to more pronounced dynamic yield stress. The power-law model was adapted to find out the slope of the Mn-Zn ferrite based MR fluid

$$\tau_y \propto H^m \qquad\qquad (8.4)$$

Where, the exponent m can be obtained by fitting the above model with the applied magnetic field strength. It should be noted that the slope of dynamic yield stress at low magnetic field strengths as a magnetic field function was considered to be 2.0 based on the magnetic polarization model, which was related to the magnetic forces.

At high magnetic field strengths, local saturation in magnetization becomes important near particle-particle contacts, the slope of dynamic yield stress as a function of magnetic field strength shown in Fig.8.6.
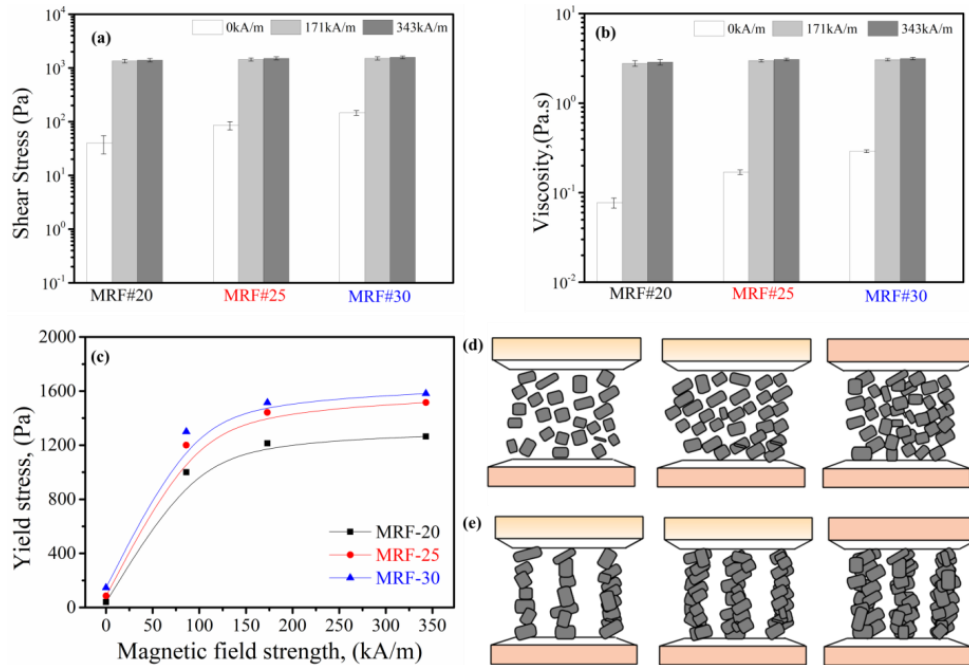
Fig.8.6 Bar graph dependence of (a) shear stress (b) shear viscosity at a maximum shear rate and (c) yield stress versus at different magnetic field strengths and (d) Illustration of particle arrangement of Mn-Zn ferrite based MRF

Transition of slope from 2.0 to 1.5 were reported in the CIPs based MRFs. For Mn-Zn ferrite-based MRF fluids, the slope of the plot was determined to be 1.5 that was possibly due to the complete saturation of the MR fluid under the magnetic field strength applied. While the particle yield stress was independent of the strength of the magnetic field when the particles achieve magnetic saturation. While the Mn-Zn ferrite-based MRFs showed moderate yield stress compared to iron particles based MRF, the ferrite based MRF was stable at high temperatures, showed high chemical and sedimentation stability, which make these Mn-Zn ferrite-based MRFs suitable candidate for applications where MRF stability in harsh working environments is a major requirement rather than comparable yield stress or strength of MRF.

The dynamic yield stress values obtained were compared to more than the previous ferrite-based MRFs. Magnetic saturation was present in all particles at a high magnetic field and the yield stress was independent of the external magnetic field. This phenomenon is mainly due to the relatively low value of M_s of Mn-Zn ferrite particles compared to typical MRF magnetic materials. The arrangement of plate-like Mn-Zn ferrite particles without and with the magnetic field is shown schematically in Figure 8.6(d) and (e). In the case of MRF-20 containing lower concentrations, the particles are shown to form chains consisting of single strands of particles. For MRF-25 and MRF-30 with the highest concentration of particles, the number of particles was high enough to form a strong column-like structure. In the case of the MRF#30 sample, the Mn-Zn particles have a low mass density resulting in accommodation a large number of particles in the MRF. Many columns were formed due to large number of particles, which are placed nearby, causing the particles also to interact perpendicularly to the length of the columns.
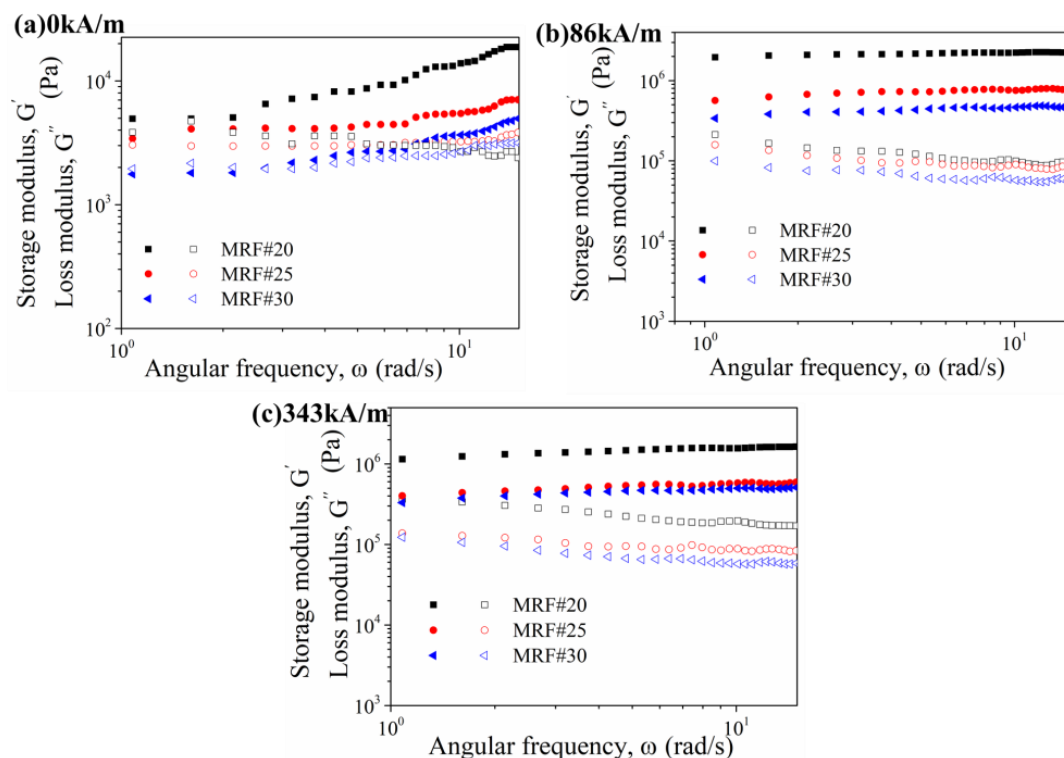
Fig.8.7 Frequency sweep test at different magnetic field strength applied (a) 0kA/m (b) 86kA/m and (c) 343 kA/m with a (γ) constant shear strain (0.001%)

Fig. 8.7 shows the frequency sweep range of 0.1–10 rad/s test which was undertaken with constant shear strain (γ) 0.001% under three various magnetic field strengths to determine the storage modulus (closed symbols) (G′) indicates the viscous response and loss (G″) modulus (open symbol) represents changes an elastic properties. Fig.8.7(a) depicts the absence of magnetic field (0 kA/m) MRF#20, 25, and 30 samples exhibit liquid-like behaviour. Figure (b)-(c) indicate with the application of the magnetic field of 86kA/m and 343 kA/m MRF#20, 25, and 30 samples shows a stable plateau-shaped at the entire over the range of frequency, indicating that the storage module was larger than the loss modulus indicating the stronger elastic nature of the samples (Vinod et al. 2016). As a result, MRF#20, 25, and 30 based MRFs exhibited solid-like rather than liquid-like behaviour, as demonstrated by the improved elastic properties. This is typical behaviour due to the Mn-Zn ferrite particles which form a more robust particle chain structure within the MRFs.

8.5.5 Sedimentation analysis

The stability of sedimentation of particles is considered an essential factor for measuring MR fluids. Fig.8.8 shows the curves of sedimentation ratio versus time of Mn-Zn ferrite particles based MRFs. Fig. 8.8(a) shows the measured sedimentation ratio for MRF#20 MRF#25 and MRF#30 based MR fluids using a visual observation method under the static condition without disturbance of the samples. The picture shown in Fig.8.8(b) are photographs of the MRF#20, 25, and 30 samples at regular intervals of sedimentation time.

As seen from the figure, within 1 day, MRF#20 settled much faster than MRF#25 and 30. On the other hand, MRF#30 demonstrated a low sedimentation ratio of about 67% than MRF#20 and 25 sedimentation ratio which was 55% and 57 %, respectively. The stearic acid from the carboxyl group mixed in silicone oil, it was forms a gel-like structure that hinders the fast settling of Mn-Zn ferrites. It can be noted that the increase in solid volume fraction the liquidity of the sample was very low; for example, in MRF#30 samples, the settling of the Mn-Zn ferrite particle has decreased. In the case of MRF#25 and 20, as the liquidity of the sample was high, it resulted in

fast sedimentation of particles concerning time of 1 day, as can be observed in Fig 9(b).
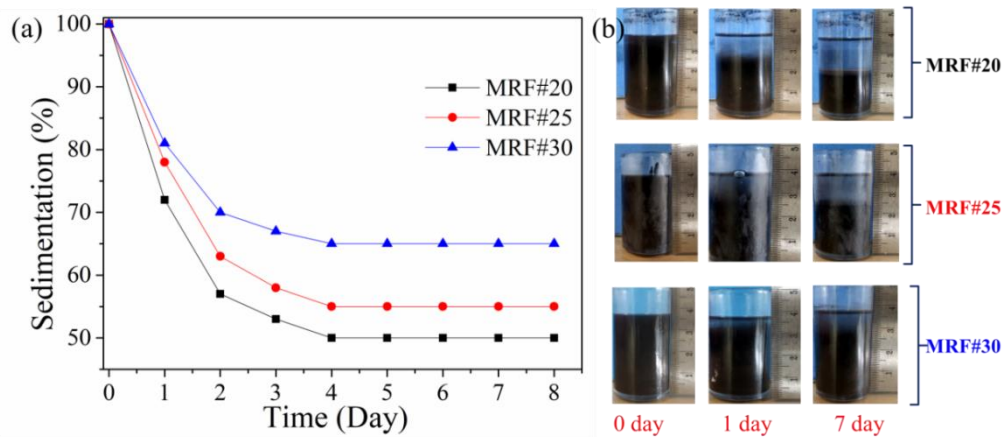
Fig.8.8(a) Sedimentation ratio as a function of time (b) snapshots of MRFs poured for visual inspection at 0hr, 24hr and 48hr for MRF#20, 25, and 30 samples.

8.6 Summary

Mn-Zn ferrite particles with different volume fractions (20, 25, and 30%) were dispersed in a silicone carrier fluid. The importance of the plate-like shape of magnetic particles and their concentration in the fluid in measuring the efficiency of MRFs is thus highlighted in this work. With increasing magnetic fill fraction and applied magnetic field strength, the yield strength increases. It was observed that Mn-Zn ferrite showed plate-like shape, presence of small aggregation, and spinel structure in phase. The magnetic measurement showed saturation magnetization (M_s) of 77.12 emu/gm at room temperature. The particles interact with one other when a magnetic field is applied, forming stronger magnetic particle columns and increasing the MRF's solidity. The saturation magnetization, particle size, size-distribution, and concentration of the particles in the MRF were found to have a considerable influence on the dynamic yield stress of the MRFs. At the maximum particle concentration (30 vol. percent) in the fluid, the Mn-Zn ferrite powder based MRF showed good yield stress (1.6 kPa). These figures are comparable to those seen in MRFs with CIPs. The Mn-Zn ferrite particles' ready-dispersibility after sedimentation renders these MRFs dependable for repeated use.

CHAPTER-9

CONCLUSIONS

Present work deals with developing lab scale magneto-rheological fluids for MR damper application with low sedimentation rate and analysing the effect of particle loading of carbonyl iron particles and on rheological and sedimentation properties. Carbonyl iron particles and different types of additives, carrier liquids, and thixotropic fumed silica as coating materials were used to synthesize MRFs containing different volumes (%) of magnetic particles. Important conclusions are summarized based on the archived outcome.

- SEM and XRD confirmed that the morphology and excellent crystalline structure of the CIPs (α-Fe phase) used in the MR fluid and additives had small and large sheet aggregates like morphology.
- SQUID magnetometer conformed to the 250emu/g at 10 kOe saturation magnetization value of CIPs.
- The Lord-132DG presented much lower shear stress and a viscosity at zero magnetic fields when compared with MRFp-1, MRFp-2, MRFp-3, and MRFp-4. It was observed that MRFp-2, 3, and 4 have slightly low shear rate v/s shear stress and shear rate v/s viscosity at the applied magnetic field (0 to 0.7 Tesla) when compared to LORD 132 DG but MRFp-1 had better response.
- Sedimentation problem was found to be greatly reduced in house prepared MRFp-2, 3, and 4 and when compared with commercially available Lord-132DG due to the addition of additives like claytone APA, baragell and garamite 1958. The MRF-3 gave a good competition to the Lord 132 DG fluid in terms of off/on state shear stress, viscosity.
- The base magnetic particle with 70wt% CIPs along with plain PAO oil and CIPs/claytone APA/molyvan 855 as an additive, friction reducer was adjusted in PAO oil-based MRF was prepared to prevent the sedimentation problems.

- The dynamic yield stress and the shear stress of the CIPs/claytone APA MRF exhibited lower than that of the CIPs MRF. Also, SEM confirmed that the surface of the CIPs connected well with claytone APA confirming improved sedimentation.

- The magnetic properties of the CIPs MRF showed higher saturation magnetization compared with the CIP/claytone APA MRF. The fabricated MR damper against 72 hrs sedimentation testing of CIPs/claytone MRF produced higher compression (F_{co}) and rebound (F_{re}) damping force than of pure CIPs MRF in off-state (i.e., 0A) condition, and also slightly lower compression (F_{co}) and rebound(F_{re}) damping force than CIPs MRF in on-state (i.e., 0.4A) condition.

- The SEM morphological analysis of CIPs/fumed silica particles mixture, which fills the interspace between the CIPs and reduces particle density, improved the sedimentation ratio. The sedimentation stability was considerably improved by the addition of different surface area types of fumed silica in MRF2, 3, 4, and 5 rather than MRF1. Finally, MRF 4 and 5 samples containing hydrophilic fumed silica showed a better sedimentation ratio of about 98% and 99% up to 7 days.

- The magnetic properties of MRF1, 2, 3, 4, and 5 samples measured using VSM showed that MRF1 has maximum saturation values of 132.92 emu/gm with applied magnetic field in the range of -15000Oe to 15000Oe, while MRF4 and 5 have better magnetic saturation values.

- The experimental rheological test of MRF1, 2, 3, 4, and 5 fluids was conducted under different magnetic field strengths using a magnetorheometer. Three constitutive models were applied to shear stress versus shear rate rheology curves, and among the three models, the H-B model well-fitted the Adj-R^2 values rather than the BP and Casson models. While the MRF4 and MRF5 hydrophilic type with larger surface area samples show dynamic yield stress of maximum of about 7.9 kPa and 8.1 kPa respectively, at an applied magnetic field strength of 343 kA/m.

- The prepared MR fluids containing carbonyl iron/fumed silica with three different carrier liquid, viscosity (5, 30, and 400 cSt). The MR performance for prepared MR fluids was studied by using a twin drive rheometer. The maximum shear stresses reached values of 15000, 12000, and 9000 Pa respectively in the magnetic field range 0–0.9 T at 40^{0}C.

- Regarding sedimentation stability during direct observation it was seen that the MR fluid with fumed silica as thixotropic additive showed slower sedimentation stability and the ratio was observed to be 90, 93, and 96% of MRF-1, MRF-2, and MRF-3 respectively during 800 hrs.

- In this chapter, MRFs were prepared with different volume concentrations ($\phi_1 = 20$, $\phi_2 = 25$ and $\phi_3 = 30$) by dispersing solid-phase these ferrite particles in a silicone oil as continuous phase along with stearic acid as an additive to minimize the sedimentation problem

- The SEM, XRD, and EDS results showed plate-like morphology, pure spinel structure phase, and presence of Mn-Zn ferrite elemental composition, respectively. The VSM analysis showed that the amount of magnetic saturation was about 19.138emu/gm. The sedimentation stability ratio of MRF#30 showed a better sedimentation ratio of 67% up to 8 days than the MRF#20 and MRF#25 samples

- The outcomes of the rheological experiments on Mn-Zn ferrites-based MR fluids showed that an increase in the volume fraction ($\phi_1 > \phi_2 > \phi_3$) and the magnitude of the magnetic field strength gives rise to higher yield stress for MRF#30 sample.

- The MRF#30 showed values than the MRF#20 and 25 sample*s* in terms of shear stress(τ), viscosity (η), and yield stress (τ_0) with increasing applied magnetic field strengths (H). The results were in good agreement with experimental flow curves fitted to the Herschel-Bulkley rather than the Bingham, and Casson constitutive rheological models. Also frequency sweep test was performed to suggest the MRF#20, #25, and # 30 samples have more solid-like behaviour with the application of the magnetic field.

SCOPE OF FUTURE WORK

The present work demonstrates the feasibility of lab-scale magneto-rheological fluids for MR damper applications. Though the approach is successful, the sedimentation rate is considerably reduced in micron-sized carbonyl iron particles-based MRFs. Further, the synthesizing (1-2μm) sized carbonyl iron particles and use of low viscosity base oil needs to be addressed through a proper synthesizing technique and sedimentation stability minimized further without affecting the rheological properties. Cost-effective MRF needs are required for commercially available MRF. Further, the performances of the developed MRFs are to be tested in a real field application.

References

Anupama, A. V., Kumaran, V., and Sahoo, B. (2018). "Magnetorheological fluids containing rod-shaped lithium-zinc ferrite particles: The steady-state shear response." *Soft Matter*, 14(26), 5407–5419.

Arief, I., and Mukhopadhyay, P. K. (2014). "Preparation of spherical and cubic $Fe_{55}Co_{45}$ microstructures for studying the role of particle morphology in magnetorheological suspensions." *J. Magn. Magn. Mater.*, 360, 104–108.

Ashour, O., Rogers, C. A., and Kordonsky, W. (1996). "Magnetorheological Fluids: Materials, Characterization, and Devices." *J. Intell. Mater. Syst. Struct.*, 7(2), 123–130.

Ashtiani, M., Hashemabadi, S. H., and Ghaffari, A. (2015). "A review on the magnetorheological fluid preparation and stabilization." *J. Magn. Magn. Mater.*, Elsevier B.V.

Bae, D. H., Choi, H. J., Choi, K., Nam, J. Do, Islam, M. S., and Kao, N. (2017). "Microcrystalline cellulose added carbonyl iron suspension and its magnetorheology." *Colloids Surfaces A Physicochem. Eng. Asp.*, 514, 161–167.

Bell, R. C., Karli, J. O., Vavreck, A. N., Zimmerman, D. T., Ngatu, G. T., and Wereley, N. M. (2008). "Magnetorheology of submicron diameter iron microwires dispersed in silicone oil." *Smart Mater. Struct.*, 17(1).

Boelter, R., and Janocha, H. (1997). "Design rules for MR fluid actuators in different working modes" *Smart Struct. Mater., 1997* 148–159.

Branch, T., and Knudsen, S. K. D. (2018). "Highlighting cooperative research performed at the Laboratory of Magnetic Fluids-Romanian Academy As featured in." *Soft Matter*, 14, 6648.

C, B. J. (2010). "An Introduction to Interfaces & Colloids: The Bridge to Nanoscience." World Scientific.

Carlson, J. D. (2003). "Critical factors for MR fluids in vehicle systems." *Int. J. Veh. Des.*, 33(1–3), 207–217.

Carlson, J. D. (2005). "MR fluids and devices in the real world." *Int. J. Mod. Phys. B*, World Scientific Publishing Company , 1463–1470.

Çeşmeci, Ş., and Engin, T. (2010). "Modeling and testing of a field-controllable magnetorheological fluid damper." *Int. J. Mech. Sci.*, 52(8), 1036–1046.

Chae, H. S., Kim, S. D., Hao Piao, S., Hyoung, &, and Choi, J. (n.d.). "Core-shell structured $Fe_3O_4@SiO_2$ nanoparticles fabricated by sol-gel method and their magnetorheology."

Chae, H. S., Piao, S. H., Maity, A., and Choi, H. J. (2015). "Additive role of attapulgite nanoclay on carbonyl iron-based magnetorheological suspension." *Colloid Polym. Sci.*, 293(1), 89–95.

Chambers, J. M., and Wereley, N. M. (2017). "Vertical axis inductance monitoring system to measure stratification in a column of magnetorheological fluid." *IEEE Trans. Magn.*, 53(1).

Chand, M., Kumar, S., Shankar, A., Porwal, R., and Pant, R. P. (2013). "The size induced effect on rheological properties of Co-ferrite based ferrofluid." *J. Non. Cryst. Solids*, 361(1), 38–42.

Chand, M., Shankar, A., Noorjahan, Jain, K., and Pant, R. P. (2014). "Improved properties of bidispersed magnetorheological fluids." *RSC Adv.*, 4(96), 53960–53966.

Charles, S. W. (2002). "The Preparation of Magnetic Fluids." 3–18.

Chaudhuri, A., Wang, G., Wereley, N. M., Tasovksi, V., and Radhakrishnan, R. (2005). "Substitution of micron by nanometer scale powders in magnetorheological fluids." *Int. J. Mod. Phys. B*, 1374–1380.

Chaudhuri, A., Wereley, N. M., Radhakrishnan, R., and Choi, S. B. (2006). "Rheological Parameter Estimation for a Ferrous Nanoparticle-based Magnetorheological Fluid using Genetic Algorithms." *J. Intell. Mater. Syst. Struct.*, 17(3), 261–269.

Cheng, H., Zhang, X., Liu, G., Ma, W., and Wereley, N. M. (2016). "Measuring the sedimentation rate in a magnetorheological fluid column via thermal conductivity monitoring." *Smart Mater. Struct.*, 25(5).

Choi, J., Han, S., Nam, K. T., and Seo, Y. (2020). "Hierarchically Structured Fe3O4Nanoparticles for High-Performance Magnetorheological Fluids with Long-Term Stability." *ACS Appl. Nano Mater.*, 3(11), 10931–10940.

Choi, J. S., Park, B. J., Cho, M. S., and Choi, H. J. (2006). "Preparation and magnetorheological characteristics of polymer coated carbonyl iron suspensions." *J. Magn. Magn. Mater.*, 304(1).

Chuah, W. H., Zhang, W. L., Choi, H. J., and Seo, Y. (2015). "Magnetorheology of Core-Shell Structured Carbonyl Iron/Polystyrene Foam Microparticles Suspension with Enhanced Stability." *Macromolecules*, 48(19), 7311–7319.

Cvek, M., Mrlík, M., Ilčíková, M., Mosnáček, J., Babayan, V., Kuceková, Z., Humpolíček, P., and Pavlínek, V. (2015). "The chemical stability and cytotoxicity of carbonyl iron particles grafted with poly(glycidyl methacrylate) and the magnetorheological activity of their suspensions." *RSC Adv.*, 5(89), 72816–72824.

Dong, X., Tong, Y., Ma, N., Qi, M., and Ou, J. (2015). "Properties of cobalt nanofiber-based magnetorheological fluids." *RSC Adv.*, 5(18), 13958–13963.

Dong, Y. Z., Piao, S. H., Zhang, K., and Choi, H. J. (2018). "Effect of $CoFe_2O_4$ nanoparticles on a carbonyl iron based magnetorheological suspension." *Colloids Surfaces A Physicochem. Eng. Asp.*, 537, 102–108.

Du, C., Chen, W., and Wan, F. (2010). "Influence of HLB parameters of surfactants on properties of magneto-rheological fluid." *Adv. Mater. Res.*, Trans Tech Publications Ltd, 843–847.

Dyke, S. J., Spencer, B. F., Sain, M. K., and Carlson, J. D. (1998). "An experimental study of MR dampers for seismic protection." *Smart Mater. Struct.*, 7(5), 693–703.

Eshaghi, M., Rakheja, S., and Sedaghati, R. (2015). "An accurate technique for pre-yield characterization of MR fluids." *Smart Mater. Struct.*, 24(6), 065018.

Fang, F. F., Choi, H. J., and Jhon, M. S. (2009). "Magnetorheology of soft magnetic carbonyl iron suspension with single-walled carbon nanotube additive and its yield stress scaling function." *Colloids Surfaces A Physicochem. Eng. Asp.*, 351(1–3), 46–51.

Fang, F. F., Jang, I. B., and Choi, H. J. (2007). "Single-walled carbon nanotube added carbonyl iron suspension and its magnetorheology." *Diam. Relat. Mater.*, 16(4-7 SPEC. ISS.), 1167–1169.

Fang, F. F., Liu, Y. D., and Choi, H. J. (2012). "Carbon nanotube coated magnetic carbonyl iron microspheres prepared by solvent casting method and their magneto-responsive characteristics." *Colloids Surfaces A Physicochem. Eng. Asp.*, 412, 47–56.

Fang, F. F., Liu, Y. D., Choi, H. J., and Seo, Y. (2011). "Core-shell structured carbonyl iron microspheres prepared via dual-step functionality coatings and their magnetorheological response." *ACS Appl. Mater. Interfaces*, 3(9), 3487–3495.

Fei, C., Zuzhi, T., and Xiangfan, W. (2015). "Novel Process to Prepare High-Performance Magnetorheological Fluid Based on Surfactants Compounding." *Mater. Manuf. Process.*, 30(2), 210–215.

Gabriel, C., and Laun, · H M. (2009). "Combined slit and plate-plate magnetorheometry of a magnetorheological fluid (MRF) and parameterization using the Casson model." *Rheol Acta*, 48, 755–768.

Gao, F., Liu, Y. N., and Liao, W. H. (2017). "Optimal design of a magnetorheological damper used in smart prosthetic knees." *Smart Mater. Struct.*, 26(3), 035034.

Ginder, J. M., Davis, L. C., and Elie, L. D. (1996). "Rheology of magnetorheological fluids: Models and measurements." *Int. J. Mod. Phys. B*, 10(23–24), 3293–3303.

Gómez-Ramírez, A., López-López, M. T., González-Caballero, F., and Durán, J. D. G. (2012). "Wall slip phenomena in concentrated ionic liquid-based magnetorheological fluids." *Rheol. Acta*, 51(9), 793–803.

Guerrero-Sanchez, C., Lara-Ceniceros, T., Jimenez-Regalado, E., Raşa, M., and Schubert, U. S. (2007). "Magnetorheological fluids based on ionic liquids." *Adv. Mater.*, 19(13), 1740–1747.

Guo, C., Yang, Z., Shen, S., Liang, J., and Xu, G. (2018a). "High microwave attenuation performance of planar carbonyl iron particles with orientation of shape anisotropy field." *J. Magn. Magn. Mater.*, 454, 32–38.

Guo, Y. Q., Sun, C. L., Xu, Z. D., and Jing, X. (2018b). "Preparation and tests of MR fluids with CI particles coated with MWNTS." *Front. Mater.*, 5.

Hajalilou, A., Mazlan, S. A., and Shila, S. T. (2016). "Magnetic carbonyl iron suspension with Ni-Zn ferrite additive and its magnetorheological properties." *Mater. Lett.*, 181, 196–199.

Han, J. K., and Choi, H. J. (2018). "Non-stoichiometric zinc-doped spinel ferrite nanoparticles with enhanced magnetic property and their magnetorheology." *Colloid Polym. Sci.*, 296(2), 405–409.

Han, Y. M., Kim, S., Park, Y. D., Kang, J. W., and Choi, S. B. (2015). "Field-dependent characteristics of magnetorheological fluids containing corroded iron particles." *Smart Mater. Struct.*, 24(11), 115016.

Hato, M. J., Choi, H. J., Sim, H. H., Park, B. O., and Ray, S. S. (2011). "Magnetic carbonyl iron suspension with organoclay additive and its magnetorheological properties." *Colloids Surfaces A Physicochem. Eng. Asp.*, 377(1–3), 103–109.

Hemanth, K., Kumar, H., and Gangadharan, K. V. (2017). "Vertical dynamic analysis of a quarter car suspension system with MR damper." *J. Brazilian Soc. Mech. Sci. Eng.*, 39(1), 41–51.

Holm, C., and Weis, J. J. (2005). "The structure of ferrofluids: A status report." *Curr. Opin. Colloid Interface Sci.*, Elsevier.

Holzwarth, U., and Gibson, N. (2011). "The Scherrer equation versus the 'Debye-Scherrer equation.'" *Nat. Nanotechnol.*, Nature Publishing Group.

Hong, C. H., Liu, Y. D., and Choi, H. J. (2013). "Carbonyl iron suspension with halloysite additive and its magnetorheology." *Appl. Clay Sci.*, 80–81, 366–371.

Hong, S.-R., and Choi, S.-B. (2005). "Vibration Control of a Structural System Using Magneto-Rheological Fluid Mount." *J. Intell. Mater. Syst. Struct.*, 16(11–12), 931–936.

Huang, L., Li, J., and Zhu, W. (2017). "Mathematical model of a novel small magnetorheological damper by using outer magnetic field." *AIP Adv.*, 7(3), 035114.

Jackson, J. A., Messner, M. C., Dudukovic, N. A., Smith, W. L., Bekker, L., Moran, B., Golobic, A. M., Pascall, A. J., Duoss, E. B., Loh, K. J., and Spadaccini, C. M. (2018). "Field responsive mechanical metamaterials." *Sci. Adv.*, 4(12).

Jang, D. S., Liu, Y. D., Kim, J. H., and Choi, H. J. (2015). "Enhanced magnetorheology of soft magnetic carbonyl iron suspension with hard magnetic γ-Fe2O3 nanoparticle additive." *Colloid Polym. Sci.*, 293(2), 641–647.

Jiang, W., Zhang, Y., Xuan, S., Guo, C., and Gong, X. (2011). "Dimorphic magnetorheological fluid with improved rheological properties." *J. Magn. Magn. Mater.*, 323(24), 3246–3250.

Jolly, M. R., Bender, J. W., and Carlson, J. D. (1999). "Properties and Applications of Commercial Magnetorheological Fluids." *J. Intell. Mater. Syst. Struct.*, 10(1), 5–13.

Jolly, M. R., Carlson, J. D., and Muñoz, B. C. (1996). "A model of the behaviour of magnetorheological materials." *Smart Mater. Struct.*, 5(5), 607–614.

Ju, B., Yu, M., Fu, J., Zheng, X., and Liu, S. (2013). "Magnetic field-dependent normal force of magnetorheological gel." *Ind. Eng. Chem. Res.*, 52(33), 11583–11589.

Jun, J. B., Uhm, S. Y., Ryu, J. H., and Suh, K. Do. (2005). "Synthesis and characterization of monodisperse magnetic composite particles for magnetorheological fluid materials." *Colloids Surfaces A Physicochem. Eng. Asp.*, 260(1–3), 157–164.

Jung, I. D., Kim, M., and Park, S. J. (2016). "A comprehensive viscosity model for micro magnetic particle dispersed in silicone oil." *J. Magn. Magn. Mater.*, 404, 40–44.

Keyoonwong, W., Guo, Y., Kubouchi, M., Aoki, S., and Sakai, T. (2012). "Corrosion behavior of three nanoclay dispersion methods of epoxy/organoclay nanocomposites." *Int. J. Corros.*, 2012.

Kim, I. G., Song, K. H., Park, B. O., Choi, B. I., and Choi, H. J. (2011). "Nano-sized

Fe soft-magnetic particle and its magnetorheology." *Colloid Polym. Sci.*, 289(1), 79–83.

Kim, J. E., Ko, J. Do, Liu, Y. D., Kim, I. G., and Choi, H. J. (2012a). "Effect of medium oil on magnetorheology of soft carbonyl iron particles." *IEEE Trans. Magn.*, 48(11), 3442–3445.

Kim, M. H., Choi, K., Nam, J. Do, and Choi, H. J. (2017). "Enhanced magnetorheological response of magnetic chromium dioxide nanoparticle added carbonyl iron suspension." *Smart Mater. Struct.*, 26(9).

Kim, M. S., Liu, Y. D., Park, B. J., You, C. Y., and Choi, H. J. (2012b). "Carbonyl iron particles dispersed in a polymer solution and their rheological characteristics under applied magnetic field." *J. Ind. Eng. Chem.*, 18(2), 664–667.

Kim, M. W., Han, W. J., Kim, Y. H., and Choi, H. J. (2016). "Effect of a hard magnetic particle additive on rheological characteristics of microspherical carbonyl iron-based magnetorheological fluid." *Colloids Surfaces A Physicochem. Eng. Asp.*, 506, 812–820.

Kordonski, W. I., and Gorodkin, S. R. (1996). "Magnetorheological Fluid-Based Seal." *J. Intell. Mater. Syst. Struct.*, 7(5), 569–572.

Kumar, J. S., Paul, P. S., Raghunathan, G., and Alex, D. G. (2019). "A review of challenges and solutions in the preparation and use of magnetorheological fluids." *Int. J. Mech. Mater. Eng.*, Springer.

Kumbhar, B. K., Patil, S. R., and Sawant, S. M. (2015). "Synthesis and characterization of magneto-rheological (MR) fluids for MR brake application." *Eng. Sci. Technol. an Int. J.*, 18(3), 432–438.

Kwon, S. H., Choi, H. J., Lee, J. W., Hong, K. P., and Cho, M. W. (2013). "Magnetorheology of xanthan-gum-coated soft magnetic carbonyl iron microspheres and their polishing characteristics." *J. Korean Phys. Soc.*, 62(12), 2118–2122.

Kwon, S. H., Jung, H. S., Choi, H. J., Strecker, Z., and Roupec, J. (2018). "Effect of octahedral typed iron oxide particles on magnetorheological behavior of carbonyl iron dispersion." *Colloids Surfaces A Physicochem. Eng. Asp.*, 555, 685–690.

Lambrou, T. P., Anastasiou, C. C., and Panayiotou, C. G. (2010). "A nephelometric turbidity system for monitoring residential drinking water quality." *Lect. Notes Inst. Comput. Sci. Soc. Telecommun. Eng.*, Springer, Berlin, Heidelberg, 43–55.

Lijesh, K. P., Muzakkir, S. M., and Hirani, H. (2016). "Rheological measurement of redispersibility and settling to analyze the effect of surfactants on MR particles." *Tribol. - Mater. Surfaces Interfaces*, 10(1), 53–62.

Lim, S. T., Cho, M. S., Jang, I. B., and Choi, H. J. (2004). "Magnetorheological characterization of carbonyl iron based suspension stabilized by fumed silica." *J. Magn. Magn. Mater.*, 170–173.

Liu, J., Wang, X., Tang, X., Hong, R., Wang, Y., and Feng, W. (2015). "Preparation and characterization of carbonyl iron/strontium hexaferrite magnetorheological fluids." *Particuology*, 22, 134–144.

Liu, Y. D., Lee, J., Choi, S. B., and Choi, H. J. (2013). "Silica-coated carbonyl iron microsphere based magnetorheological fluid and its damping force characteristics." *Smart Mater. Struct.*, 22(6), 065022.

Manzoor, M. T., Kim, J. E., Jung, J. H., Han, C., Choi, S. B., and Oh, I. K. (2018). "Two-Dimensional rGO-MoS2 Hybrid Additives for High-Performance Magnetorheological Fluid." *Sci. Rep.*, 8(1).

Marinicə, O., Susan-Resiga, D., Bələnean, F., Vizman, D., Socoliuc, V., and Vékás, L. (2016). "Nano-micro composite magnetic fluids: Magnetic and magnetorheological evaluation for rotating seal and vibration damper applications." *J. Magn. Magn. Mater.*, 406, 134–143.

Mazlan, S. A., Issa, A., Chowdhury, H. A., and Olabi, A. G. (2009). "Magnetic circuit design for the squeeze mode experiments on magnetorheological fluids." *Mater. Des.*, 30(6), 1985–1993.

Moon, I. J., Kim, M. W., Choi, H. J., Kim, N., and You, C. Y. (2016). "Fabrication of dopamine grafted polyaniline/carbonyl iron core-shell typed microspheres and their magnetorheology." *Colloids Surfaces A Physicochem. Eng. Asp.*, 500, 137–145.

Morillas, J. R., and Vicente, J. de. (2019). "On the yield stress in magnetorheological fluids: A direct comparison between 3D simulations and experiments." *Compos. Part B Eng.*, Elsevier Ltd.

Ngatu, G. T., Wereley, N. M., Karli, J. O., and Bell, R. C. (2008). "Dimorphic magnetorheological fluids: Exploiting partial substitution of microspheres by nanowires." *Smart Mater. Struct.*, 17(4).

Nguyen, P. B., Do, X. P., Jeon, J., Choi, S. B., Liu, Y. D., and Choi, H. J. (2014a). "Brake performance of core-shell structured carbonyl iron/silica based magnetorheological suspension." *J. Magn. Magn. Mater.*, 367, 69–74.

Nguyen, Q., Choi, S., and Woo, J. (2014b). "Optimal design of magnetorheological fluid-based dampers for front-loaded washing machines." *Proc. Inst. Mech. Eng. Part C J. Mech. Eng. Sci.*, 228(2), 294–306.

Ni, X., Zheng, Z., Hu, X., and Xiao, X. (2010). "Silica-coated iron nanocubes:

Preparation, characterization and application in microwave absorption." *J. Colloid Interface Sci.*, 341(1), 18–22.

Park, B. J., Kim, M. S., and Choi, H. J. (2009). "Fabrication and magnetorheological property of core/shell structured magnetic composite particle encapsulated with cross-linked poly(methyl methacrylate)." *Mater. Lett.*, 63(24–25), 2178–2180.

Park, J. H., Chin, B. D., and Park, O. O. (2001). "Rheological properties and stabilization of magnetorheological fluids in a water-in-oil emulsion." *J. Colloid Interface Sci.*, 240(1), 349–354.

Patel, J., Parekh, K., and Upadhyay, R. V. (2017). "Performance of Mn-Zn ferrite magnetic fluid in a prototype distribution transformer under varying loading conditions." *Int. J. Therm. Sci.*, 114, 64–71.

Patel, R. (2011). "Mechanism of chain formation in nanofluid based MR fluids." *J. Magn. Magn. Mater.*, 1360–1363.

Piao, S. H., Bhaumik, M., Maity, A., and Choi, H. J. (2015). "Polyaniline/Fe composite nanofiber added softmagnetic carbonyl iron microsphere suspension and its magnetorheology." *J. Mater. Chem. C*, 3(8), 1861–1868.

Premalatha, S. E., Chokkalingam, R., and Mahendran, M. (2012). "Magneto Mechanical Properties of Iron Based MR Fluids." *Am. J. Polym. Sci.*, 2012(4), 50–55.

Purandare, S., Zambare, H., and Razban, A. (2019). "Analysis of magnetic flux in magneto-rheological damper." *J. Phys. Commun.*, 3(7).

Rabbani, Y., Hajinajaf, N., and Tavakoli, O. (2019). "An experimental study on stability and rheological properties of magnetorheological fluid using iron nanoparticle core–shell structured by cellulose." *J. Therm. Anal. Calorim.*, 135(3), 1687–1697.

Rabinow, J. (2013). "The magnetic fluid clutch." *Electr. Eng.*, 67(12), 1167.

Sapiński, B., and Gołdasz, J. (2015). "Development and performance evaluation of an MR squeeze-mode damper." *Smart Mater. Struct.*, 24(11), 115007.

Sedlacik, M., and Pavlinek, V. (2014). "A tensiometric study of magnetorheological suspensions' stability." *RSC Adv.*, 4(102), 58377–58385.

Shafer, A. S., and Kermani, M. R. (2011). "On the feasibility and suitability of mr fluid clutches in human-friendly manipulators." *IEEE/ASME Trans. Mechatronics*.

Shah, K., and Choi, S. B. (2015). "The influence of particle size on the rheological properties of plate-like iron particle based magnetorheological fluids." *Smart Mater.*

Struct., 24(1), 015004.

Shah, K., Phu, D. X., Seong, M. S., Upadhyay, R. V., and Choi, S. B. (2014). "A low sedimentation magnetorheological fluid based on plate-like iron particles, and verification using a damper test." *Smart Mater. Struct.*, 23(2), 27001–27011.

Si, H., Peng, X., and Li, X. (2008). "A Micromechanical Model for Magnetorheological Fluids." *J. Intell. Mater. Syst. Struct.*, 19(1), 19–23.

Sidpara, A., Das, M., and Jain, V. K. (2009a). "Rheological Characterization of Magnetorheological Finishing Fluid." *Mater. Manuf. Process.*, 24(12), 1467–1478.

Sidpara, A., Das, M., and Jain, V. K. (2009b). "Rheological Characterization of Magnetorheological Finishing Fluid." *Mater. Manuf. Process.*, 24(12), 1467–1478.

Singh, A. K., Jha, S., and Pandey, P. M. (2015). "Performance Analysis of Ball End Magnetorheological Finishing Process with MR Polishing Fluid." *Mater. Manuf. Process.*, 30(12), 1482–1489.

Snyder, R. A., Kamath, G. M., and Wereley, N. M. (2001). "Characterization and analysis of magnetorheological damper behavior under sinusoidal loading." *AIAA J.*, 39(7), 1240–1253.

Stanway, R., Sproston, J. L., and El-Wahed, A. K. (1996). "Applications of electro-rheological fluids in vibration control: A survey." *Smart Mater. Struct.*, IOP Publishing.

Vékás, L. (2008). "Ferrofluids and magnetorheological fluids." *CIMTEC 2008 - Proc. 3rd Int. Conf. Smart Mater. Struct. Syst. - Smart Mater. Micro/Nanosystems*, Trans Tech Publications Ltd, 127–136.

Vinod, S., John, R., and Philip, J. (2016). "Magnetorheological properties of sodium sulphonate capped electrolytic iron based MR fluid: a comparison with CI based MR fluid."

Wang, G., Ma, Y., Li, M., Cui, G., Che, H., Mu, J., Zhang, X., Tong, Y., and Dong, X. (2016). "Magnesium ferrite nanocrystal clusters for magnetorheological fluid with enhanced sedimentation stability."

Wang, G., Ma, Y., Li, M., Cui, G., Che, H., Mu, J., Zhang, X., Tong, Y., and Dong, X. (2017a). "Magnesium ferrite nanocrystal clusters for magnetorheological fluid with enhanced sedimentation stability." *Solid State Sci.*, 63, 70–75.

Wang, G., Zhao, D., Ma, Y., Zhang, Z., Che, H., Mu, J., Zhang, X., Tong, Y., and Dong, X. (2017b). "Synthesis of calcium ferrite nanocrystal clusters for magnetorheological fluid with enhanced sedimentation stability." *Powder Technol.*,

322, 47–53.

Wang, J., and Meng, G. (2001). "Magnetorheological fluid devices: Principles, characteristics and applications in mechanical engineering." *Proc. Inst. Mech. Eng. Part L J. Mater. Des. Appl.*, 215(3), 165–174.

Wang, X., and Gordaninejad, F. (1999). "Flow Analysis of Field-Controllable, Electro- and Magneto-Rheological Fluids Using Herschel-Bulkley Model." *J. Intell. Mater. Syst. Struct.*, 10(8), 601–608.

Weiss, K. D., Carlson, J. D., and Nixon, D. A. (1994). "Viscoelastic properties of magneto- and electro-rheological fluids." *J. Intell. Mater. Syst. Struct.*, 5(6), 772–775.

Wereley, N. M., Chaudhuri, A., Yoo, J.-H., John, S., Kotha, S., Suggs, A., Radhakrishnan, R., Love, B. J., and Sudarshan, T. S. (2006). "Bidisperse Magnetorheological Fluids using Fe Particles at Nanometer and Micron Scale." *J. Intell. Mater. Syst. Struct.*, 17(5), 393–401.

Wu, S., Sun, A., Xu, W., Zhang, Q., Zhai, F., Logan, P., and Volinsky, A. A. (2012). "Iron-based soft magnetic composites with Mn-Zn ferrite nanoparticles coating obtained by sol-gel method." *J. Magn. Magn. Mater.*, 324(22), 3899–3905.

Xia, Z., Wu, X., Peng, G., Wang, L., Li, W., and Wen, W. (2017). "A novel nickel nanowire based magnetorheological material." *Smart Mater. Struct.*, 26(5).

Xu, Y., Gong, X., and Xuan, S. (2013). "Soft magnetorheological polymer gels with controllable rheological properties." *Smart Mater. Struct.*, 22(7), 075029.

Xu, Z., Fan, J., Han, Y., Liu, T., Zhang, H., Song, K., and Zhang, C. (2019). "Preparation and characterization of Mn–Zn ferrites via nano-in-situ composite method." *Solid State Sci.*, 98, 106006.

Yang, J., Yan, H., Dai, J., Hu, Z., and Zhang, H. (2017). "The rheological response of carbonyl iron particles suspended in mineral oil solution of 12-hydroxy stearic acid." *J. Rheol. (N. Y. N. Y).*, 61(3), 515–524.

Yang, J., Yan, H., Wang, X., and Hu, Z. (2016). "Enhanced yield stress of magnetorheological fluids with dimer acid." *Mater. Lett.*, 167, 27–29.

Yang, P., Yu, M., Fu, J., and Luo, H. (2018). "Rheological properties of dimorphic magnetorheological gels mixed dendritic carbonyl iron powder." *J. Intell. Mater. Syst. Struct.*, 29(1), 12–23.

Yao, G. Z., Yap, F. F., Chen, G., Li, W. H., and Yeo, S. H. (2002). "MR damper and its application for semi-active control of vehicle suspension system." *Mechatronics*, 12(7), 963–973.

Yu, M., Yang, C., Bian, X., Zhao, S., Wang, T., Liu, S., and Guo, T. (2016). "Application of Fe78Si9B13 amorphous particles in magnetorheological fluids." *RSC Adv.*, 6(27), 22511–22518.

Zhang, H., Yan, H., Hu, Z., Yang, J., and Niu, F. (2018). "Magnetorheological fluid based on thixotropic PTFE-oil organogel." *J. Magn. Magn. Mater.*, 451, 102–109.

Zhang, X.-J., Farjoud, A., Ahmadian, M., Guo, K.-H., and Craft, M. (2011). "Dynamic Testing and Modeling of an MR Squeeze Mount." *J. Intell. Mater. Syst. Struct.*, 22(15), 1717–1728.

Zhou, C., Fang, Q., Yan, F., Wang, W., Wu, K., Liu, Y., Lv, Q., Zhang, H., Zhang, Q., Li, J., and Ding, Q. (2012). "Enhanced microwave absorption in ZnO/carbonyl iron nano-composites by coating dielectric material." *J. Magn. Magn. Mater.*, 324(9), 1720–1725.

Zhu, W., Dong, X., Huang, H., and Qi, M. (2019). "Iron nanoparticles-based magnetorheological fluids: A balance between MR effect and sedimentation stability." *J. Magn. Magn. Mater.*, 491, 165556.

BIO DATA

Personal Information
ARUNA M N
E-mail: arunamn400@gmail.com
Mobile: +91-9164774565
DOB : 07-09-1991.
Nationality: Indian.
Permanent Address: Nagaraju M N S/o Muttige Village, Malalikere   Post,
Arakalgud Taluk, Hassan District,
 Karnataka State India-5730102

Education details

Course and University	**Duration**
(Ph.D.,) Metallurgical and Materials Engineering National Institute of Technology Karnataka (NITK) Surathkal Mangalore, India.	**2016-**
M.Tech., Computational analysis in Mechanical sciences Government Engineering College., Hassan ., Karnataka., India**.**	**2013-2015**
B.E., Mechanical Engineering Sapthagiri College of Engineering (S.C.E)., Bangalore., Karnataka., India**.**	**2010-2013**
DME., Diploma in Mechanical Engineering Government Polytechnic Kushalangar., Kodagu., Karnataka., India.	**2007-2010**

Declaration

I hereby declare that the above-mentioned information is correct up to my knowledge and I bear the responsibility for the correctness of the above-mentioned particulars

Date:29/10/2021
Place: Mangalore   **ARUNA M N**

List of Publications based on the Ph.D. Research Work

Sl.No	Title of the paper	Authors name (In the same order as in the paper, underline the research scholar's name	Name of the Journal / Conference / Symposium, Vol., No., Pages	Month & Year Of Publication	Category*
1	Influence of additives on the synthesis of carbonyl iron suspension on rheological and sedimentation properties of magnetorheological (MR) fluids	<u>MN Aruna</u>, MR Rahman, S Joladarashi, H Kumar	Materials Research Express, 6(8), 086105.	May, 2019	1
2	Investigation of sedimentation, rheological, and damping force characteristics of carbonyl iron magnetorheological fluid with/without additives.	<u>MN Aruna</u>, MR Rahman, S Joladarashi, H Kumar	Journal of the Brazilian Society of Mechanical Sciences and Engineering, 42(5)	April, 2020	1
3	Investigating Sedimentation and Rheological properties of Magnetorheological Fluids using various carrier fluids	<u>MN Aruna</u>, MR Rahman, S Joladarashi, H Kumar	In IOP Conference Series: Materials Science and Engineering (Vol. 577, No. 1, p. 012049).	November, 2019	3
4	Influence of Different Fumed Silica as Thixotropic Additive on Carbonyl Particles Magnetorheological Fluids for Sedimentation Effects. .	<u>M N Aruna</u>, Rahman, M. R., Joladarashi, S., Kumar, H., & Bhat, P. D.	*Journal of Magnetism and Magnetic Materials*, 167910	April 2021	1

Category*
1 : Journal paper, full paper reviewed   2 : Journal paper, Abstract reviewed
3 : Conference/Symposium paper, full paper reviewed   4 : Conference/Symposium paper, abstract reviewed 5 : Others (including papers in Workshops, NITK Research Bulletins, Short notes etc.)

Research Scholar
(ARUNA M N.)

Research Guide
(Dr. MR Rahman)